

**THE UNIVERSITY OF NAIROBI**  
**COLLEGE OF BIOLOGICAL AND PHYSICAL SCIENCES**  
**SCHOOL OF PHYSICAL SCIENCES**  
**DEPARTMENT OF GEOLOGY**



**MODELLING HYDROLOGICAL RESPONSE TO URBANIZATION: CASE STUDY**  
**SYOKIMAU – KATANI AREA, MACHAKOS COUNTY, KENYA**

By

Karen Nguna Masila

I56/82940/2015

**Supervisors**

Dr. E. Dindi


Dr. L. Olaka

A dissertation submitted in partial fulfilment of the requirements for the award of the  
Master of Science Degree in Applied Geophysics

©November, 2020

## DECLARATION

I declare that this dissertation is my original work and has not been submitted elsewhere for examination, the award of a degree or publication. Where other people's work or my work has been used this has properly been acknowledged and referenced under the University of Nairobi's requirements.

**SIGNATURE:**  \_\_\_\_\_

**DATE:** 27/11/2020 \_\_\_\_\_

MASILA KAREN NGUNA

I56/82940/2015

karennguna@gmail.com

DEPARTMENT OF GEOLOGY

This dissertation is submitted with our approval as research supervisors.

**SIGNATURE:** \_\_\_\_\_

**DATE:** \_\_\_\_\_

DR. EDWIN W. DINDI

[edwin.dindi@uonbi.ac.ke](mailto:edwin.dindi@uonbi.ac.ke)

DEPARTMENT OF GEOLOGY

UNIVERSITY OF NAIROBI

**SIGNATURE:** \_\_\_\_\_

**DATE:** \_\_\_\_\_

DR. LYDIA A. OLAKA

[lydiaolaka@uonbi.ac.ke](mailto:lydiaolaka@uonbi.ac.ke)

DEPARTMENT OF GEOLOGY

UNIVERSITY OF NAIROBI

## ABSTRACT

The Syokimau – Katani peri-urban catchment has over time been affected by adverse urban development related flooding. The encroachment of the expanding Nairobi city on this metropolitan space has spurred the mushrooming of impervious surfaces on an already poorly drained gently sloping clay-filled landscape. This has, in turn, reduced rainfall losses by interception and infiltration and increased net rainfall-runoff amounts and flood frequency, thus posing a livelihood safety challenge in the area. From the analysis done of the problem-solving approach countries such as Belgium, Rwanda, Slovakia and Iran have assimilated, a physically-based hydrological modelling approach using the WetSpa tool has been chosen and adopted in this project for this catchment. This framework has made provision for the use of geologically and geophysically validated readily-available datasets on the topography, soils and land-use of the Syokimau – Katani region in a rapid-prototyping approach to determine the area’s hydrological response.

Herein, a delineation of the study area’s watershed was achieved alongside an analysis of its land-use (over the years 1999, 2000, 2010 and 2016), soils, stratigraphy and geology. Also, an added analysis of locally acquired ERT and drillhole data was used to aid in the interpretation and justification of the study area’s soils and geology coverage. From the validated topography, soils and land-use datasets, spatially indexed potential runoff coefficient values were generated using the WetSpa tool upon which hotspot runoff areas within the study area were mapped. A time series of the rainfall-runoff depth estimates was also generated based on both the **LULC-only** and **unique scenarios** to isolate the effects of rainfall intensity and land-use/land cover to these estimates.

Even though weather and climate play a significant role in generating runoff depths in this study area, land use and land cover have also significantly contributed to runoff depth yields shown from the **LULC-only** and **unique scenarios**. This has been exemplified by the 1999-2000 drought case and the 2016 increase in urbanization discussed in this project. The highlighted impact of urbanization to flooding in this research can therefore be used to inform urban development policies and settlement procedures in the Syokimau – Katani area, as well as in urban/peri-urban centres and metropolitan spaces within the country. The potential runoff coefficient maps generated herein are viable in aiding the placement and design of storm management systems in

more effective ways that can help control this urban-flooding problem. It is also recommended to use an advanced form of the Wetspa tool known as WetSpa-Python for the increased spatial and temporal resolution flexibility for a varied distribution of urban catchments.

**TABLE OF CONTENTS**

***DECLARATION**..... I*

***ABSTRACT**..... II*

***TABLE OF CONTENTS**..... IV*

***LIST OF FIGURES**..... VII*

***LIST OF MAPS**..... IX*

***LIST OF PLATES**..... X*

***LIST OF TABLES**..... X*

***LIST OF ACRONYMS & UNITS**..... X*

***ACKNOWLEDGEMENTS**..... XII*

**Chapter 1: Introduction ..... 1**

    1.1 Introduction ..... 1

    1.2 Problem Statement..... 5

    1.3 Aims and Objectives..... 5

    1.4 Justification..... 5

**Chapter 2: Literature Review ..... 7**

    2.1 The peri-urban flooding problem ..... 7

    2.2 Flood modelling methods ..... 7

    2.3 The WetSpa Approach..... 8

**Chapter 3: Materials and Methods ..... 10**

    3.1 The Study Area..... 10

        3.1.1 Physiography and Drainage ..... 10

        3.1.2 Soils and geology ..... 10

        3.1.3 Hydrogeology..... 14

        3.1.4 Vegetation and Climate..... 15

---

3.1.5	Population.....	15
3.1.6	Available Data for modelling.....	16
3.2	Model Framework and Validation.....	17
3.2.1	Introduction.....	17
3.2.2	Topographical model (T) validation.....	17
3.2.3	Land use model (LU) validation.....	18
3.2.4	Soil model (S) validation.....	19
3.2.4.1	<i>Electrical resistivity tomography data</i> .....	19
3.2.4.2	<i>Borehole data</i> .....	26
3.3	Methods.....	27
3.3.1	Introduction.....	27
3.3.2	The WetSpa model.....	27
3.3.2.1	<i>Introduction</i> .....	27
3.3.2.2	<i>Model structure</i> .....	28
3.3.2.3	<i>Watershed Delineation</i> .....	29
3.3.2.4	<i>Data Preparation</i> .....	32
3.3.2.5	<i>Model Formulation</i> .....	36
i.	Flow response at cell level.....	37
ii.	Flow response at a flow path level.....	37
iii.	Flow response of the catchment.....	38
3.3.2.6	<i>Model Parameters</i> .....	38
i.	Default parameters for Soil texture classes.....	38
ii.	Default parameters for Land use classes.....	38
iii.	Potential runoff coefficient.....	40
3.3.2.7	<i>Model Assumptions</i> .....	41

---

<b>Chapter 4: Results and Discussion .....</b>	<b>43</b>
4.1 Results .....	43
4.1.1 Landuse and land cover changes in the Syokimau-Katani area .....	43
4.1.2 Soil textural classes in the Syokimau-Katani area .....	46
4.1.3 Potential runoff coefficients and ‘hotspots’ of the Syokimau-Katani area .....	49
4.1.4 Topography, land-use and soil overlays with runoff coefficient results .....	52
4.1.4.1 Topography overlaid by the 2016 runoff coefficient results .....	53
4.1.4.2 Landuse overlaid by the 2016 runoff coefficient results .....	54
4.1.4.3 Soil overlaid by the 2016 runoff coefficient results.....	55
4.1.5 Runoff depth time series from 1999 to 2016.....	55
4.2 Discussion.....	58
<b>Chapter 5: Conclusions and Recommendations.....</b>	<b>60</b>
5.1 Conclusion .....	60
5.2 Recommendations .....	60
<b>APPENDICES .....</b>	<b>62</b>
<b>Appendix 1: Sample page of borehole completion report from WRMA (2018) .....</b>	<b>62</b>
<b>REFERENCES .....</b>	<b>63</b>

**LIST OF FIGURES**

*Fig. 1.1: An elevation map of the study area and its relative location on google earth ..... 2*

*Fig. 1.2: Nairobi Metropolitan region (Source: (UN-Habitat, 2010))..... 3*

*Fig. 1.3: Change of water balance due to urbanization (Source: www.sieker.de, 2018) ..... 4*

*Fig. 3.1: Graph of average mean monthly precipitation of the 1999 - 2016 period (Generated from KMD data) ..... 15*

*Fig. 3.2: Graph of average mean monthly temperature of the 1999 - 2016 period (Generated from KMD data) ..... 16*

*Fig. 3.3: The Syokimau-Katani watershed showing variable topography and derived waterways at 30m resolution. .... 18*

*Fig. 3.4: A comparison between land-use data provided online (shown by the upper map divided into land-use classes) and a google earth image (shown by the lower map) of the study area ..... 19*

*Fig. 3.5: Electrical Resistivity Tomography typical layout; (A) Measurement sequencing used to generate apparent resistivity pseudo-section. (B) Example of a measured apparent resistivity pseudo-section (Reynolds, 2011) ..... 21*

*Fig. 3.6: Location and resistivity profile of the first ERT survey line, with respect to the Syokimau-Katani soil map ..... 23*

*Fig. 3.7: An illustration of soil/rock types and their respective resistivities ..... 24*

*Fig. 3.8: Location and resistivity profile of the second ERT survey line, with respect to the Syokimau-Katani soil map ..... 24*

*Fig. 3.9: Location and resistivity profile of the third ERT survey line, with respect to the Syokimau-Katani soil map ..... 25*

*Fig. 3.10: An excerpt of a driller's borehole log from one of the neighbouring boreholes within the locality of the study area (See Appendix 1) ..... 27*

*Fig. 3.11: WetSpa model structure (Source: (Liu and De Smedt, 2004)) ..... 29*

*Fig. 3.12: Profile view of a sink before and after running the Fill tool (Source: ArcGIS documentation) ..... 30*

*Fig. 3.13: Flow direction matrix (Source: ArcGIS documentation) ..... 31*

*Fig. 3.14: Determining the accumulation of flow (Source: ArcGIS documentation)..... 31*



**Fig. 3.15:** Various stages of the Syokimau-Katani DEM processing using the WetSpa extension on ArcView: (a) Filled elevation, (b) Flow direction, (c) Flow accumulation, (d) Flow length, (e) Stream link, (f) Slope, (g) Hydrologic radius, (i) Subwatersheds. .... 33

**Fig. 3.16:** Steps involved in land-use dataset processing: (a) General clip result of the original 300m X 300m grid file, (b) An array of points generated from the original 300m X 300m grid file, (c) An Interval Distance Weighting (idw) result at 30m X 30m cell spacing, and (d) A classified watershed clipped to the boundary extent. .... 34

**Fig. 3.17:** An overview of the ArcView window and corresponding soil parameters during the processing of soil data using the WetSpa extension. .... 35

**Fig. 4.1:** Graphical representation of land use and land cover variations in percentages for the years 1999, 2004, 2010 and 2016..... 46

**Fig. 4.2:** (RC) A 3-D spatial representation of the 2016 runoff coefficient values in the Syokimau-Katani area with streams generated from DEM, correlated with (T) A 3-D image of the study area's DEM; (IT) A 2-D overlay of runoff coefficient on DEM..... 53

**Fig. 4.3:** (RC) A 3-D spatial representation of runoff coefficient values in Syokimau-Katani area with streams generated from DEM correlated with (LU) A 3-D image of the study area's land use map (ILU) A 2-D overlay of runoff coefficient on land-use..... 54

**Fig. 4.4:** (RC) A 3-D spatial representation of runoff coefficient values in Syokimau-Katani area with streams generated from DEM correlated with (S) A 3-D image of the study area's soil map (IS) A 2-D overlay of runoff coefficient on soils..... 55

**Fig. 4.5:** Runoff depths for the March-April-May periods of the years 1999, 2004, 2010 and 2016 ..... 56

**Fig. 4.6:** Runoff depths with only change in land-use/land cover for the March-April-May period in the years 1999, 2004, 2010 and 2016..... 57

**LIST OF MAPS**

*Map. 3.1: Drainage and DEM map of the Syokimau-Katani watershed ..... 10*

*Map. 3.2: Percentage slope distribution in the Syokimau-Katani area ..... 11*

*Map. 3.3: Soil types of Syokimau-Katani (Adopted from 1962 Soil map)..... 11*

*Map. 3.4: Regional geology map of the study area with attached corresponding cross section A-B (right). Note that the cross-section has inferred surfaces to show unknown strata depths. The gap between the “Athi Tuffs & Lake Beds” and the “Undifferentiated crystalline rocks of the MMB” represents any unknown strata. Drillhole data is recommended to fill this gap..... 13*

*Map. 3.5: Geology of the Syokimau-Katani area (Adopted from the Geological map sheets 51NE, 1964 and 52NW, 1954) ..... 14*

*Map. 3.6: Spatial placement of boreholes within the vicinity of the study area..... 14*

*Map. 3.7: Map showing the ERT quarry site survey with respect to Syokimau-Katani's soil map that was processed using online data ..... 22*

*Map. 4.1: Land cover land use distribution in the Syokimau-Katani area 1999 ..... 43*

*Map. 4.2: Land cover land use in Syokimau-Katani in 2004 ..... 44*

*Map. 4.3: Land cover land use in Syokimau-Katani in 2010 ..... 44*

*Map. 4.4: Land cover land use in Syokimau-Katani in 2016 ..... 45*

*Map. 4.5: Clay soil distribution map of the Syokimau-Katani area (%)..... 47*

*Map. 4.6: Sand soil distribution map of the Syokimau-Katani area (%) ..... 47*

*Map. 4.7: Silt soil distribution map of the Syokimau-Katani area (%)..... 48*

*Map. 4.8: Soil textural and coverage map of the Syokimau-Katani..... 48*

*Map. 4.9: Potential runoff coefficient distribution of the Syokimau-Katani area (1999)..... 49*

*Map. 4.10: Percentage slope distribution in the Syokimau-Katani area ..... 50*

*Map. 4.11: Potential runoff coefficient distribution of the Syokimau-Katani area (2004)..... 50*

*Map. 4.12: Potential runoff coefficient distribution of the Syokimau-Katani area (2010)..... 51*

*Map. 4.13: Potential runoff coefficient distribution of the Syokimau-Katani area (2016)..... 52*

**LIST OF PLATES**

*Plate: 1.1 Floods in Syokimau (Source: www.braced.org, 2015) ..... 1*  
*Plate: 3.1: Section of the ERT survey area with outcropping volcanic rocks. .... 26*

**LIST OF TABLES**

*Table 3.1: Default parameters characterizing soil textural classes (Source: WetSpa Manual by (Liu and De Smedt, 2004))..... 39*  
*Table 3.2: Default parameters characterizing land use classes (Source: WetSpa Manual by (Liu and De Smedt, 2004))..... 39*  
*Table 3.3: Slope constant  $S_0$  for determining potential runoff coefficient (Source: WetSpa Manual by (Liu and De Smedt, 2004) ..... 40*  
*Table 3.4: Potential runoff coefficient for different land use, soil type and slope (Source: WetSpa Manual by (Liu and De Smedt, 2004))..... 41*

**LIST OF ACRONYMS & UNITS**

ANN	Artificial Neural Network
ASCII	American Standard Code for Information Interchange
bgl	Below ground level
CST	Constant Separation Traversing
DEM	Digital Elevation Model
ERT	Electrical Resistivity Tomography
ESA	European Space Agency
GIS	Geographical Information System
GoK	Government of Kenya
HBV	Hydrologiska Byråns Vattenbalansavdelning
IDW	Interval Distancing Weighting
IGBP	International Geosphere – Biosphere Program
ISRIC	International Soil Reference & Information Centre
IUH	Instantaneous Unit Hydrograph

JKIA	Jomo Kenyatta International Airport
Km <sup>2</sup>	Square kilometers
KMD	Kenya Meteorological Department
LULC	Land Use Land Cover
m/m	Metre per metre
m/s	Metre per second
MAM	March-April-May
max	Maximum
MIKE SHE model	MIKE Système Hydrologique Européen model
min	Minimum
MMB	Mozambique Mobile Belt
RC	Runoff Coefficient
RCMRD	Regional Centre for Mapping of Resources for Development
SRTM	Shuttle Radar Topography Mission
UN FAO	United Nations' Food & Agriculture Organization
USDA	United States Department of Agriculture
VES	Vertical Electrical Sounding
WetSpa	Water & Energy Transfer through Soils, Plants & the Atmosphere
WRMA	Water Resources Management Authority

## **ACKNOWLEDGEMENTS**

I would like to thank the University of Nairobi, particularly the Department of Geology for offering me a scholarship for my graduate studies. I also appreciate the support I have received from the Chairman – Dr. D. W. Ichang’i and my project supervisors – Dr. E. Dindi and Dr. L. Olaka.

Many thanks to Professor Abdolreza Bahreman from Iran and Mr. Kavianpour for the help and guidance they gave me in managing and operating the WetSpa tool. I also appreciate the Vrije Universiteit of Brussels team and my colleagues from Rwanda for their correspondence with regards to WetSpa.

I am greatly humbled by the immense mental, emotional and intellectual support I have continually received from my close friends and family. And above all, I thank God for the opportunity to do this project.

*“No substantial part of the universe is so simple that it can be grasped and controlled without abstraction. Abstraction consists in replacing the parts of the universe under consideration by a model of similar but simpler structure. Models, formal or intellectual on the one hand, or material on the other, are thus a central necessity of scientific procedure.”~ Xu (2002)*

## Chapter 1: Introduction

### 1.1 Introduction

Urbanization-induced land cover conversion has of late become an issue of environmental concern (Karamage et al., 2017; Panyako, 2018). The detrimental effects of poorly planned and ever-expanding urban spaces, more so in developing countries, include the increase of impervious surfaces. These surface types consequently lead to a reduction in the infiltration capacity of the ground (Karamage et al., 2017); a reduction that often translates to an increase in rainfall-runoff and eventually poses as a flood risk. **Plate: 1.1** shows a newly developed estate in Syokimau affected by flooding during the 2015 long rains season.



*Plate: 1.1 Floods in Syokimau (Source: www.braced.org, 2015)*

Situated in the peripheral settlements of Kenya's capital city Nairobi, the Syokimau - Katani area represents one of many metropolitan spaces in the region that face frequent flooding during the rainy season (Panyako et al., 2015). The study area is approximately 20.7km<sup>2</sup> in extent and it lies between longitudes 36.91<sup>0</sup> E and 37.05<sup>0</sup>E, and latitudes 1.33<sup>0</sup>S and 1.36<sup>0</sup>S. This region forms part of the Upper Athi River basin and is drained by one of the river's tributaries, at an elevation range

of 1464m to 1634m. **Fig. 1.1** below gives a relative position of the study area with respect to Nairobi city.

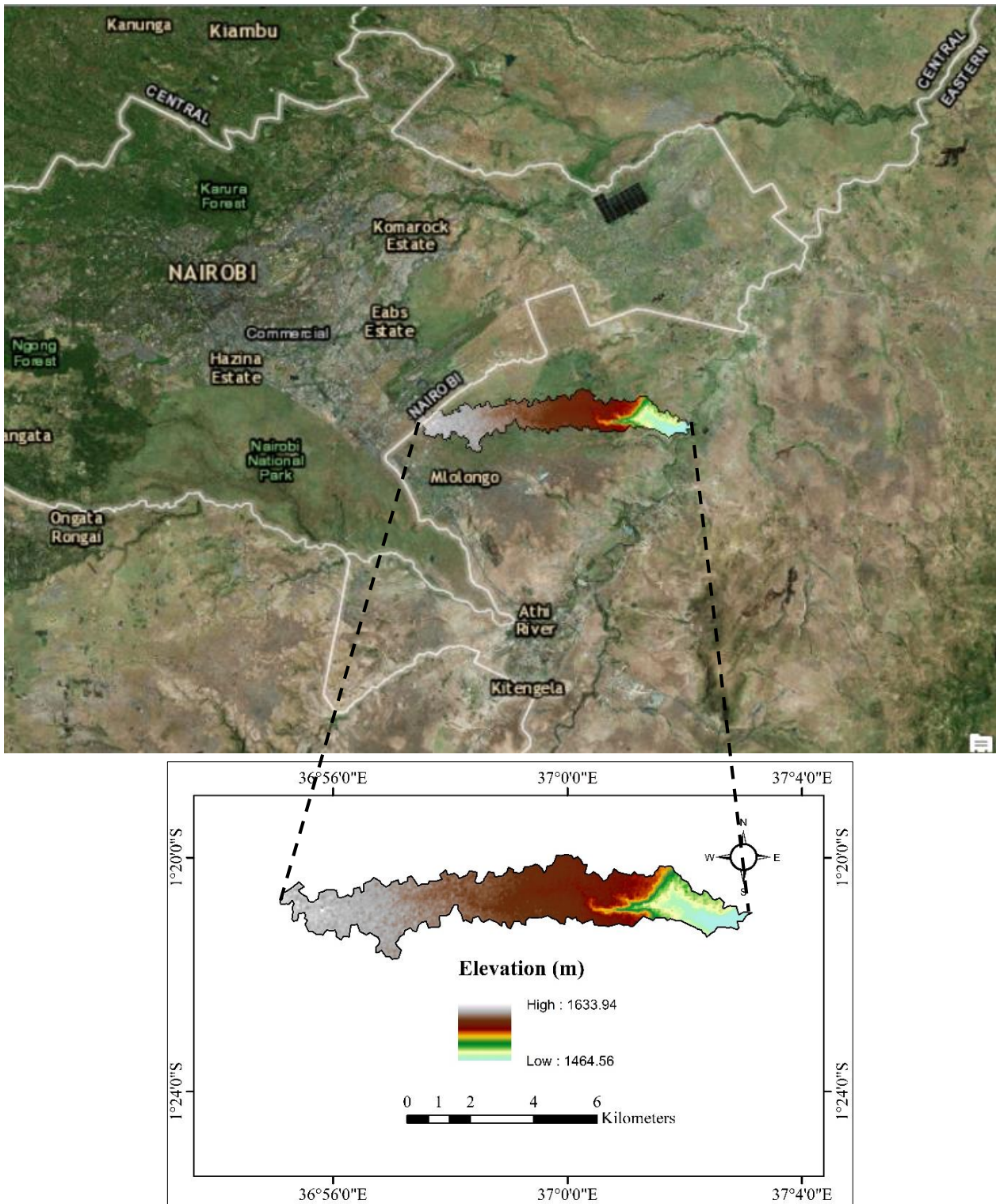


*Fig. 1.1: An elevation map of the study area and its relative location on google earth*



The Syokimau-Katani area is a transitional zone between the urban city of Nairobi and the rural region of Machakos County (within the Mavoko municipality – as shown in **Fig. 1.2**). It has experienced what Panyako et al. (2015) describes as a ‘rapid socio-economic transformation’ with mushrooming urban activities. The increase of impervious surfaces in this area (among them houses, malls, all-weather roads and paved compounds) has directly translated to the increase of rainfall-runoff amounts. Even with the operationalization of the National Disaster and Management Agency, the response to urban and peri-urban flooding in the area has been slow and the safety responsibility has been taken up by affected individuals and their respective households (Panyako et al., 2015); an approach that has borne futile results.

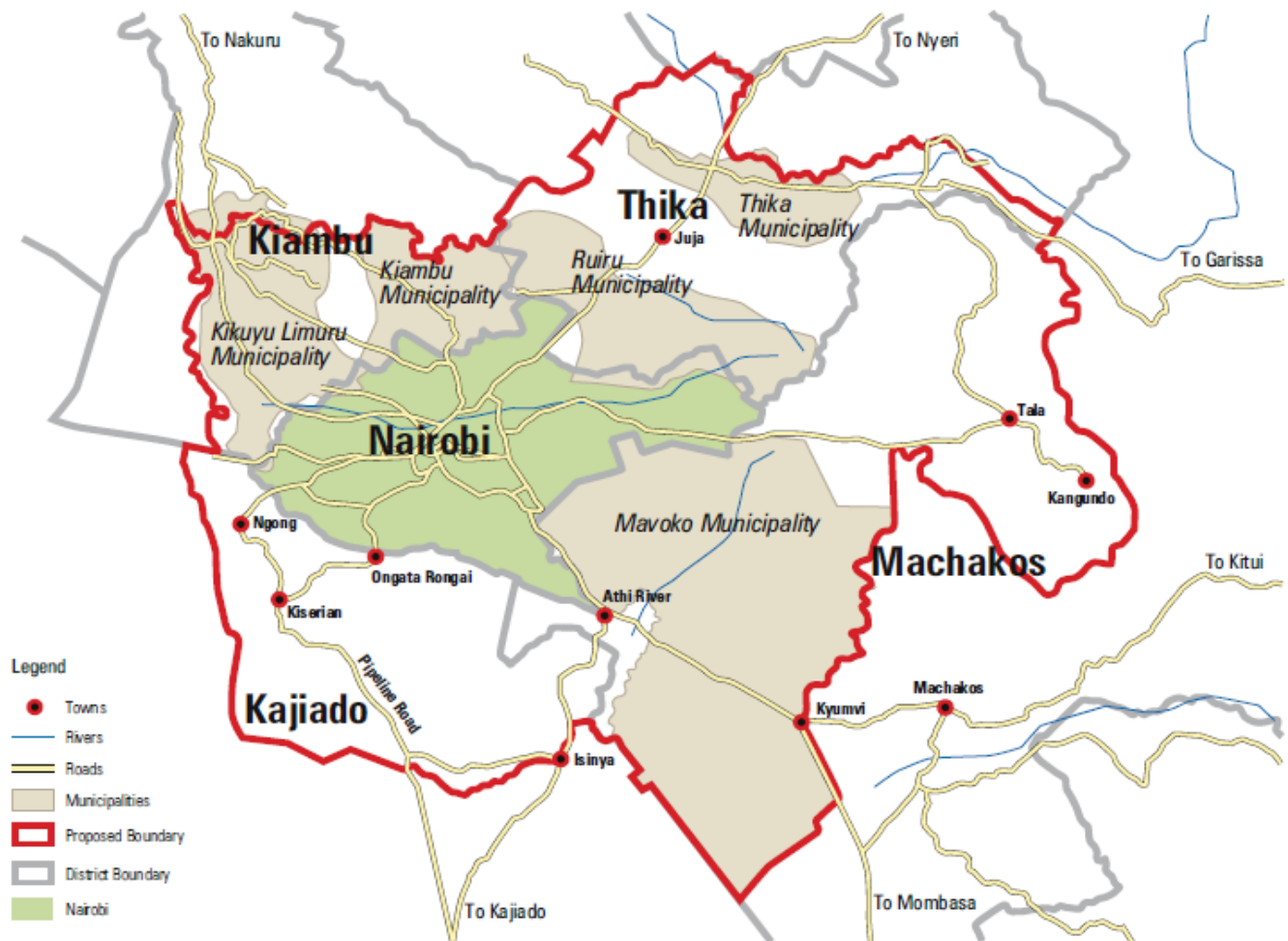


*Fig. 1.2: Nairobi Metropolitan region (Source: (UN-Habitat, 2010))*

Rapid land use transformations associated with urban (or peri-urban) development influence both direct and indirect transformations of land surface properties. Direct transformations include variations in soil water content, vegetation density and variety, heat capacity and surface coarseness (Wirion et al., 2017). Indirect transformations involve changes in evapotranspiration regimes by vegetation removal, precipitation patterns and ‘heat island’ effects (Shuster et al., 2005). The sealing of formerly natural landscapes through building and road construction reduces rainfall losses by interception and infiltration which then increase the net rainfall-runoff amounts. As a result, this limits the number and type of possible precipitation pathways/outlets in such urban settings (Shuster et al., 2005; Wirion et al., 2017). **Fig. 1.3** provides a summary of water balance variations with different types of ground cover.



*Fig. 1.3: Change of water balance due to urbanization (Source: [www.sieker.de](http://www.sieker.de), 2018)*

Hydrological models are used in runoff simulations for their typical design in the characterization of watershed conditions i.e. soil type, degree of soil saturation, topography, land use, drainage

density and even rainfall properties (Karamage et al., 2017). Countries such as Belgium (Smedt et al., 2002; Wirion et al., 2017), Rwanda (Karamage et al., 2017), Slovakia (Bahremand, 2006) and Iran (Almasi and Soltani, 2017) have explored hydrological modelling as a guide to help solve their flooding problems and highlighted a physical-based distributed approach to this problem.

## **1.2 Problem Statement**

The Mavoko region (in which the Syokimau – Katani area is situated) has been labelled as the fastest-growing municipality in Kenya (UN-Habitat, 2006). This rapid growth has been attributed to the industrial expansion in the area and the developing settlements just outside Nairobi city. The growth in infrastructure has involved the introduction of impervious roads, pavements and house roofs - all of which have contributed to the rise in surface runoff and the reduction of the infiltration capacities of the study area. This development has increased both flood frequency and rainfall-runoff amounts, thus posing a livelihood safety challenge to the occupants of this peri-urban space.

## **1.3 Aims and Objectives**

The main aim of this project was to determine the hydrological response of the Syokimau – Katani area due to urbanization. To achieve this, the project sought to:

1. Determine and analyze runoff coefficients predicated upon topography, land-use and soil maps.
2. Generate a time series of rainfall-runoff depth estimates (for the years 1999, 2004, 2010 and 2016).
3. Map out hotspot runoff areas within the Syokimau – Katani area, to aid in mitigation measures by informed administrative action.

## **1.4 Justification**

According to (UN-Habitat, 2010), Kenya's urbanized population stood at an approximate 19.73% in the year 2000, around 22.18% in 2010 and is projected to reach 48.14% in 2050. Today, there are nearly 230 urban centres in Kenya, where 45% of residents found in these centres live in the capital city of Nairobi and its environs (Mundia, 2017). Consequently, flood events in such urban and respective peri-urban spaces (like the Syokimau-Katani area) have markedly increased with increasing settlement activities and with this, a decreased effectiveness in flood management approaches has also been noted (Mundia, 2017).

Hydrological modelling makes provision for watershed analyses by using model inputs to comprehensively describe the catchment in question. This approach applies simulations that attempt to mimic the catchment's behaviour and then yield outputs that capture its response to varied weather conditions. These outputs are then used to inform flood management. Hydrological modelling has been used in different environments around the globe to solve similar problems. Examples of countries that have adopted this approach include Belgium, France, United Kingdom, United States and Rwanda.

## **Chapter 2: Literature Review**

### **2.1 The peri-urban flooding problem**

The development of peri-urban spaces on previously natural landscapes along the periphery of large towns and cities has been a direct result of growing urban populations, majorly experienced in developing countries (Braud et al., 2013; Koti and Weiner, 2006; Miller et al., 2014; Sahoo and Sreeja, 2014; Zellner et al., 2016). (The term ‘peri-urban’ is used herein to refer to areas with a patchwork of urbanized sections intertwined with undeveloped natural surfaces and agricultural/croplands). This transformation brings about physical changes to natural hydrological systems, thus reducing infiltration into soils, introducing artificial drainage that replaces natural pathways and consequently increasing river flow magnitudes and flooding frequencies.

Countries that have committed to tackling this problem greatly value the necessity of hydrological model application to provide data on urbanization-related hydrological effects on the long-term. (Miller et al., 2014). Requirements to map out areas that are vulnerable to flood risks and quantify the contributions made by watersheds as a response to urbanization are guided by the need for mitigation and management strategies in peri-urban areas. The facilitation provided by hydrological models with regards to temporal and spatial physical change manipulation abilities helps development stakeholders ascertain resulting impacts on simulated watershed hydrological response. This fact presents hydrological modelling as a necessary tool for planning and development.

Information on the geology, soils, drainage and urban development of the Syokimau-Katani area is readily available. Analyses on the region’s Mozambique mobile belt (MMB) deformation, lava flow layering, intercalation of weathered surfaces and later peneplanation exists (Fairburn, 1963; Matheson, 1966), alongside later borehole drilling (Simiyu and Dulo, 2015) and soil analyses reports (Ellenkamp, 2004). Digital elevation models and land-use digital datasets have been developed from international projects using remotely sensed images. Unfortunately, no published work exists concerning any technical approaches to tackle the flooding problem in the study area.

### **2.2 Flood modelling methods**

Rainfall-runoff modelling began in the early 19th Century (Xu, 2002). The need for hydrological modelling then revolved around the design of land reclamation drainage systems, urban sewage systems and reservoir spillways, and grew into the need to forecast the impact of land use change.

A clear necessity to understand the metrics and mechanisms behind land drainage at considerably high resolutions, in addition to flood peak discharge calculations, had been established.

A wide variation of hydrological models has developed over the years with the increase of identified hydrological challenges and watershed complexities – among them peri-urbanization (Devi et al., 2015; Xu, 2002). These variations have been based on criteria (deterministic and stochastic models), the time factor (static and dynamic models), and model parameters (lumped and distributed models) (Devi et al., 2015). The inputs needed for these models can then be obtained by empirical, conceptual or physically-based means, depending on both the purpose for which the model in use has been chosen and the prevailing conditions of operation (Devi et al., 2015; Dhimi and Pandey, 2013).

A varied number of hydrological models exist based on their problem-solving approach. Just to give a few examples; we have empirical or data-driven models such as the ANN model that use unit hydrographs and regression and correlation models to establish input-output relationships, conceptual models the HBV and TOPMODEL models that make interpretations by complex curve-fitting mechanisms, and physically-based models such as MIKE SHE, SWAT and WetSpa models that derive their interpretations from the mathematical idealization of physical processes that occur within a hydrological basin (Devi et al., 2015; Dhimi and Pandey, 2013; Xu, 2002). In this project, however, the physically-based models have been preferred. These models use finite difference equations and evaluate a substantial number of descriptive parameters highlighting the physical properties of the basin, which are then used to derive large amounts of information applicable in a wide range of scenarios. Physically-based models do not require extensive hydrological data as input, as an exhaustive description of the basin's physical characteristics is satisfactory. In our case, there exists sufficient physical data to describe the basin's characteristics without loss of scientific rigour and therefore a physically-based model will suffice for this exercise.

### **2.3 The WetSpa Approach**

This continuous, distributed and physically-based hydrological model has been applied to both small and fairly larger catchments in France, Belgium, Luxembourg, Iran, the United States and Rwanda (Naipal and Smedt, 2006). It has proven its ability to simulate watershed response to land-use change in different climatic environments. The WetSpa program is also user friendly and is

set up to easily extract necessary watershed parameters from high-resolution maps of land-use, soil and DEMs.

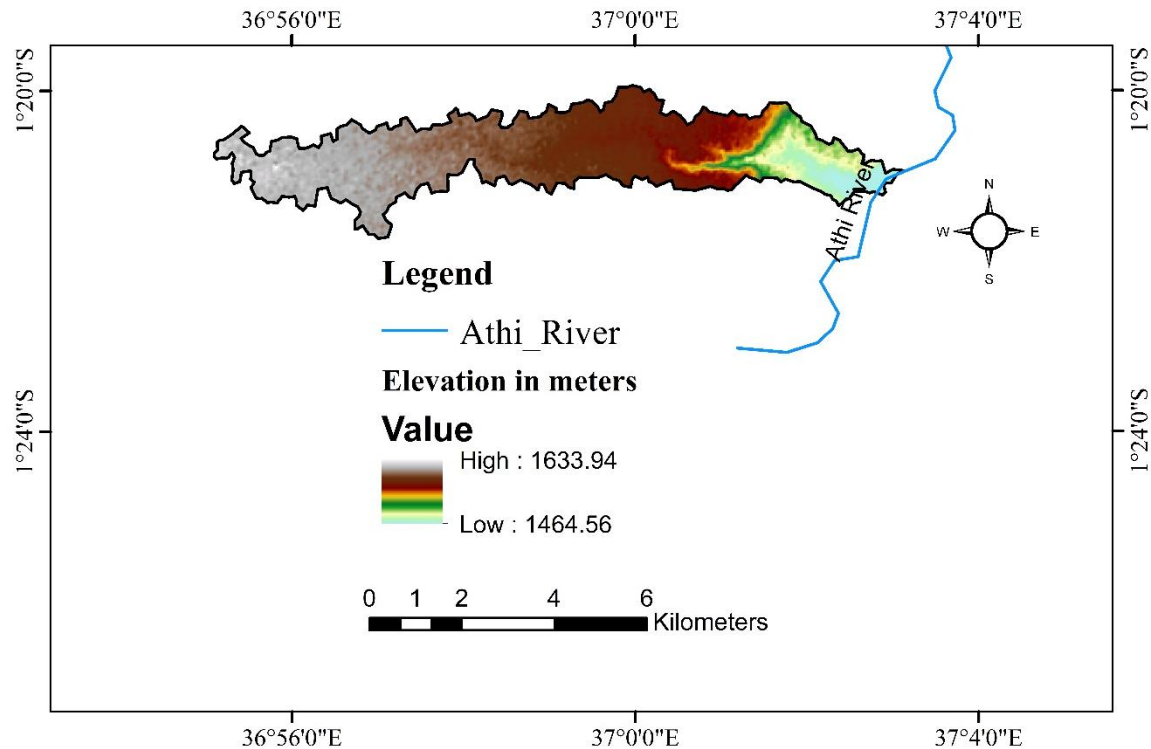
In conclusion, peri-urban flooding problems similar to those in the Syokimau-Katani area have been successfully assessed before using WetSpa in varied environments around the global.

## Chapter 3: Materials and Methods

### 3.1 The Study Area

#### 3.1.1 Physiography and Drainage

Situated within the depositional environment of the Kapiti plains, the Syokimau-Katani watershed drains easterly into the upper section of the Athi River, as shown on **Map. 3.1**, near the boundary between the Nairobi and Machakos counties. The area appears to gently slope (with a slope ranging between 0.02% and 12.4%) for the larger part and then develop steepness (with a slope ranging between 12.4% and 50%) towards the east into the tributary valley, as depicted on **Map. 3.2**. The steep easterly-face of the valley (evident on the DEM) represents a rock boundary.



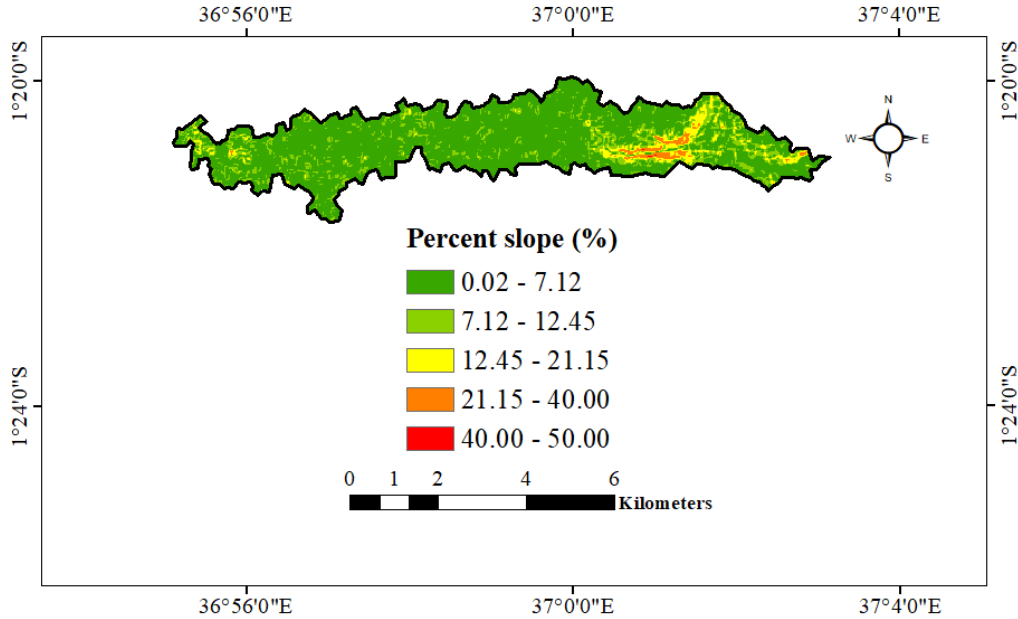
*Map. 3.1: Drainage and DEM map of the Syokimau-Katani watershed*

#### 3.1.2 Soils and geology

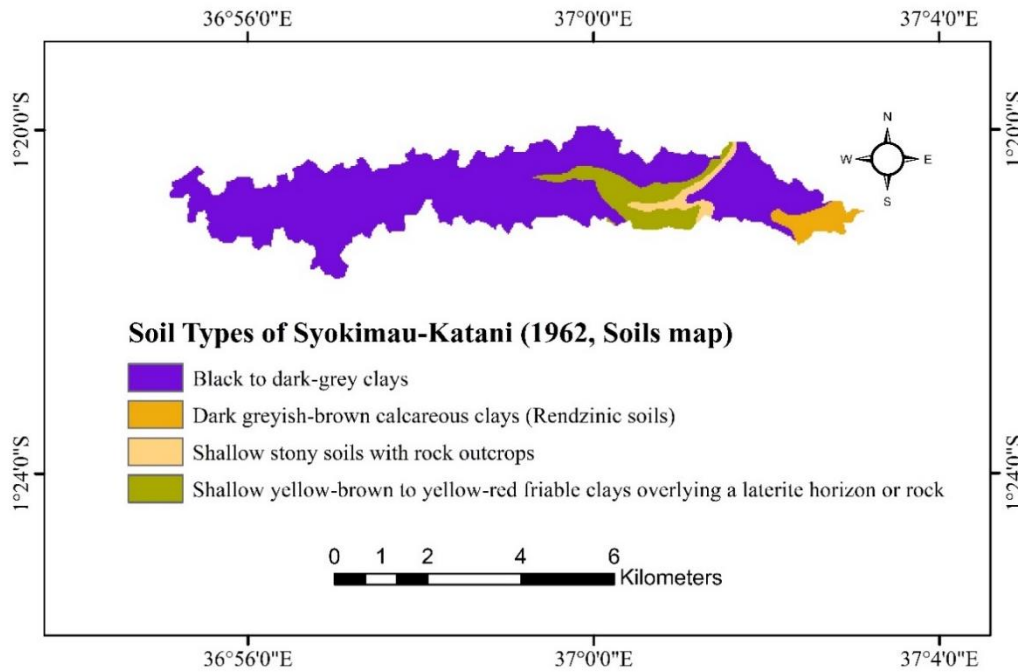
The region is dominated by black to dark-grey clay soils with localized zones bearing shallow yellow-brown to yellow-red friable clays, shallow stony soils (around rock outcrops) and dark greyish-brown Rendzinic soils. A spatial representation of this distribution is shown on **Map. 3.3**. These soil variations are closely related to the geology and landforms in the area i.e. the Athi-Kapiti plains (Ellenkamp, 2004).



**NB:** The significant figures displayed in all the numeric maps in this report (i.e. those that have a numerical distribution like **Map. 3.2**) are only a result of software generation and do not insinuate precision of any kind.

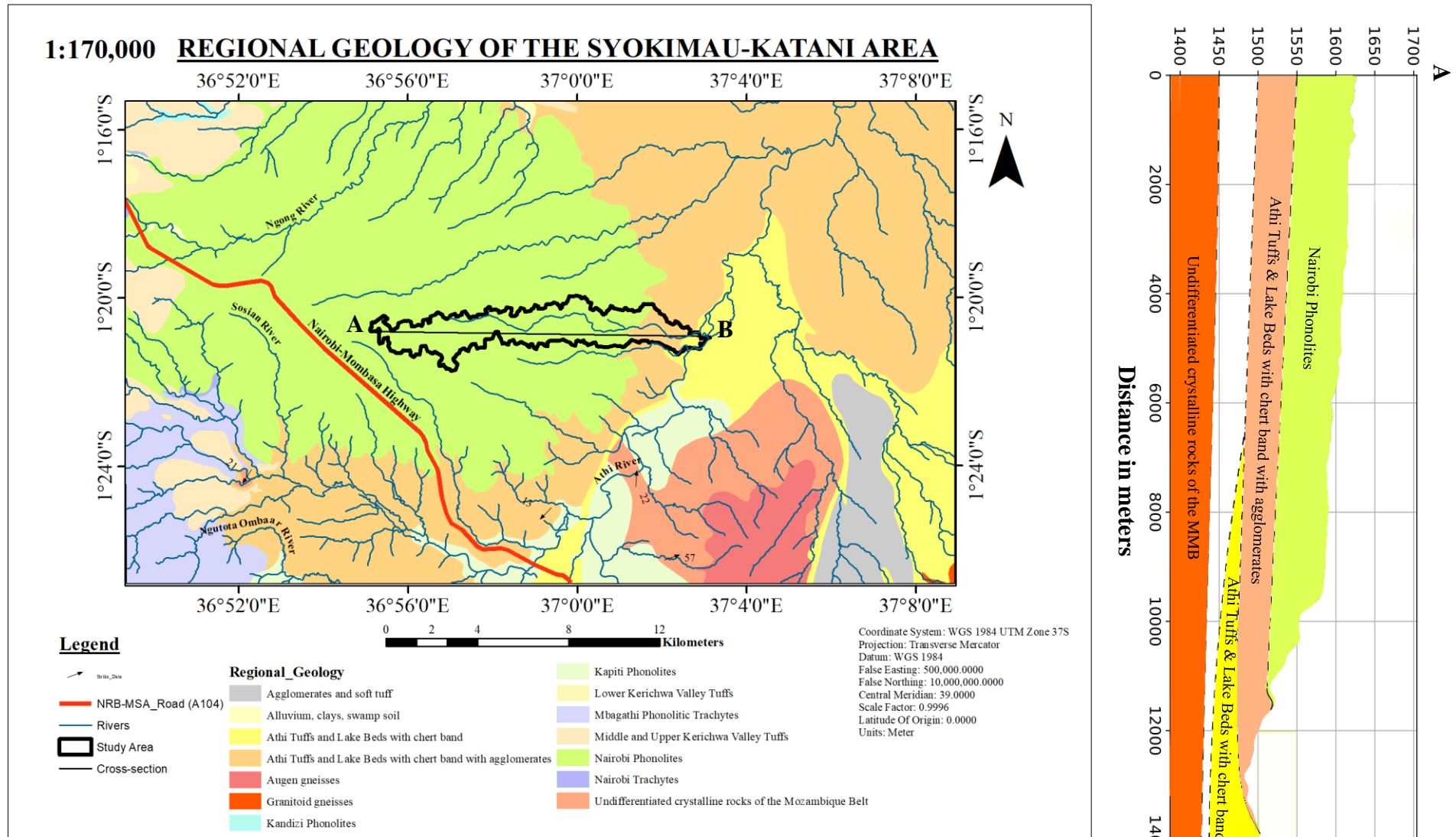


*Map. 3.2: Percentage slope distribution in the Syokimau-Katani area*

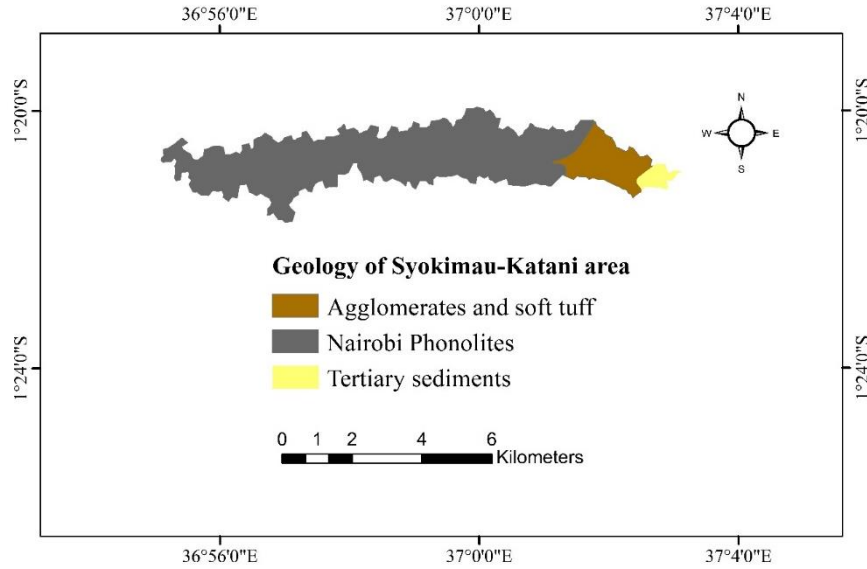


*Map. 3.3: Soil types of Syokimau-Katani (Adopted from 1962 Soil map)*

The recent black cotton soils in this area are derived from the underlying Nairobi Phonolites. Under these phonolites are the Athi agglomerate tuffs, the Simbara basalts and the relatively old Kapiti Phonolites; all of which represent episodes of volcanic flow deposition on the heavily deformed MMB during the formation of the Rift Valley (Fairburn, 1963; Matheson, 1966; Onyancha et al., 2011; Simiyu and Dulo, 2015). There are no faults or fractures notable in the study area (as shown in **Map. 3.5**) and its immediate environs (as evidenced by **Map. 3.4**).



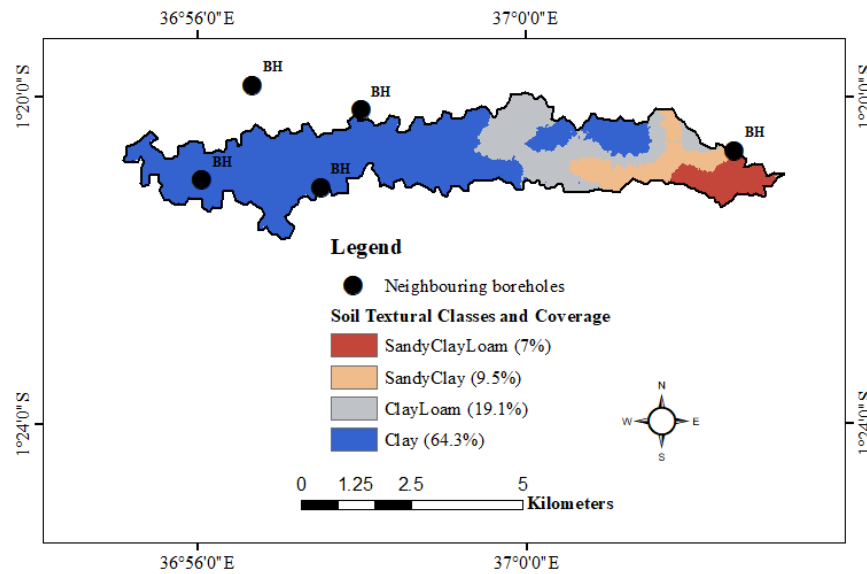
**Map. 3.4:** Regional geology map of the study area with attached corresponding cross section A-B (right). Note that the cross-section has inferred surfaces to show unknown strata depths. The gap between the “Athi Tuffs & Lake Beds” and the “Undifferentiated crystalline rocks of the MMB” represents any unknown strata. Drillhole data is recommended to fill this gap.



*Map. 3.5: Geology of the Syokimau-Katani area (Adopted from the Geological map sheets 51NE, 1964 and 52NW, 1954)*

### 3.1.3 Hydrogeology

Several boreholes have been drilled within the vicinity of the study area as (shown on **Map. 3.6**) for domestic and industrial purposes. The area has been reported to have medium groundwater potential, with subsurface and deep aquifers found at weathered zones and volcanic-basement contacts. Major aquifers in that region have been reported to occur at depths of 114m to 146m bgl, with the borehole water rest levels ranging from 96m to 137m bgl (Kuria, 2018).



*Map. 3.6: Spatial placement of boreholes within the vicinity of the study area*

### 3.1.4 Vegetation and Climate

Machakos County has a generally hot and dry climate with a 500mm to 1300mm annual average rainfall range, and a bimodal rainfall distribution; the March to May long rains (with April as the wettest month) and the October to December short rains. The region's mean monthly temperature ranges between 18<sup>0</sup>C and 25<sup>0</sup>C; with July as the coldest month and October/March as the hottest (Ngugi et al., 2011). **Fig. 3.1** and **Fig. 3.2** provide a graphical representation of these statistics.

The vegetation here consists mainly of closed shrublands (48.4%), croplands (25.6%), and grasslands (20.7%), with rare occurrences of barren/sparsely vegetated lands (1.24%) and woody savannah (0.4%). Details on this are provided in **section** Error! Reference source not found.**4.1.1**.

### 3.1.5 Population

With an estimated population of 65,000, the Mavoko region (in which the study area is situated, about 25km southeast of Nairobi) is the fastest-growing municipality (UN-Habitat, 2006). The area has been absorbing the industrial and settlement expansion of the metropolitan area of Nairobi city. It is the rapid urban growth in the area that has exacerbated flooding.

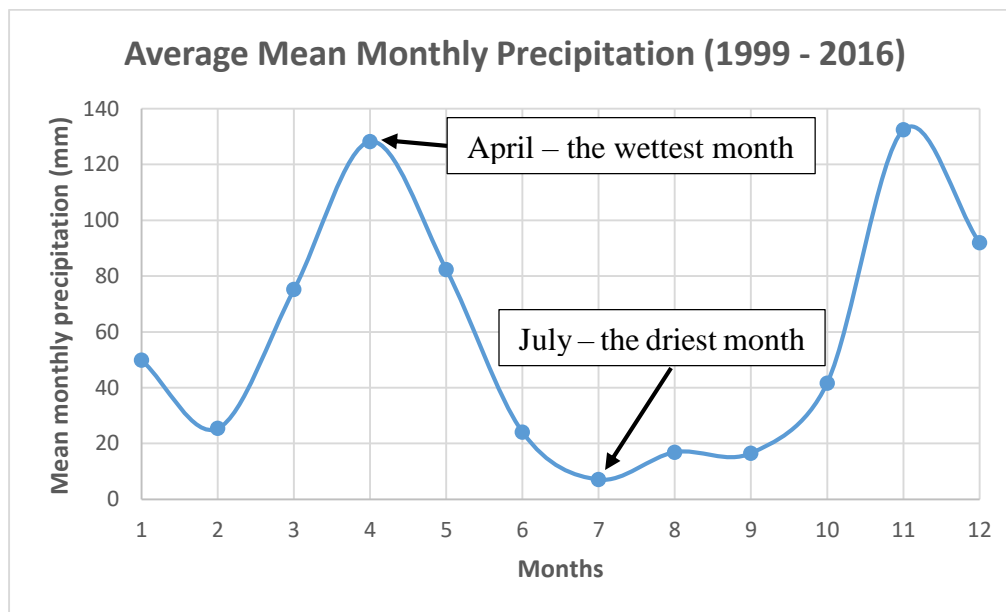


*Fig. 3.1: Graph of average mean monthly precipitation of the 1999 - 2016 period (Generated from KMD data)*

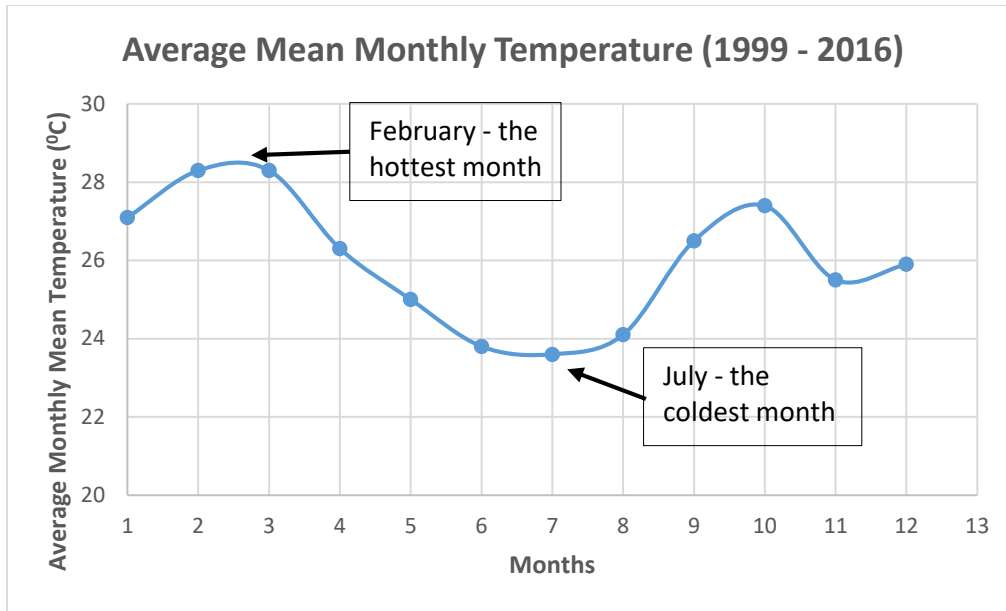


Fig. 3.2: Graph of average mean monthly temperature of the 1999 - 2016 period (Generated from KMD data)

### 3.1.6 Available Data for modelling

#### a) Digital Elevation Model

A 30m resolution SRTM level 3 DEM from the *NASA Jet Propulsion Laboratory website* ([www2.jpl.nasa.gov/srtm/](http://www2.jpl.nasa.gov/srtm/)) was used for watershed elevation analysis.

#### b) Soil data

Soil maps of clay, sand and silt percentages were obtained from *ISRIC World Soil Information website* (<http://isric.org/projects>) for Africa at 250m resolution.

#### c) Land use

Land use data grids were obtained from *UN FAO Africover* (<http://www.fao.org/>), *ESA* (<http://maps.elie.ucl.ac.be/CCI/viewer/>) and the *RCMRD websites* (<http://geoportal.rcmrd.org>)

#### d) Meteorological data

Total monthly rainfall intensity data was sourced from the Kenya Meteorological Department for the period 1999 to 2016.

## 3.2 Model Framework and Validation

### 3.2.1 Introduction

In this chapter, a framework for rapid prototyping that lends itself to simulation by a physically-based modelling tool is presented. This is done by defining the following generic models:

$$\mathbf{M}_1(\mathbf{T}) \rightarrow \mathbf{M}_2(\mathbf{LU}) \rightarrow \mathbf{M}_3(\mathbf{S}) \equiv \mathbf{M}(\mathbf{T}, \mathbf{LU}, \mathbf{S}) \rightarrow \mathbf{RC} \quad (\text{Expression 3.1})$$

where  $\mathbf{M}_1$  takes the topography map  $\mathbf{T}$  as input to yield model  $\mathbf{M}_2$  which takes the land use map  $\mathbf{LU}$  as input to yield model  $\mathbf{M}_3$  which takes the soil type map  $\mathbf{S}$  as input to yield model  $\mathbf{M}$ , which then takes topography, land use and soil type maps respectively to yield model  $\mathbf{RC}$ ; the runoff coefficient map. Also,

$$\mathbf{T} \times \mathbf{RC} \rightarrow \mathbf{I}_T$$

$$\mathbf{LU} \times \mathbf{RC} \rightarrow \mathbf{I}_{LU}$$

$$\mathbf{S} \times \mathbf{RC} \rightarrow \mathbf{I}_S \quad (\text{Expression 3.2})$$

Where model  $\mathbf{T}$  overlaid by model  $\mathbf{RC}$  yields an interpretation for  $\mathbf{T}$ , model  $\mathbf{LU}$  overlaid by model  $\mathbf{RC}$  yields an interpretation for  $\mathbf{LU}$  and model  $\mathbf{S}$  overlaid by model  $\mathbf{RC}$  yields an interpretation for  $\mathbf{S}$ . *Expressions 3.1* and *3.2* are an original contribution to the rapid prototyping modelling approach adopted in this dissertation.

In this rapid prototyping approach, all the data inputs for models  $\mathbf{T}$ ,  $\mathbf{LU}$  and  $\mathbf{S}$  are readily available and are derived from digital elevation models (provided online), digital land-use grids (provided online as datasets developed from remote sensing data) and digital soil grids (provided online) respectively. Our only concern and additional input to this framework is the validation of the various datasets selected.

### 3.2.2 Topographical model ( $T$ ) validation

In practice, the topographical dataset used as input for hydrological simulation is chosen by virtue of resolution – the higher the resolution, the more representative the results. The choice of resolution must near actual representation of an area's topography to allow for accurate determination of a watershed's boundaries and its physical properties i.e. river networks and slope variations.

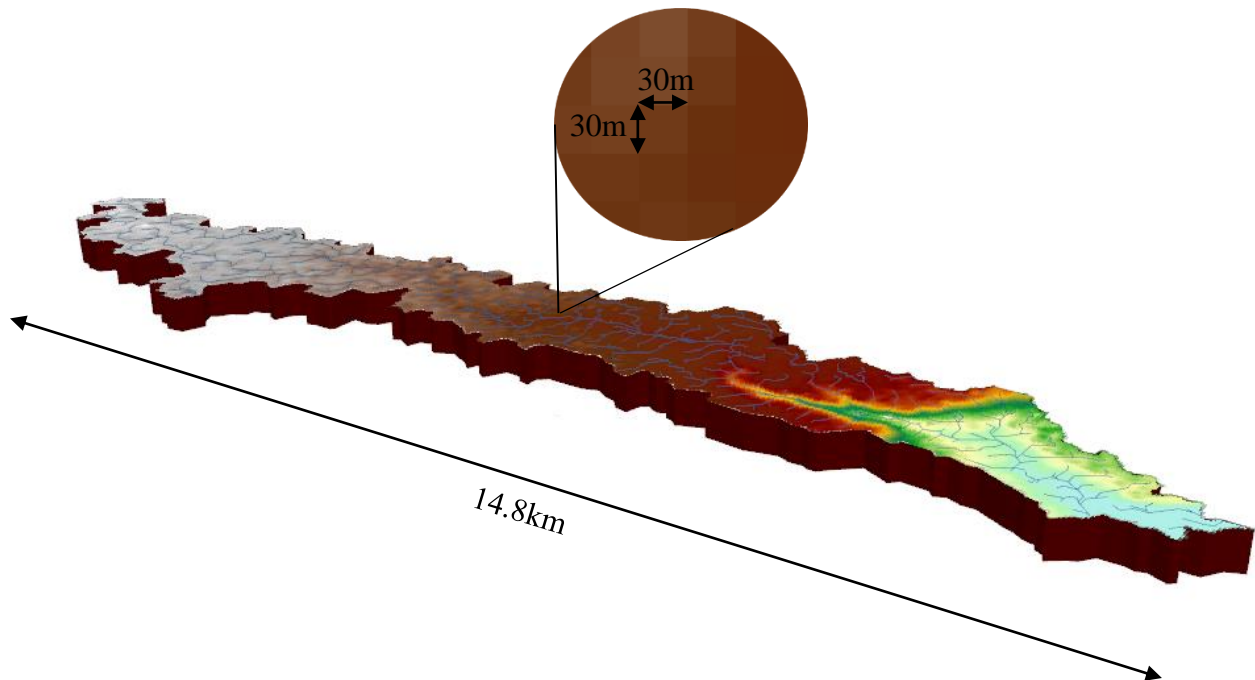


*Fig. 3.3: The Syokimau-Katani watershed showing variable topography and derived waterways at 30m resolution.*

The digital elevation model used for hydrological simulation in the study area was a 30m resolution grid file obtained online. It was used to define the boundaries of the basin in question, the possible waterways within the catchment and the slope used as input for the determination of the area's spatial distribution of runoff coefficient. **Fig. 3.3** shows derived waterways within the study area at 30m resolution. Being the first model in *Expression 1*, its resolution dictates the resolution to be used in the whole simulation process.

### **3.2.3 Land use model (LU) validation**

All input data used in simulation MUST be of the same resolution or grid cell size to ensure correct representation of the information overlaid in one pixel. The land use digital maps obtained online were regrided to 30m resolution to match that of the digital elevation model. A quick comparison of the data used and historical google earth images shows a correlation between land use types in the study area as displayed in **Fig. 3.4**.



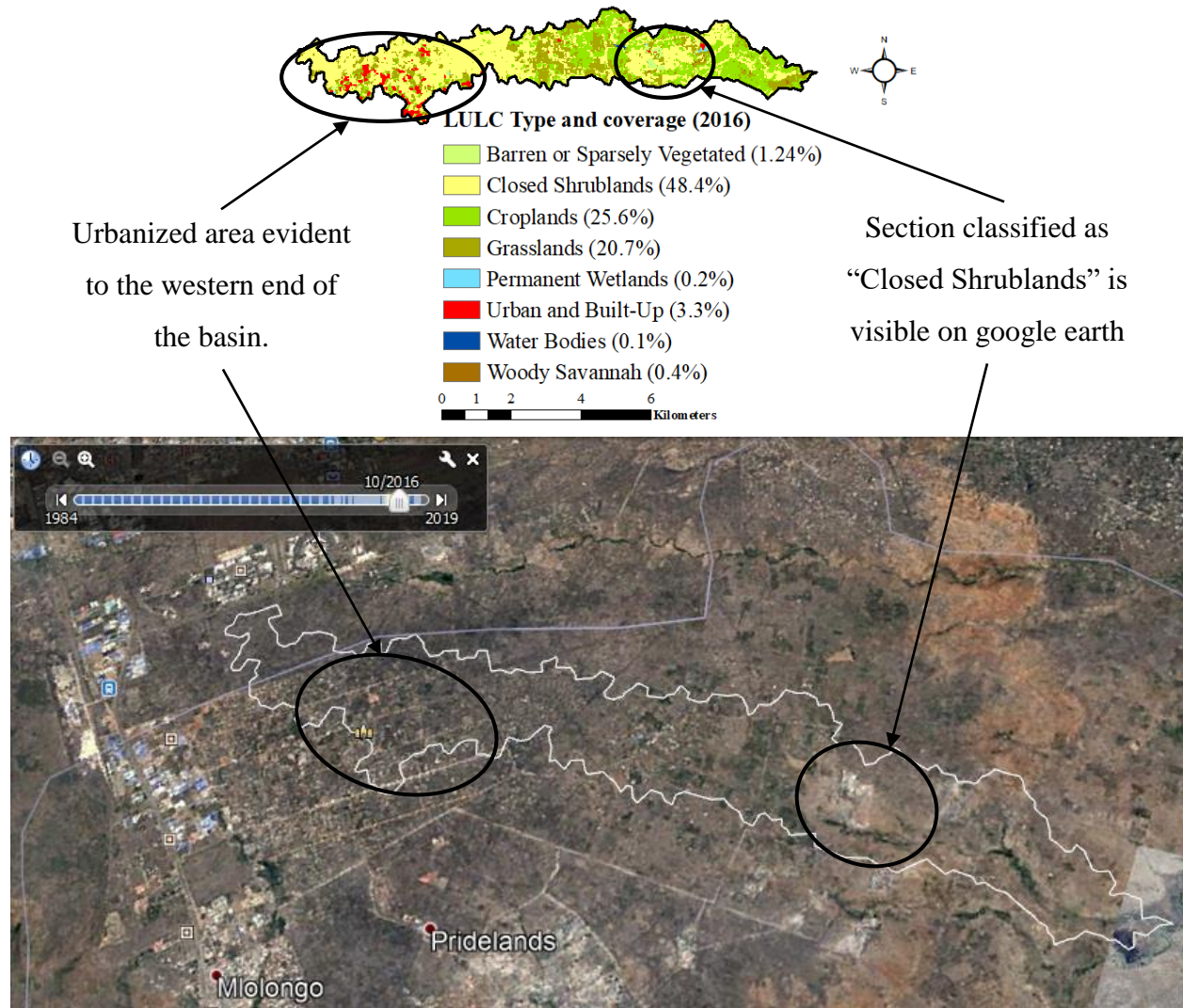


*Fig. 3.4: A comparison between land-use data provided online (shown by the upper map divided into land-use classes) and a google earth image (shown by the lower map) of the study area*

### 3.2.4 Soil model (S) validation

Apart from ensuring the soil data maps are of similar resolution to that of the digital elevation model, the soil information obtained can be validated using geophysical data and borehole data where available. In our case, 3 electrical resistivity tomography profiles and 3 boreholes are available for analysis in tandem with the information available on the area's regional geology.

#### 3.2.4.1 Electrical resistivity tomography data

In general, resistivity is a physical property that can be measured in rocks (both 'true' and 'apparent') to determine their types, their compactness (porosity and permeability), their age, as well as their depth of occurrence (Reynolds, 2011). Resistivity-based geophysical methods of

exploration rely on the transmission of direct current via certain electrode setups or arrays to measure the amount of resistivity in subsurface rocks. There are three main modes of electrode array in practice; VES (Vertical Electrical Sounding) for depth sounding, CST (Constant separation traversing) for generating horizontal profiles, and ERT (Electrical Resistivity Tomography) for imaging both lateral and vertical variances in resistivity (Reynolds, 2011). The ERT array is favoured for high resolution mapping of the near-surface (Reynolds, 2011).

ERT images a section of the earth's sub-surface by determining the apparent resistivity of rocks and/or soil material present (Onyancha et al., 2014; Reynolds, 2011) identifying them, and consequently defining layer thicknesses, depth of soils and rocks, depth to the water table (OHPA, 2008) possibly locating fracture zones (Valois et al., 2011). The procedure involves an array of ground-sunken electrode take-outs connected by a cable to an automated system that scans the near-surface in successive electrode sets by passing a flow of electrical current through the ground via these electrodes. At first, attention is given to successive groups of four electrodes (as shown in part A of **Fig. 3.5**), moving each instance by one electrode separation laterally. After scanning the entire array, the electrode separation is increased by one electrode increment i.e. groups of five electrodes, and so on. This process is repeated until all appropriate levels of the array are scanned. The whole procedure is software-controlled from a laptop computer (Reynolds, 2011).

The results are usually displayed as a pseudo-section (as shown in part B of **Fig. 3.5**) of contoured apparent resistivity values along the path travelled by the current for the entire array extent (Onyancha et al., 2014; Reynolds, 2011).

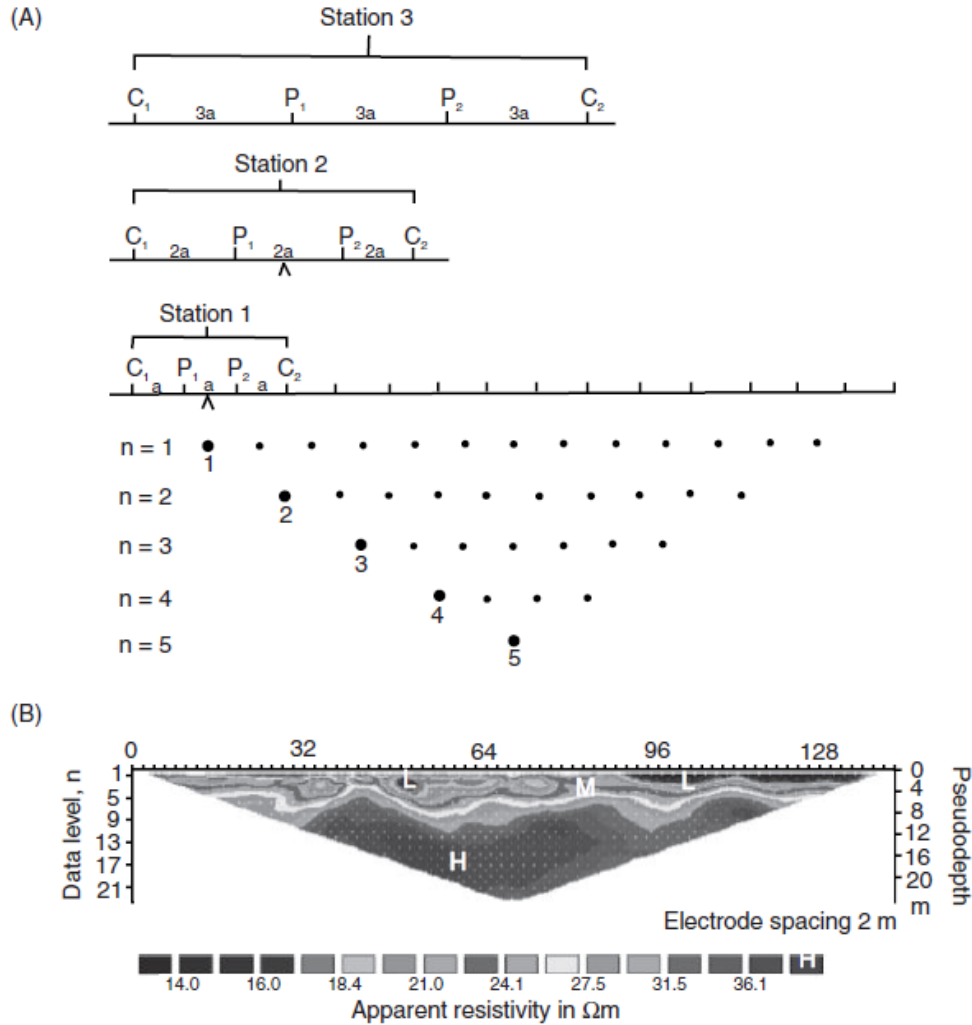
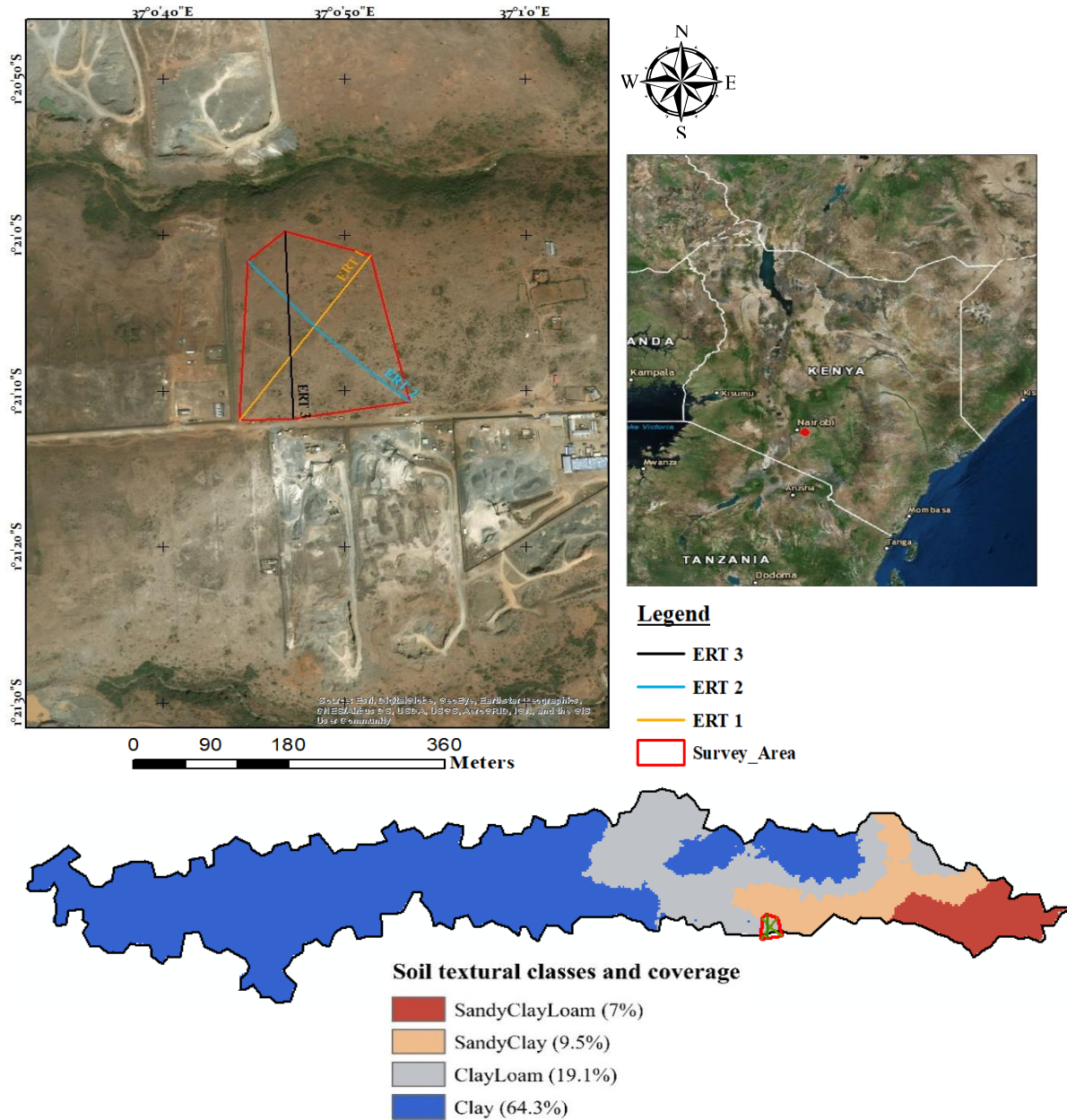


*Fig. 3.5: Electrical Resistivity Tomography typical layout; (A) Measurement sequencing used to generate apparent resistivity pseudo-section. (B) Example of a measured apparent resistivity pseudo-section (Reynolds, 2011)*

This ERT data was initially acquired for quarry site investigations using an ABEM Terrameter LS system, with a 41 electrode take-out array at 10 m spacing. Three survey lines were chosen; two diagonally orientated (NE-SW and NW-SE) and one across the stretch of the plot (almost N-S) as shown in **Map. 3.7**. This ERT dataset was adopted for this research as readily available information for soil validation. It is duly noted that longer ERT profiles with wider coverage of the study area would add value to the project, but the dataset at hand is deemed substantial.



*Map. 3.7: Map showing the ERT quarry site survey with respect to Syokimau-Katani's soil map that was processed using online data*

A least-squares inversion was performed on the raw ERT data collected, at a 5m spacing (even though the original electrode spacing set up during acquisition was 10m) to cater for the highly variable resistivity values on the ground surface. Other than the high resistivity features visible on the first resistivity profile shown on the final inversion profile as orange-yellow 'pockets' in **Fig. 3.6** within a depth range of 5m to 55m postulated to be phonolites surrounded by welded tuffs, the localized overburden of about 4.5m in thickness from the surface appears to have resistivity values ranging from 25.5Ωm to 77.7Ωm. According to (OHPA, 2008), such values would indicate loam

soils as shown by the scale provided in **Fig 3.7**, a near correlation to the classification provided by the digital map accessed online.

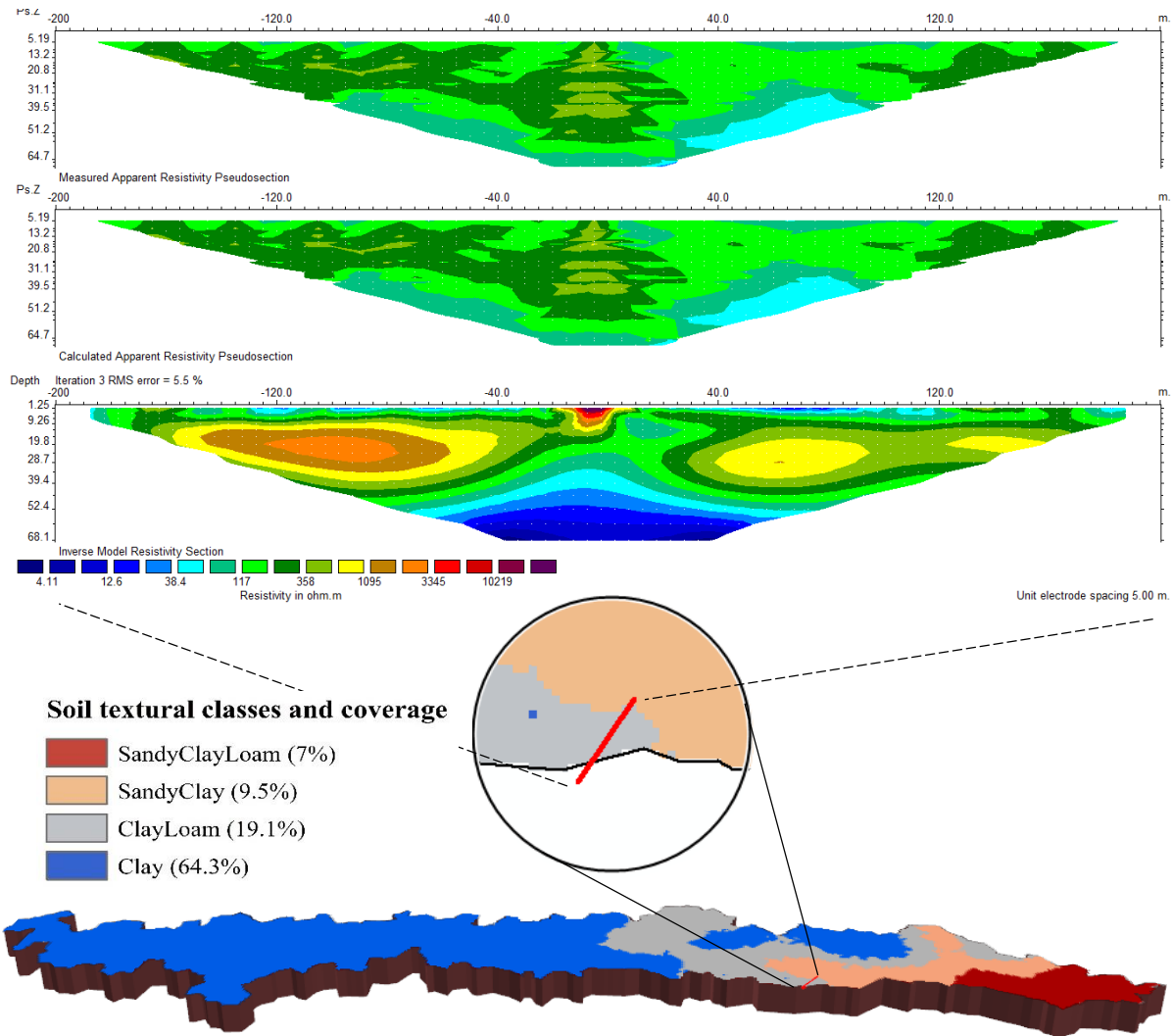


*Fig. 3.6: Location and resistivity profile of the first ERT survey line, with respect to the Syokimau-Katani soil map*

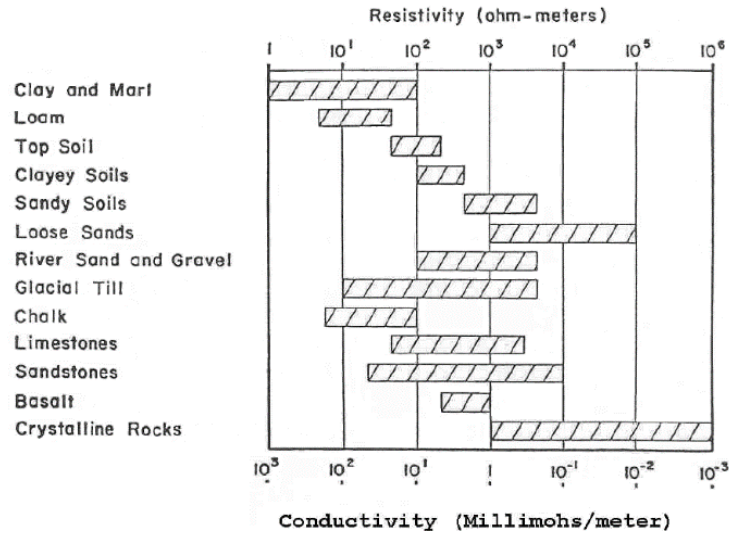


Fig. 3.7: An illustration of soil/rock types and their respective resistivities

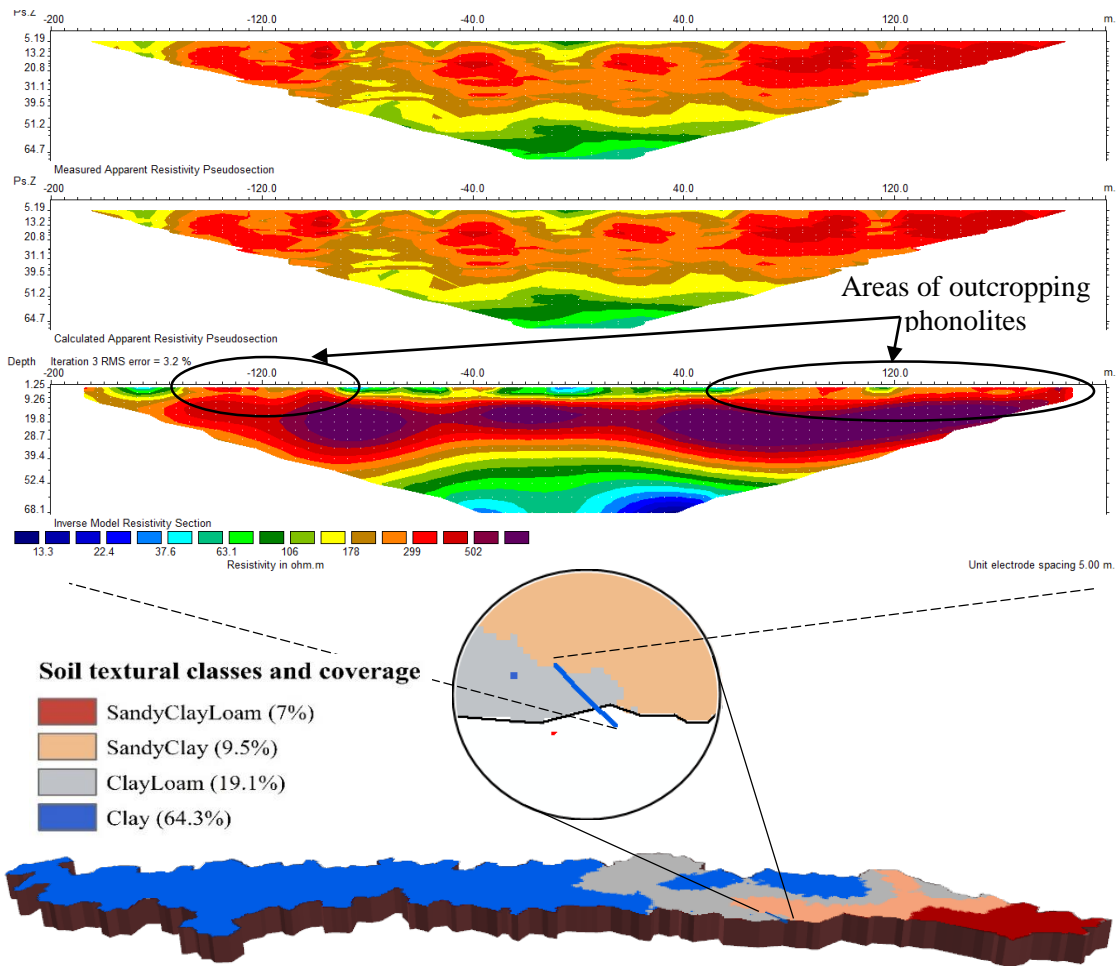
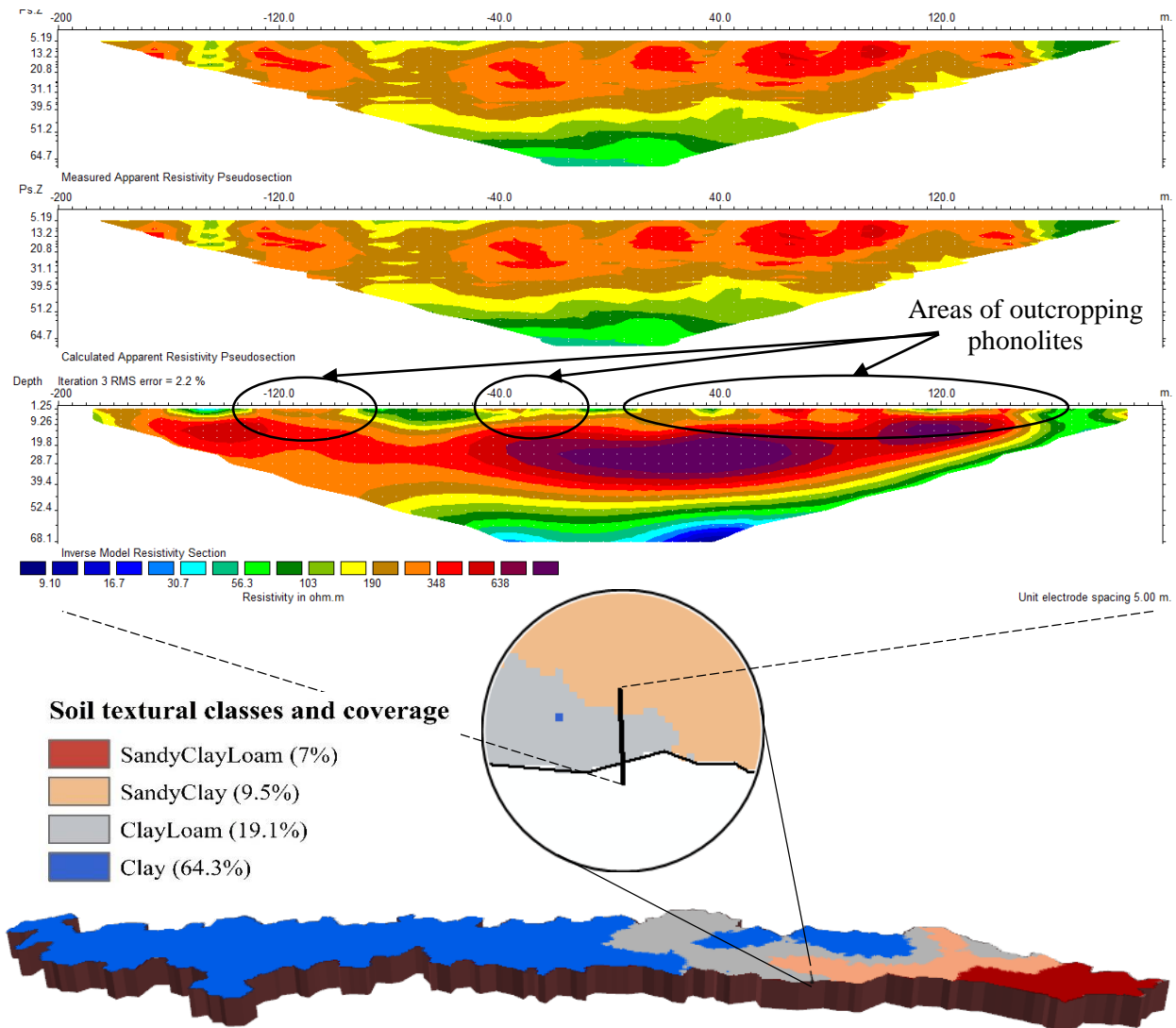
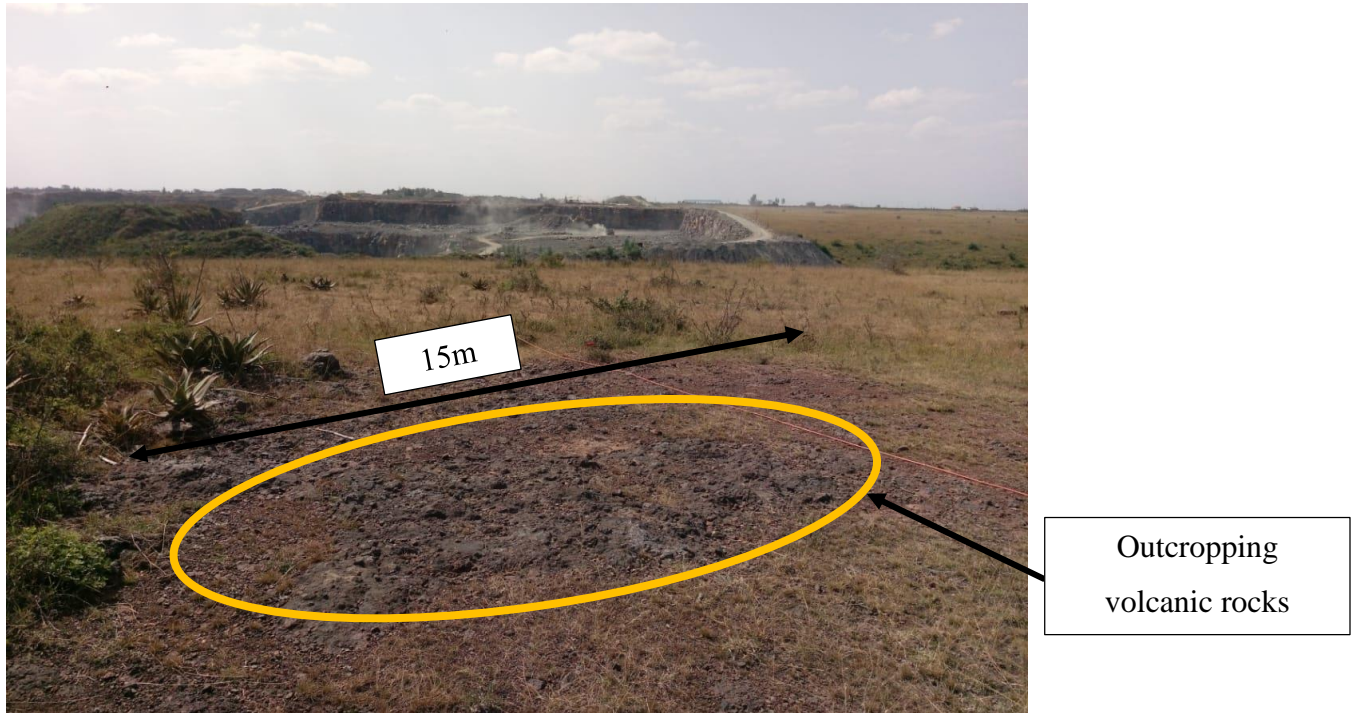


Fig. 3.8: Location and resistivity profile of the second ERT survey line, with respect to the Syokimau-Katani soil map

The overburden in the second ERT profile shown in **Fig. 3.8** appears to be slightly thinner with an approximate 4m thickness of material bearing low resistivity values ranging from 37.6Ωm to 178Ωm, while the resistivity values on the third ERT profile shown in **Fig. 3.9** range from 43.5Ωm to 190Ωm. These value ranges lie in the clayey-loam-soil classification, providing a good correlation to the online digital soil data. However, the sections of outcropping rock material (phonolites) on both profiles evidenced by the photograph on **Plate: 3.1** show sections of ground surface that have undergone possible erosion for a while, as the time difference between the resistivity data and the digital soil data is three years. No faults were noted in the three profiles.



**Fig. 3.9:** Location and resistivity profile of the third ERT survey line, with respect to the Syokimau-Katani soil map



*Plate: 3.1: Section of the ERT survey area with outcropping volcanic rocks.*

#### 3.2.4.2 Borehole data

Samples obtained during borehole drilling are one of the best sources of information used to characterize subsurface petrology (Sterrett, 2007). These representative samples collected at specified intervals down the borehole using varied sampling methods are commonly used in aquifer identification and are dependable for stratigraphic analyses (Sterrett, 2007).

In the Syokimau-Katani study area, several neighbouring boreholes have been drilled and an excerpt (as shown in **Fig. 3.10**) from a driller's borehole log from one of these boreholes mentioned in *section 3.1.3* correlates with the derived ERT profiles interpreted in *section 3.2.4.1*. The ERT profiles highlight top-layer surfaces filled with weathered rock material that correspond to the borehole section between 0 and 13m depth logged as a highly weathered region. The phonolites surrounded by welded tuffs interpreted from the ERT profiles also show similarity to the borehole log between 15m and 74m depth with interlayered fresh and weathered trachytes.



### 1. Driller's Log.

0-13m	Highly weathered
15-45m	Fresh trachyte
45-48m	Weathered trachyte
48-54m	Fresh trachyte
55-57m	Weathered trachyte
57-61m	Fresh trachyte
62-64m	Weathered trachyte
64-74m	Highly weathered
74-79m	Fresh trachyte

*Fig. 3.10: An excerpt of a driller's borehole log from one of the neighbouring boreholes within the locality of the study area (See Appendix 1)*

## 3.3 Methods

### 3.3.1 Introduction

All the spatial datasets (DEM, soil, land-use) used in this project were open-source. The meteorological data was sourced from the Kenya Meteorological Department. The softwares used to prepare and process this data were both open-source (i.e. WetSpa) and commercial (i.e. ArcGIS and Res2Dinv; *Courtesy of the Ministry of Petroleum & Mining*).

The main processing step involved hydrological modelling using WetSpa. This means that all the data was prepared and processed manually according to the standards required by the modelling tool.

### 3.3.2 The WetSpa model

#### 3.3.2.1 Introduction

WetSpa is a grid-based distributed hydrological model for **Water and Energy** transfers between **Soil, Plants and the Atmosphere**. It can forecast peak discharges and hydrographs which can simulate the spatial spread of a catchment's hydrologic features. Originally developed for hourly or daily time step flood prediction and water balance simulations at point sources within watersheds, this model considers four layers in the vertical orientation; the vegetation zone, root zone, transmission zone and saturated zone. It also considers the following hydrologic processes; interception, precipitation, surface runoff, depression, infiltration, evapotranspiration, percolation,

groundwater flow, interflow and water balance in the root zone and the saturated zone (Liu and De Smedt, 2004; Naporadean and Chira, 2006). It is, however, possible to use this model to generate hydrological responses without daily/hourly data.

In the WetSpa model, the total water balance in each raster cell comprises the water balance for the impervious surfaces, open water, bare soil and vegetated parts of the cell. This setup accounts for the anisotropy of the land use per cell which is consequently dependent on the resolution of the data grids chosen for the modelling process (Liu and De Smedt, 2004; Naporadean and Chira, 2006).

### 3.3.2.2 Model structure

WetSpa uses multiple layers in each grid cell for water and energy balance representation considering precipitation, snowmelt, interception, depression, evapotranspiration, infiltration, percolation, interflow, surface runoff and groundwater flow as shown in **Fig. 3.11**. Ideally, the flow of water within a watershed can be summarized as follows (Liu and De Smedt, 2004):

- a) Precipitation falls from the atmosphere.
- b) Part of the precipitation in (a) is trapped through canopy interception storage before reaching the ground.
- c) Remaining precipitation in (a) reaches the ground surface.
- d) Part of the precipitation in (c) is divided into two components depending on the land cover, soil type, slope, rainfall amounts, and the initial moisture content of the soil.
- e) Constituent 1 from (d) fills the depression storage at the first stage and runs off the ground surface instantaneously.
- f) Constituent 2 from (d) permeates into the soil.
- g) The permeated rainfall in (f) may (depending on the amount of moisture in the soil):
  - i. Be retained as soil moisture in the root zone
  - ii. Flow laterally as interflow, or
  - iii. Seep further as groundwater recharge – percolation out of the soil layer is assumed to recharge the groundwater storage.

**NB:** Drainage water from a cell moves laterally as influenced by the amount of groundwater storage and the recession coefficient.

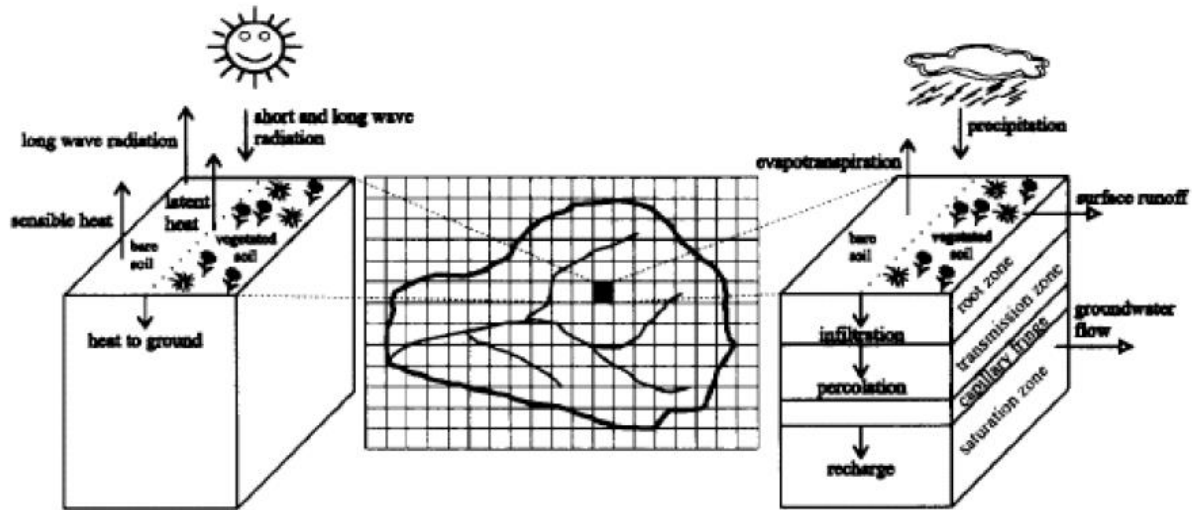


Fig. 3.11: WetSpa model structure (Source: (Liu and De Smedt, 2004))

Interflow from the root zone is anticipated to feed overland flow (Hortonian flow) which is then directed to the watershed outlet adding to surface runoff. Note that,

$$\text{Total runoff from each pixel cell} = \text{Surface runoff} + \text{Interflow} + \text{Groundwater flow}$$

The evaporation process occurs from intercepted water, depressed water and the soil surface, while that of transpiration occurs from a plant's root system in the soil layer, and a certain amount from the groundwater storage.

For this project, however, we will only use the inputs of soil, land-use and DEM with a few default parameters, to generate potential rainfall-runoff coefficients. This approach was used due to the lack of daily/hourly meteorological data to accurately capture calculated drainage values and water balance values that could be used to directly assess runoff volumes from the watershed. We will then use our potential rainfall-runoff coefficients values to manually calculate out runoff depths for the Syokimau-Katani watershed.

### 3.3.2.3 Watershed Delineation

Before delving into the rainfall-runoff coefficient calculation, a clear boundary of the watershed in question had to be defined. To define a watershed boundary, topographical data analysis is required (Greer et al., 2018). The watershed boundary of interest was delineated using the *Spatial Analyst* tool found in *ArcGIS* software.

Steps followed:

1. DEM grid section windowed from country SRTM DEM grid and exported as a Surfer grid (compatible with ArcGIS) at cell size 30m.
2. Raster analysis specification (*Geoprocessing>Environment>Raster Analysis*) set to match the original grid.
3. To create a flow direction grid of the drainage network developed from the DEM, the ‘path of flow’ of every cell in the grid must be determined. Some DEM files, however, tend to have cells that lack an associated drainage value otherwise called a ‘sink’ as shown in **Fig. 3.12**. The *Fill tool* (*ArcToolbox>Spatial Analyst Tools>Hydrology>Fill*) in ArcGIS is used to correct for this.

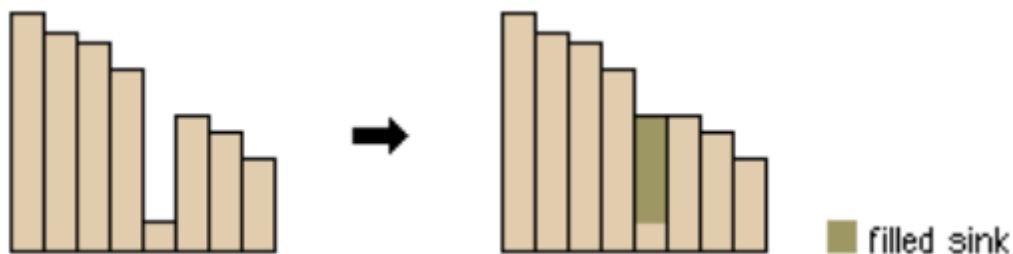


*Fig. 3.12: Profile view of a sink before and after running the Fill tool (Source: ArcGIS documentation)*

4. A flow direction grid is then created using the *Flow Direction tool* (*ArcToolbox>Spatial Analyst Tools>Hydrology>Flow Direction*). A value is assigned to each cell which is then used to indicate the flow direction from that same cell based on the underlying DEM. The collective analysis of cells within the grid defines the final destination of the water flowing across the land surface. The grid processing tool finds the lowest neighbouring cell from the centre of every 3x3 cell matrix by a simply assigned numeric code (i.e. 64 represents flow in the northerly direction, while 8 represents flow in the southwesterly direction as shown in **Fig. 3.13** below), determined using the height values from the DEM.

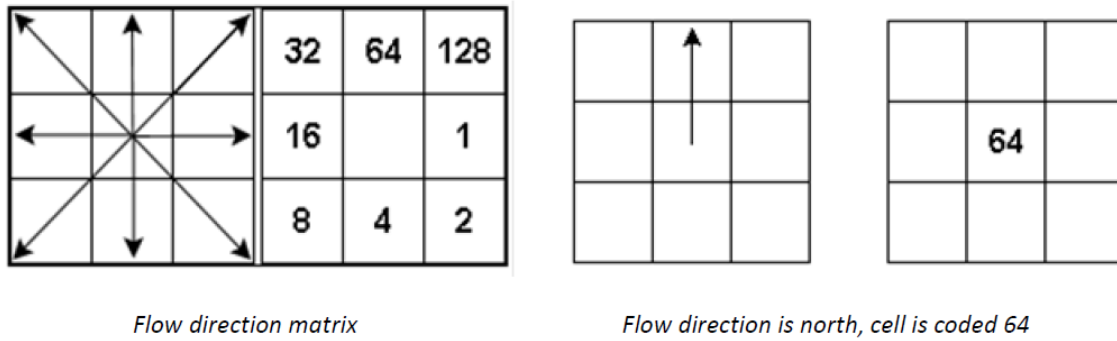


Fig. 3.13: Flow direction matrix (Source: ArcGIS documentation)

5. Using the output data from the *Flow Direction tool*, the *Flow Accumulation tool* (ArcToolbox>Spatial Analyst Tools>Hydrology>Flow Accumulation) then pinpoints the upstream cells that flow into each downslope cell and calculates the flow into each cell. The number of upstream cells flowing into a certain cell determines the flow accumulation value of that cell as shown in Fig. 3.14 based on the underlying DEM. As expected, areas with lower elevation i.e. valleys or drainage channels, are represented by cells with higher flow accumulation values.

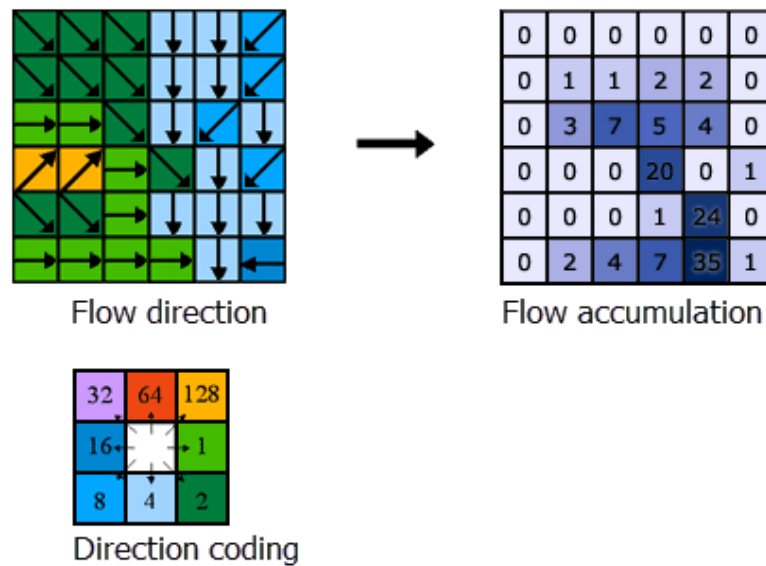


Fig. 3.14: Determining the accumulation of flow (Source: ArcGIS documentation)

6. Watershed delineation requires pour point placement. Pour points are regarded as point locations within cells with high cumulative flow since they are used to determine the total contributing water flow to that given point. In some scenarios, pour points could be represented by sampling sites, hydrometric stations or certain data sources. However, for this case, the pour

points were manually created from the flow accumulation grid, keeping in mind that these pour points must be on the path of high flow accumulation, be a natural exit for the upstream cells and define the 'end' of a catchment area. The created pour point shapefile was then snapped (*ArcToolbox>Spatial Analyst Tools>Hydrology>Snap Pour Point*) to the closest cell of high flow accumulation. This is done to account for any errors during digitization and convert the data to raster format for the delineation of watersheds.

#### 3.3.2.4 Data Preparation

Data collation and preparation in WetSpa is essential for the determination of a watershed's drainage structure, soil type spatial distribution, land use classes, as well as the compilation of available hydro-meteorological data related to the project (Liu and De Smedt, 2004). The inputs for the WetSpa model include *spatial data maps* (digital elevation model, land-use and soil type) and *time series data* (precipitation). From this input data, WetSpa generates maps on the flow direction, flow accumulation, stream network, slope, subwatersheds, soil porosity, soil hydraulic conductivity, soil wilting point, the Manning's coefficient (or terrain roughness related to water flow), runoff coefficient, depression capacity and even velocity maps (*Naporadean and Chira, 2006*).

##### 3.3.2.4.1 Digital elevation model (DEM)

To ensure compatibility, a raster DEM generated from contour or point data is preferred. The resolution of choice must adequately represent the watershed's topography, river network and sub-watersheds. After processing and error filtering of erroneous extreme values, the raster DEM is then used to determine the slope, aspect, flow direction, flow length and flow accumulation of each grid cell within the raster file. Afterwards, assuming all cells draining more than a specified upstream area are part of that network, river networks within the watershed (both more or less detailed) can be identified; with their corresponding stream links, stream orders and subwatersheds. **Fig. 3.15** shows the various stages of the study area's DEM using the WetSpa extension on ArcView.

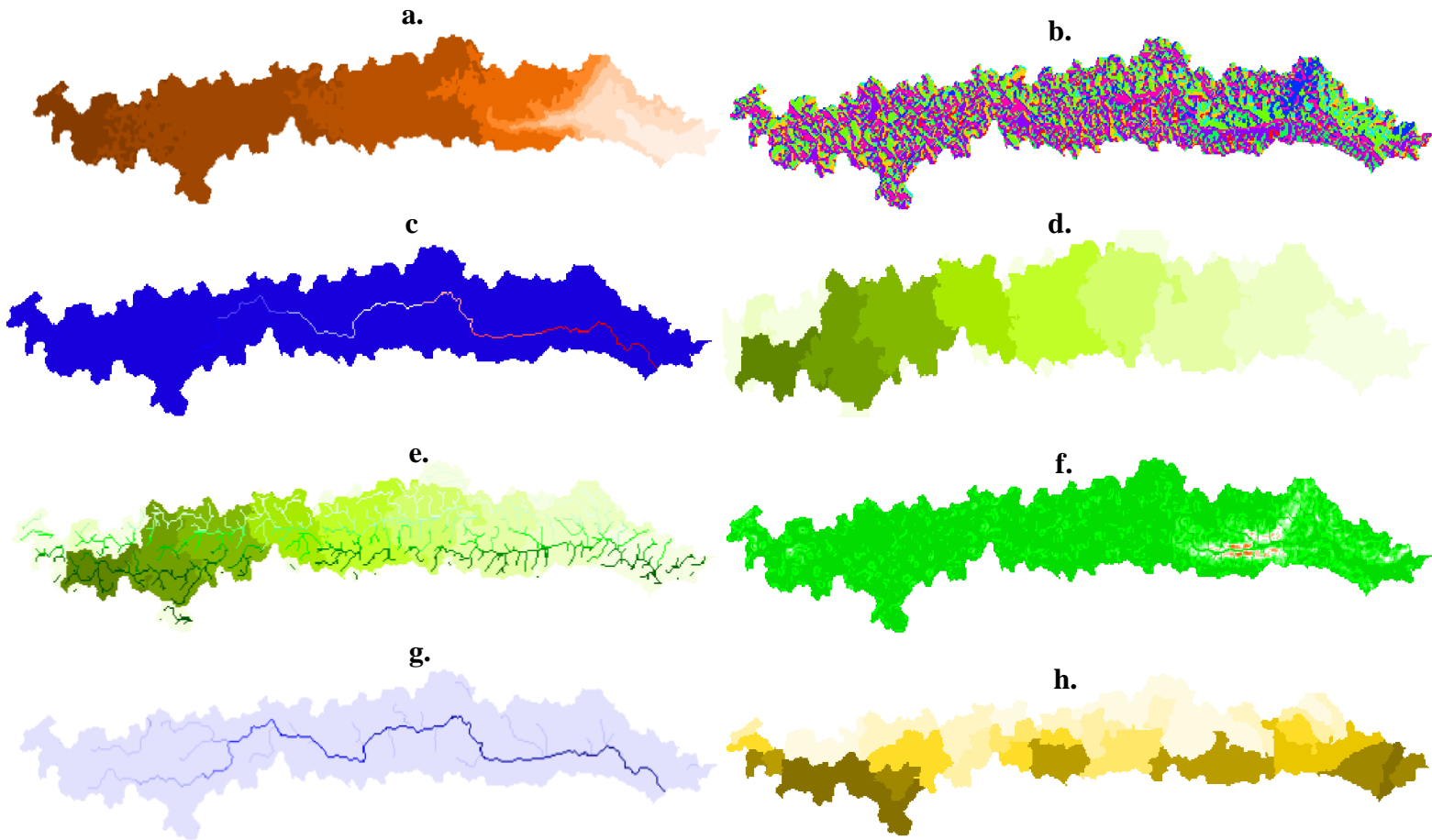


**Fig. 3.15:** Various stages of the Syokimau-Katani DEM processing using the WetSpa extension on ArcView: (a) Filled elevation, (b) Flow direction, (c) Flow accumulation, (d) Flow length, (e) Stream link, (f) Slope, (g) Hydrologic radius, (i) Subwatersheds.

#### 3.3.2.4.2 Land use data

Land use data is usually obtained from remote sensing data at the same resolution and grid cell size as the DEM file prepared in *section 3.3.2.4.1*. All initially determined land use classes are regrouped into 17 WetSpa categories and classified based on their impact on hydrological processes. They include *evergreen needleleaf forest*, *evergreen broadleaf forest*, *deciduous needleleaf forest*, *deciduous broadleaf forest*, *mixed forest*, *closed shrublands*, *open shrublands*, *woody savannah*, *savannahs*, *grasslands*, *permanent wetlands*, *croplands*, *urban and built-up*, *cropland/natural vegetation*, *snow and ice*, *barren or sparsely vegetation* and *water bodies* (Liu and De Smedt, 2004). Note that these groups (each of which is characterized by a quantitative attribute) vary with the algorithms used in the model. Estimated class percentages for each grid cell are determined from high-resolution maps.

After the land-use map has been regridded to a higher resolution map (as depicted by the steps shown in **Fig. 3.16**) and reclassified to match the WetSpa default categories, the resultant ASCII file is taken through processing on WetSpa to generate the associated parameters needed to contribute to the overall runoff coefficient values, i.e. *root depth*, *vegetated fraction*, *interception capacity*, *Manning's coefficient* and the *Leaf Area Index* (Liu and De Smedt, 2004).

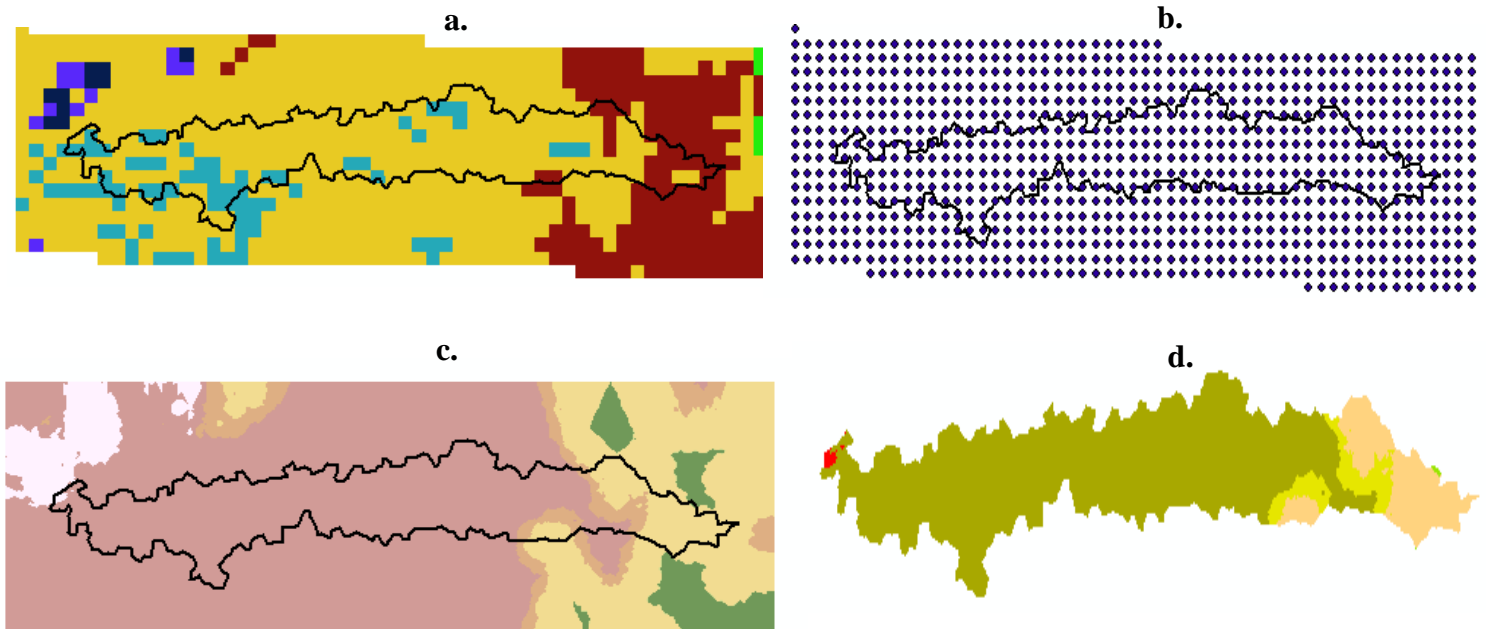


**Fig. 3.16:** Steps involved in land-use dataset processing: (a) General clip result of the original 300m X 300m grid file, (b) An array of points generated from the original 300m X 300m grid file, (c) An Interval Distance Weighting (idw) result at 30m X 30m cell spacing, and (d) A classified watershed clipped to the boundary extent.

#### 3.3.2.4.3 Soil data

Soil data is also obtained from digital soil maps of the same resolution and grid cell size as the DEM file prepared in **section 3.3.2.4.1**. The WetSpa Extension uses the soil code system created by the *United States Department of Agriculture (USDA)* that is based on soil texture and characterized by its clay percentage (fine textures), silt (intermediate textures) and sand (coarser textures). Similar to the land-use map, reclassification of the original soil raster maps to fit WetSpa's soil codes was done on ArcGIS and then the resulting data set was taken through WetSpa processing to derive parameters such as porosity, *hydraulic conductivity*, *field capacity*, and *maximum soil saturation* as shown in **Fig. 3.17**.



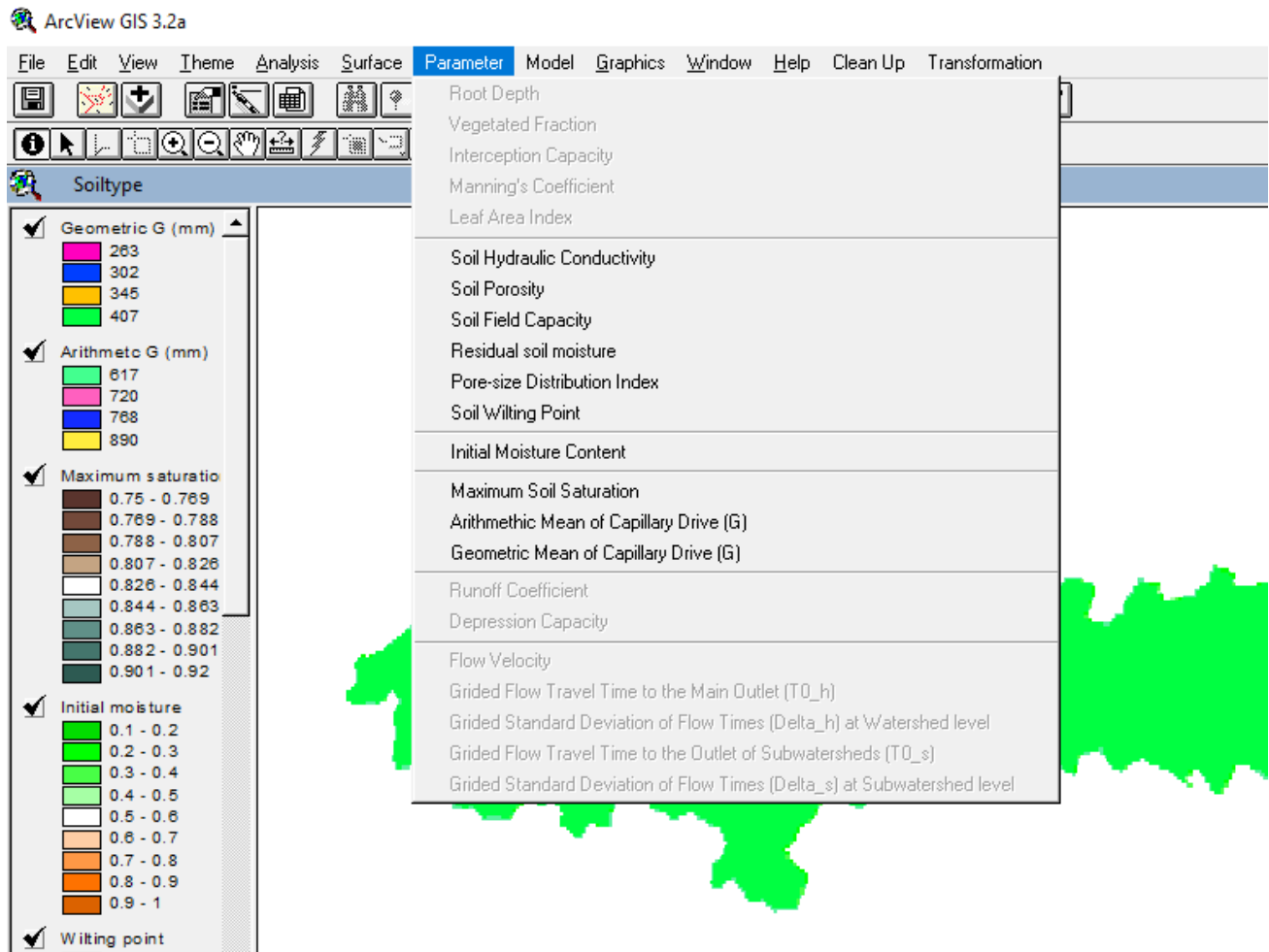


*Fig. 3.17: An overview of the ArcView window and corresponding soil parameters during the processing of soil data using the WetSpa extension.*

#### 3.3.2.4.4 Hydro-meteorological data

The WetSpa Extension requires model parameters, initial conditions, meteorological data and streamflow data as basic data inputs for model calibration and validation. These include:

- 1) **Rainfall** – needed for rainfall-runoff models, in a resolution that matches the model running time-step, i.e. daily rainfall data is needed when modelling on a daily scale. For this project, we chose to run monthly rainfall intensity data for a generalized assessment since getting daily rainfall data was a challenge. A reducing factor of 0.9 was included in the calculations for runoff depth to account for storms that do not generate runoff.

Using potential runoff coefficient values calculated per pixel, we have (Karamage et al., 2017);

$$R_d = P \times P_j \times C_0 \quad \text{Eq 3.1}$$

Where  $R_d$  is the runoff depth,  $P$  is the precipitation for the time period of interest,  $P_j$  is 90% of annual rainfall that yields runoff (a constant introduced to recognize that many small storms do not produce runoff) and  $C_0$  is the potential runoff coefficient that is derived from WetSpa after running the *runoff coefficient and depression* tool. This tool derives its parameters from the resulting maps after processing the land-use, soil and DEM datasets.

- 2) **Potential evapotranspiration, discharge (m<sup>3</sup>/s) and temperature data** – all these datasets are required for daily runoff depth and volume estimate calculations for model calibration, validation and evaluation. For this project, however, the calculations were performed manually and the validation checks made for each dataset during data preparation.
- 3) **Additional digital data (optional)** - Additional digital data can be included in the model (if available) to appraise DEM derived spatial maps, i.e. for drainage area identification and the correction of flow directions. The Thiessen polygon weighting method is used to calculate rainfall distribution whenever two or more rain gauges/station exist within the same watershed with measured data. If not, a uniform rainfall distribution is assumed for the whole catchment. Additional layers (if available) on sewer systems, communications lines, artificial channels, etc. can be used to adjust drainage structure configurations accordingly for simulations within complex terrain such as urban/peri-urban watersheds. For this case, data from one station was available (JKIA) and additional digital data was not available.

### 3.3.2.5 Model Formulation

As stated in previous sections, the WetSpa Extension describes the processes of precipitation, runoff and evapotranspiration for varied terrain types using a *distributed, continuous* and *physically-based* model (Bahremand et al., 2006; Bahremand and De Smedt, 2010; Karamage et al., 2017; Liu and De Smedt, 2004). It is noteworthy to remember that the model is:

- a) *Distributed* – since the channel network and watershed are characterized by a grid of cells each described by their initial conditions, unique characteristics and precipitation inputs.
- b) *Continuous* – the water and energy balance is retained between storms since the model has components that describe evapotranspiration and soil water movement between storms.

- c) *Physically-based* – the model components are described by mathematical models that are based on physical principles, i.e. conservation of mass and momentum.

The generation of rainfall-runoff within a watershed using the Wetspa approach can be summarized into three unique stages; *flow response at cell level*, *flow response at a flow path level* and *flow response of the catchment as a whole* (Liu and De Smedt, 2004)).

***i. Flow response at cell level***

Linear diffusive wave approximation in Wetspa implements overland flow and channel flow routing. This means that an individual cell's impulse response function can holistically be generated by considering the following aspects:

- i. assuming the cell to have 1D unsteady flow,
- ii. ignoring inertial terms,
- iii. assuming a system that is bounded by a transmitting barrier upstream and an adsorbing barrier downstream, and
- iv. using a constant flow velocity that is calculated by default Manning's roughness coefficients (adopted from literature as determined from land use categories and channel characteristics) and a diffusion coefficient. The cell impulse unit response function can then be calculated for each grid cell over the whole watershed.

***ii. Flow response at a flow path level***

Assuming a linear channeling system, the flow response at the end of a flow path, resulting from a unit impulse input to a single cell, can be calculated independently without the interference of other cell inputs. To determine the flow-path response, the impulse is routed through the corresponding sequence of cells down to the system outlet. Each of these cells along the flow path has unique unit-impulse response functions. During the channeling process, the output of any cell becomes the input to the receiving cell. The original input distribution is also continuously changed by the flow dynamics in the cells as described by their impulse response functions. The flow path response is then determined by successively applying a convolution integral.

The resulting summation can be solved for each grid cell as a weighted flow length to the water outlet or any downstream converging point with the *Flow Length tool* found in standard *GIS software*.

### *iii. Flow response of the catchment*

The catchment flow response can be determined as the sum of its elements responses from all contributing cells, considering the areal decomposability in a linear channeling system. The flow channeling involves tracking runoff along its topographically determined flow path and evaluating groundwater flow out of the subcatchment. The total discharged is the summation of overland flow, interflow and groundwater flow, and is derived by the convolution of the flow response from all the grid cells. This approach is advantageous in that it allows the spatially distributed runoff and land surface hydrological parameters to be used as model inputs, and can channel runoff from a particular land-use area to the catchment outlet or any downstream converging point.

#### *3.3.2.6 Model Parameters*

##### *i. Default parameters for Soil texture classes*

Research has proven that soil textures alone can account for most patterns of soil physical properties i.e. porosity, hydraulic conductivity, pore size distribution index, among others (Liu and De Smedt, 2004). In the WetSpa Extension, soil textures are classified into 12 United States Department of Agriculture (USDA) classes that range from 1 to 12 based on the percentage of sand, silt and clay in a soil sample as shown on **Table 3.1**. Hydraulic properties are then estimated as a function of soil texture classes using mean values extracted from literature.

##### *ii. Default parameters for Land use classes*

Landuse has a major influence on a catchment's water balance. This data type creates variations in evapotranspiration rates, interception and depression rates (during storms), infiltration and soil water redistribution processes (i.e. plant roots and pores influence the saturated hydraulic conductivity of the watershed), and surface roughness that controls overland flow velocity and floodplain flow rates. A total of 17 basic land use classes listed in **Table 3.2** and according to the International Geosphere-Biosphere Program (IGBP) classification system are specified within the WetSpa Extension. Consideration is made on both the observed physical and biophysical cover of the land surface and the purpose for which the land use is being used. Such datasets are derived from ground surveys or remote sensing images.

**Table 3.1:** Default parameters characterizing soil textural classes (Source: WetSpa Manual by (Liu and De Smedt, 2004))

Texture classes	Hydraulic conductivity <sup>1</sup> (mm/h)	Porosity <sup>1</sup> (m <sup>3</sup> /m <sup>3</sup> )	Field capacity <sup>1</sup> (m <sup>3</sup> /m <sup>3</sup> )	Wilting point <sup>1</sup> (m <sup>3</sup> /m <sup>3</sup> )	Residual moisture <sup>1</sup> (m <sup>3</sup> /m <sup>3</sup> )	Pore size distribution index <sup>2</sup> (-)
Sand	208.80	0.437	0.062	0.024	0.020	3.39
Loamy sand	61.20	0.437	0.105	0.047	0.035	3.86
Sandy loam	25.92	0.453	0.190	0.085	0.041	4.50
Silt loam	13.32	0.501	0.284	0.135	0.015	4.98
Silt	6.84	0.482	0.258	0.126	0.015	3.71
Loam	5.58	0.463	0.232	0.116	0.027	5.77
Sandy clay loam	4.32	0.398	0.244	0.136	0.068	7.20
Silt clay loam	2.30	0.471	0.342	0.210	0.040	8.32
Clay loam	1.51	0.464	0.310	0.187	0.075	8.32
Sandy clay	1.19	0.430	0.321	0.221	0.109	9.59
Silt clay	0.90	0.479	0.371	0.251	0.056	10.38
Clay	0.60	0.475	0.378	0.251	0.090	12.13

**Table 3.2:** Default parameters characterizing land use classes (Source: WetSpa Manual by (Liu and De Smedt, 2004))

Category	Cover	Interception capacity(mm)		Root depth(m)	Manning's Coefficient	Vegetated fraction(%)	Leaf area index(-)	
		Maximum	Minimum				Maximum	Minimum
1	Evergreen Needleleaf Forest	2	0.5	1.0	0.40	80	60	50
2	Evergreen Broadleaf Forest	3	0.5	1.0	0.60	90	60	50
3	Deciduous Needleleaf Forest	2	0.5	1.0	0.40	80	60	10
4	Deciduous Broadleaf Forest	3	0.5	1.0	0.80	80	60	10
5	Mixed Forest	3	0.5	1.0	0.55	83	60	30
6	Closed Shrublands	3	0.5	0.8	0.40	80	60	10
7	Open Shrublands	2	0.5	0.8	0.40	80	60	10
8	Woody Savannah	3	0.5	1.0	0.50	80	60	8
9	Savannahs	2	0.5	0.8	0.40	80	60	5
10	Grasslands	2	0.5	0.8	0.30	80	20	5
11	Permanent Wetlands	1	0.2	0.5	0.50	80	60	5
12	Croplands	2	0.5	0.8	0.35	85	60	5
13	Urban and Built-Up	0	0.0	0.5	0.05	0	0	0
14	Cropland / Natural Vegetation	2	0.5	0.8	0.35	83	40	5
15	Snow and Ice	0	0.0	0.1	0.05	0	0	0
16	Barren or Sparsely Vegetation	1	0.2	0.5	0.10	5	20	5
17	Water Bodies	0	0.0	0.1	0.05	0	0	0

### iii. Potential runoff coefficient

A catchment's runoff coefficient is defined by the ratio of runoff volume to rainfall volume. The WetSpa Extension estimates the runoff coefficient from varying land use, slope, soil type, rainfall intensity and antecedent soil moisture conditions. A linear relationship between potential runoff coefficient and surface slope is used to estimate potential runoff coefficient based on a continuous slope, as shown in *Eq. 3.14*;

$$C = C_0 + (1 - C_0) \frac{S}{S + S_0} \quad (\text{Eq. 3.14})$$

Where C is the potential runoff coefficient for a surface slope S (%) (**Table 3.4** provides a breakdown of potential runoff coefficients for various slopes),  $C_0$  is the potential runoff coefficient for a near-zero slope corresponding to the values listed on the first row of each land-use class, and soil type combinations that are calibrated (Liu and De Smedt, 2004) using the data in **Table 3.3**.

*Table 3.3: Slope constant  $S_0$  for determining potential runoff coefficient (Source: WetSpa Manual by (Liu and De Smedt, 2004))*

Land use	Sand	Loamy sand	Sandy loam	Loam	Silt loam	Silt	Sandy clay loam	Clay loam	Silty clay loam	Sandy clay	Silty clay	Clay
Forest	0.680	0.650	0.620	0.590	0.560	0.530	0.500	0.470	0.440	0.410	0.380	0.350
Grass	0.580	0.551	0.522	0.493	0.464	0.435	0.405	0.376	0.347	0.318	0.289	0.260
Crop	0.500	0.471	0.442	0.413	0.384	0.355	0.325	0.296	0.267	0.238	0.209	0.180
Bare soil	0.420	0.393	0.365	0.338	0.311	0.284	0.256	0.229	0.202	0.175	0.147	0.120

**Table 3.4:** Potential runoff coefficient for different land use, soil type and slope (Source: WetSpa Manual by (Liu and De Smedt, 2004))

Land use	Slope (%)	Sand	Loamy sand	Sandy loam	Loam	Silt loam	Silt	Sandy clay loam	Clay loam	Silty clay loam	Sandy clay	Silty clay	Clay
Forest	<0,5	0.03	0.07	0.10	0.13	0.17	0.20	0.23	0.27	0.30	0.33	0.37	0.40
	0,5-5	0.07	0.11	0.14	0.17	0.21	0.24	0.27	0.31	0.34	0.37	0.41	0.44
	5-10	0.13	0.17	0.20	0.23	0.27	0.30	0.33	0.37	0.40	0.43	0.47	0.50
	>10	0.25	0.29	0.32	0.35	0.39	0.42	0.45	0.49	0.52	0.55	0.59	0.62
Grass	<0,5	0.13	0.17	0.20	0.23	0.27	0.30	0.33	0.37	0.40	0.43	0.47	0.50
	0,5-5	0.17	0.21	0.24	0.27	0.31	0.34	0.37	0.41	0.44	0.47	0.51	0.54
	5-10	0.23	0.27	0.30	0.33	0.37	0.40	0.43	0.47	0.50	0.53	0.57	0.60
	>10	0.35	0.39	0.42	0.45	0.49	0.52	0.55	0.59	0.62	0.65	0.69	0.72
Crop	<0,5	0.23	0.27	0.30	0.33	0.37	0.40	0.43	0.47	0.50	0.53	0.57	0.60
	0,5-5	0.27	0.31	0.34	0.37	0.41	0.44	0.47	0.51	0.54	0.57	0.61	0.64
	5-10	0.33	0.37	0.40	0.43	0.47	0.50	0.53	0.57	0.60	0.63	0.67	0.70
	>10	0.45	0.49	0.52	0.55	0.59	0.62	0.65	0.69	0.72	0.75	0.79	0.82
Bare soil	<0,5	0.33	0.37	0.40	0.43	0.47	0.50	0.53	0.57	0.60	0.63	0.67	0.70
	0,5-5	0.37	0.41	0.44	0.47	0.51	0.54	0.57	0.61	0.64	0.67	0.71	0.74
	5-10	0.43	0.47	0.50	0.53	0.57	0.60	0.63	0.67	0.70	0.73	0.77	0.80
	>10	0.55	0.59	0.62	0.65	0.69	0.72	0.75	0.79	0.82	0.85	0.89	0.92
IMP		1.00	1.00	1.00	1.00	1.00	1.00	1.00	1.00	1.00	1.00	1.00	1.00

### 3.3.2.7 Model Assumptions

Every model works on certain assumptions. For WetSpa, they include the following (Liu and De Smedt, 2004):

- 1) Each raster cell has isotropic and homogeneous topography and soil characteristics.
- 2) Each raster cell has homogeneous canopy cover and ground cover.
- 3) Precipitation in each raster cell is spatially homogeneous.
- 4) Hortonian overland flow is valid for most of areas within the watershed.
- 5) Evapotranspiration is ignored during rainstorms and when residual soil moisture surpasses the soil moisture.
- 6) The amount of effective groundwater storage restricts deep evapotranspiration, which takes place when the soil is dry.
- 7) Soil moisture content is considered homogeneous within a cell, while the groundwater storage is distributed uniformly on small subcatchment scale for each time step.

- 8) Water cannot be partitioned to more than one adjacent raster cell, rather it flows along its unique pathway from one cell to the next.
- 9) The linear diffusive wave approximation method is appropriate for the channelling of both overland flow and channel flow.
- 10) Hydraulic radius is location reliant and remains constant over a flood event, but varies with flood frequency.
- 11) Interflow takes place when the soil moisture content is higher than field capacity and can be estimated by Darcy's law and kinematic approximation.
- 12) The water losses during deep percolation, overland flow and channel flow are not of importance.

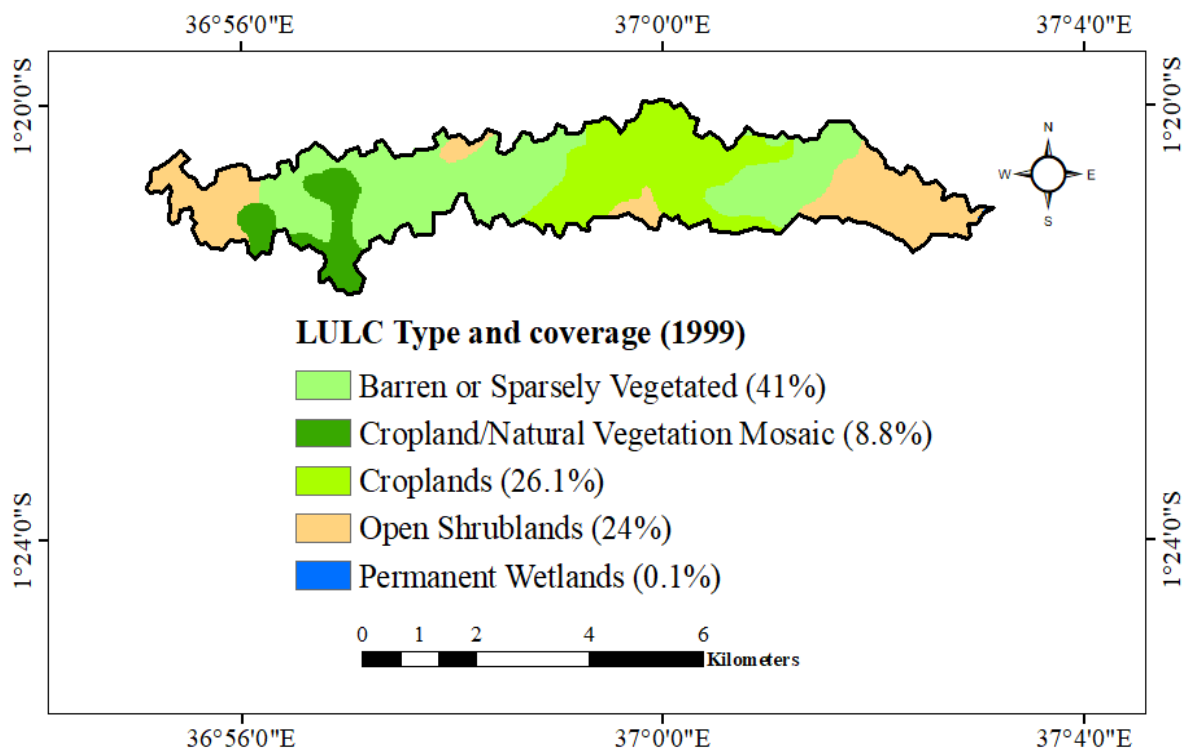


## Chapter 4: Results and Discussion

### 4.1 Results

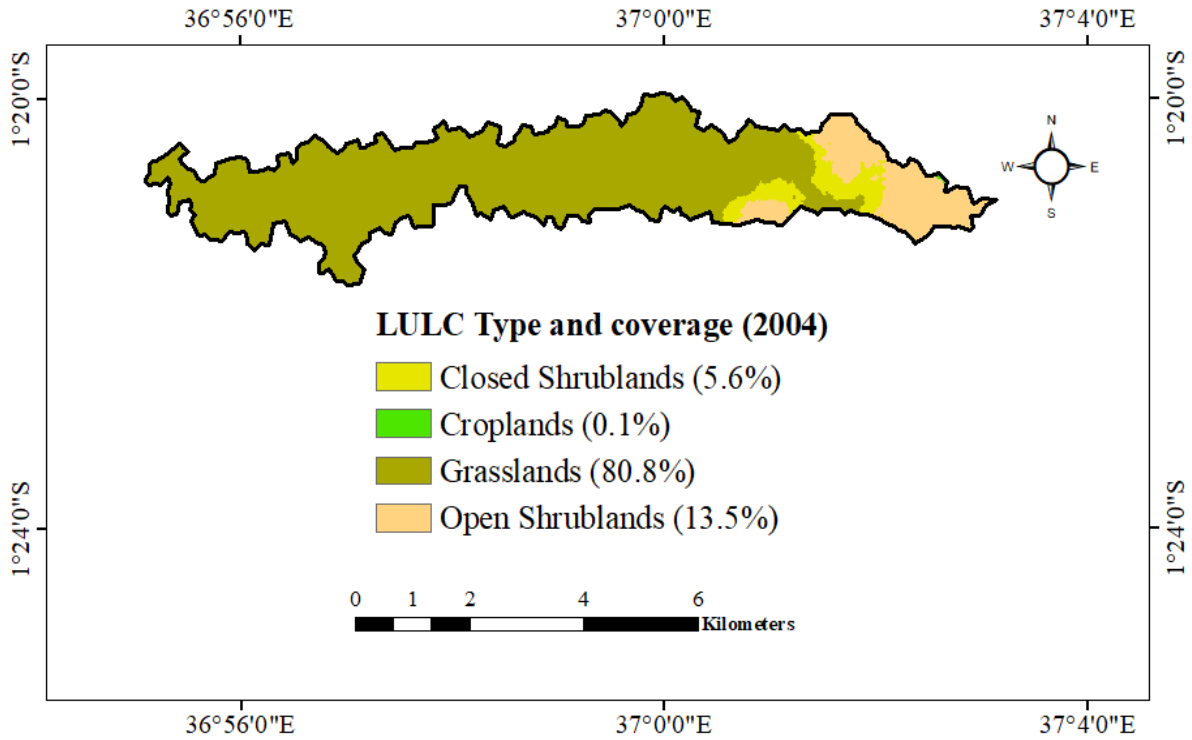
#### 4.1.1 Landuse and land cover changes in the Syokimau-Katani area

The land-use/land cover distribution within the Syokimau-Katani area in 1999 was dominated by barren/sparsely vegetated areas (41%) that could be attributed to the 1999-2001 nation-wide drought (GoK, 2009), with significantly large sections of croplands (26.1%) and open Shrublands (24%). A bit of mixed natural vegetation with cropland (8.8%) can be spotted towards the west of the study area and permanent wetlands (0.1%) to the east as shown on **Map. 4.1** below.

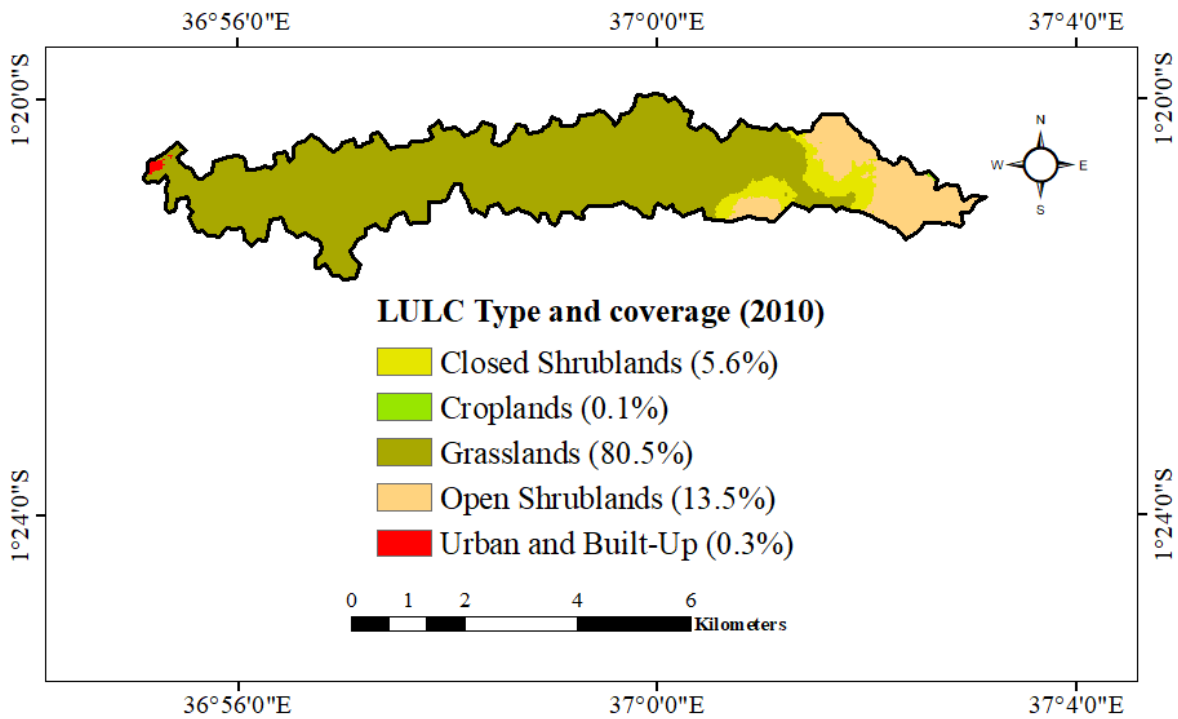


*Map. 4.1: Land cover land use distribution in the Syokimau-Katani area 1999*

In 2004 as shown on **Map. 4.2**, there seems to have been a drastic recovery in the land-use/land cover distribution of the area, with all of the barren/sparsely vegetated area, natural vegetation/cropland mosaic, and a significant section of the cropland transforming into grassland (80.8%) and closed Shrublands (5.6%). The loss of cropland can be attributed to losses in soil fertility from widespread cooperative farming in the region (Jeremiah, 2015), though a bit of spatially shifted cropland remnants (0.1%) can be spotted to the far eastern edge of the study area.



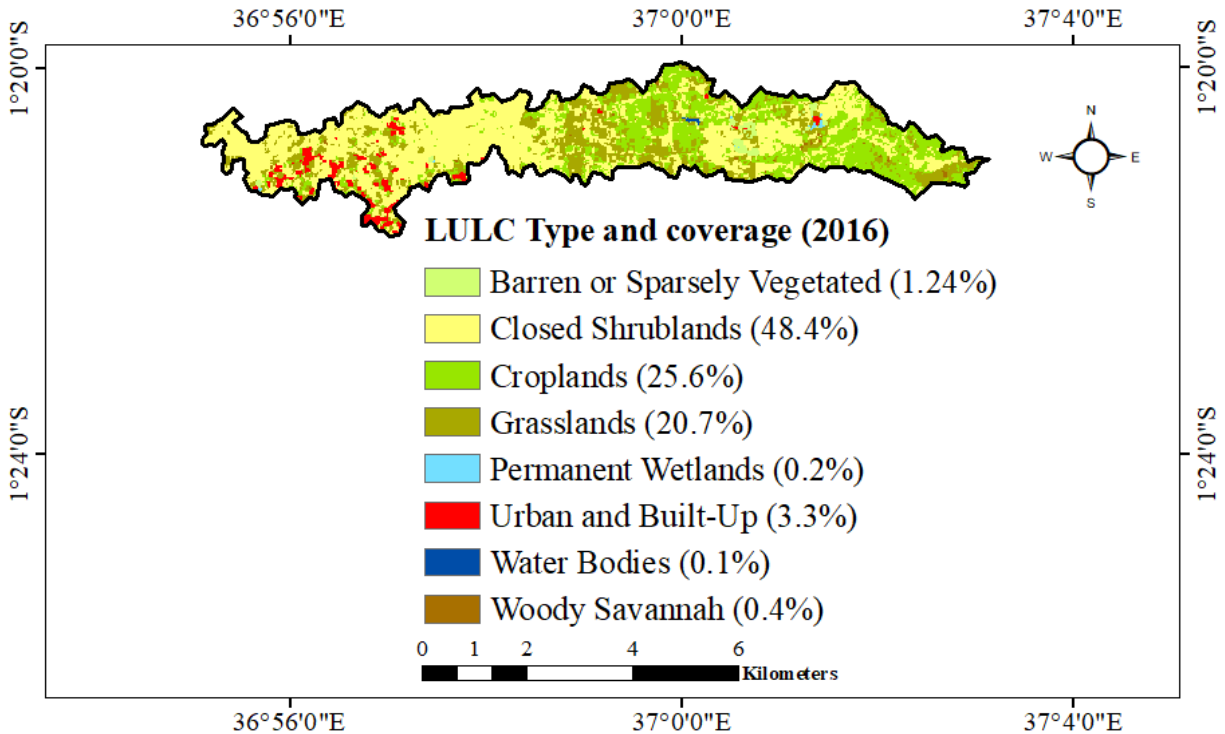
Map. 4.2: Land cover land use in Syokimau-Katani in 2004



Map. 4.3: Land cover land use in Syokimau-Katani in 2010

The land-use/land cover distribution within Syokimau-Katani in 2010 shown on **Map. 4.3** does not vary much from that in 2004. The only change noted is a patch of urban and built-up area (0.3%) that develops on the western edge of this area, replacing the natural grasslands. The closed shrublands (5.6%), open shrublands (13.5%) and croplands (0.1%) appear to have maintained their spatial extent.

Syokimau-Katani's land-use/land cover in 2016 seems quite different on **Map. 4.4**. The urban and built-up area seems to have grown from 0.3% to 3.3% and spread out deeper into the watershed. There also appears to be an increase in closed shrublands (from 5.6% to 48.4%) and a decrease in grasslands (from 80.5% to 20.7%). There is no doubt that these land-use/land cover changes came with the rise of human activity and urbanization within the watershed.



*Map. 4.4: Land cover land use in Syokimau-Katani in 2016*

**Fig. 4.1** gives a graphical representation of the variations of land-use/land cover percentages over the years 1999, 2004, 2010 and 2016.

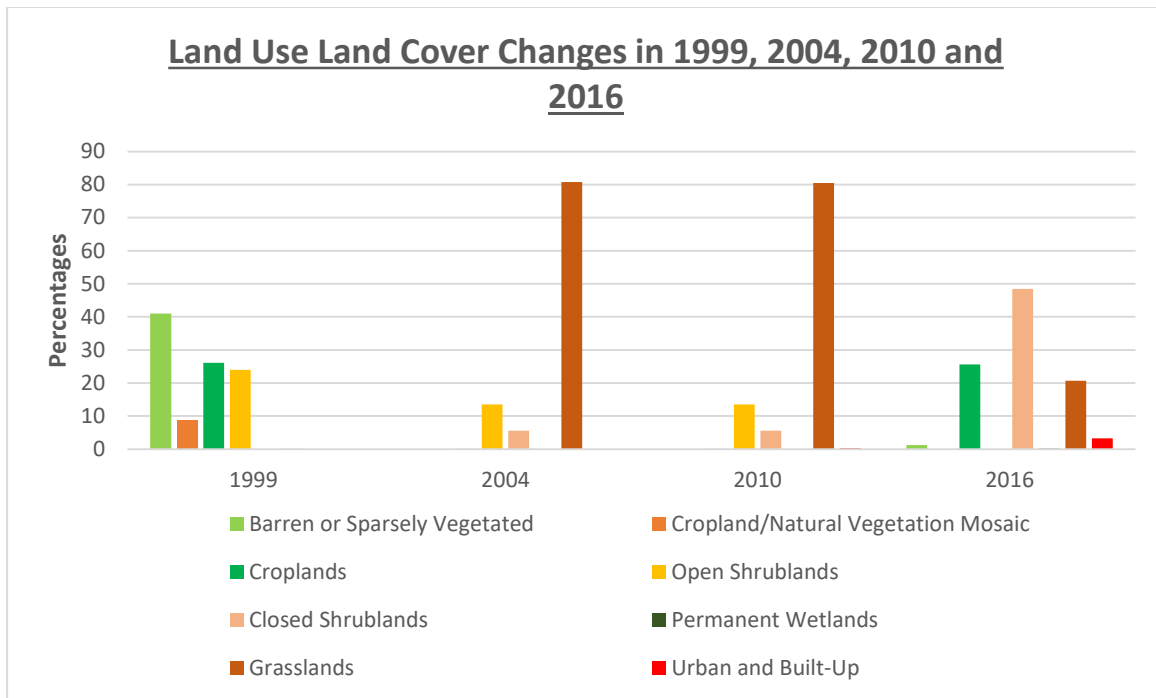
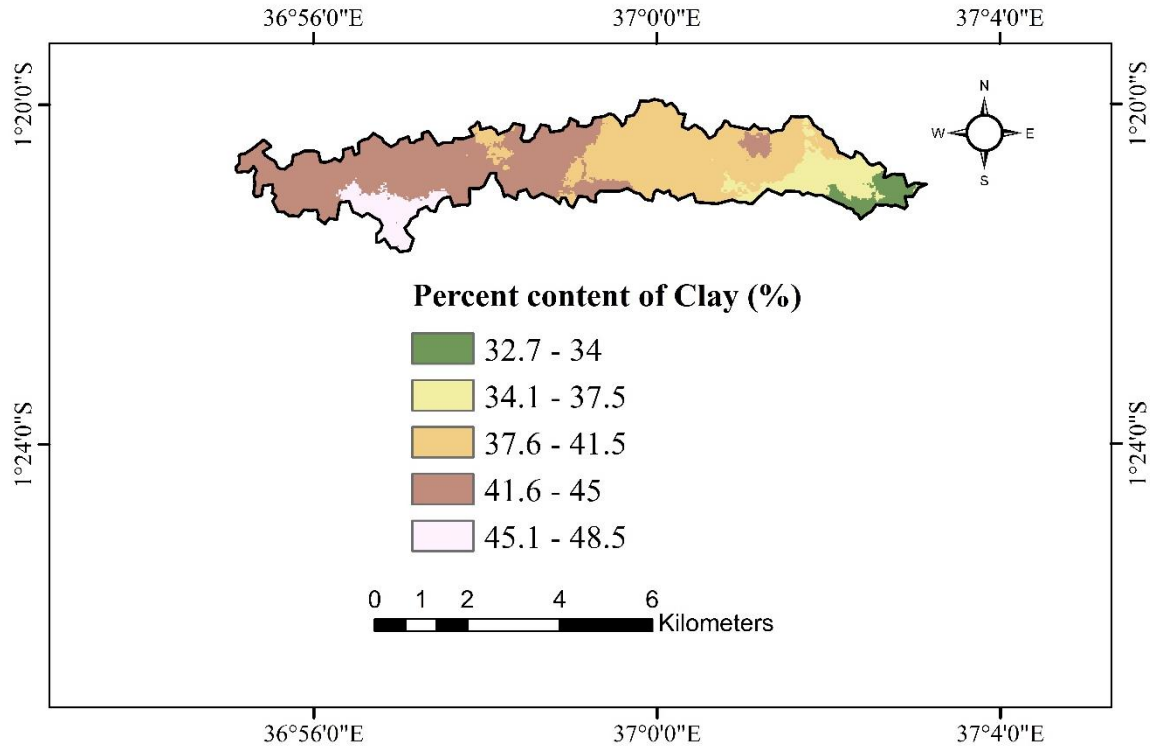


*Fig. 4.1: Graphical representation of land use and land cover variations in percentages for the years 1999, 2004, 2010 and 2016*

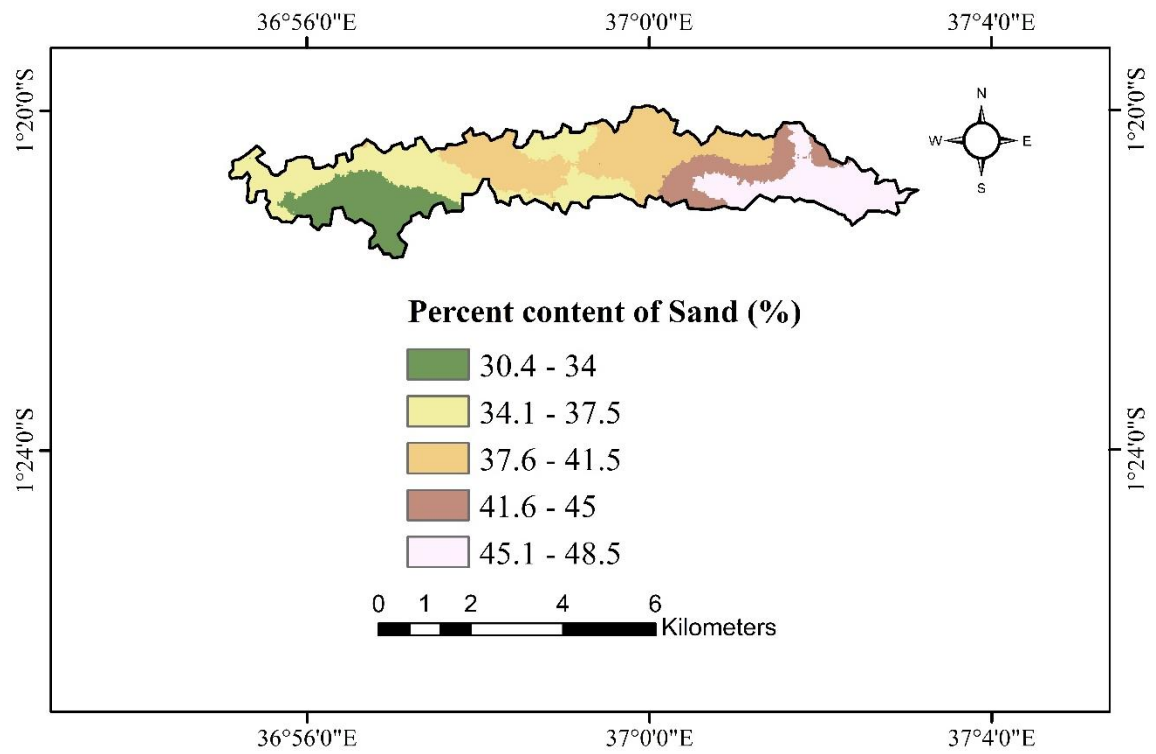
The dynamism of the Syokimau-Katani watershed with respect to land-use/land cover distribution within the 1999 – 2016 period is evident. Having been part of the metropolitan area of Nairobi city, this region has undergone various transformations – from large tracts of farmland to recent real estate related developments – which have contributed to the alterations of this once natural habitat.

#### ***4.1.2 Soil textural classes in the Syokimau-Katani area***

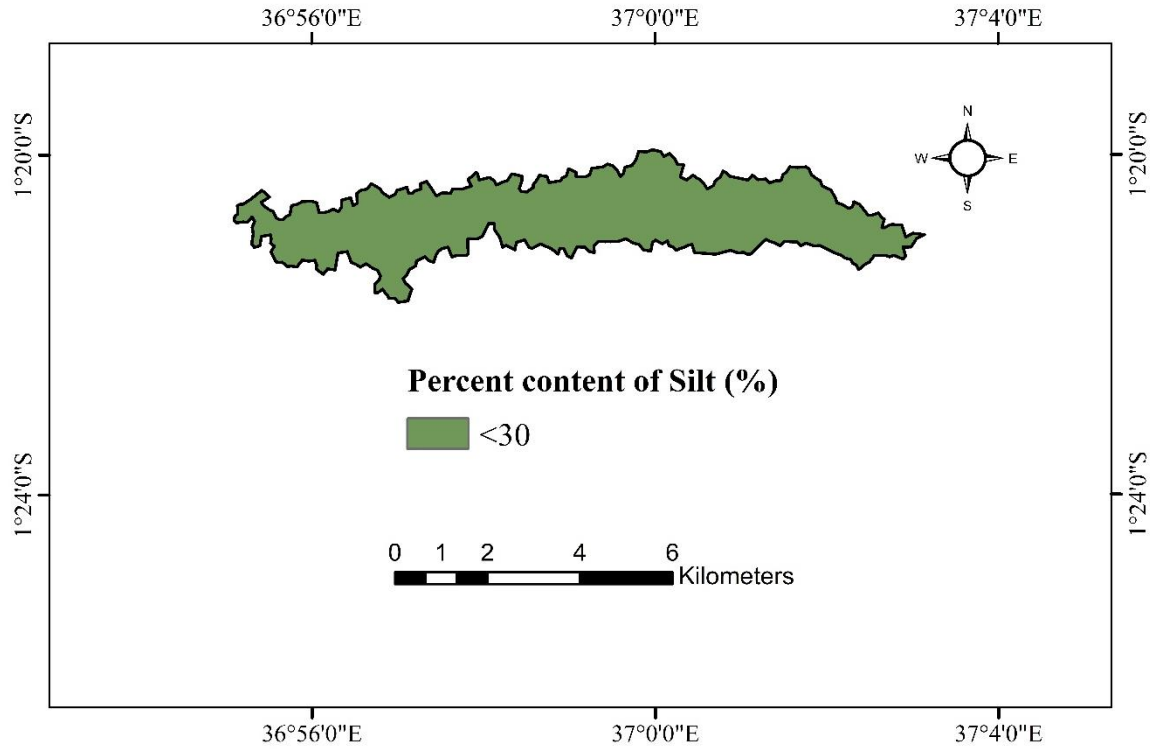
From a soil textural perspective, the Syokimau-Katani area is defined by a Sand – Clay – Loam composition. These soil combinations are an erosional result of the area's rocks (consisting of phonolites and trachytic tuffs) and its generally gently sloping nature. The silt levels are low and range between 16% and 24% in weight (g/100g). **Map. 4.5**, **Map. 4.6** and **Map. 4.7** show the spatial distribution of the sand (coarse texture) silt (medium texture) and clay (smooth texture), while **Map. 4.8** provides an overall spatial distribution of these soil combinations.



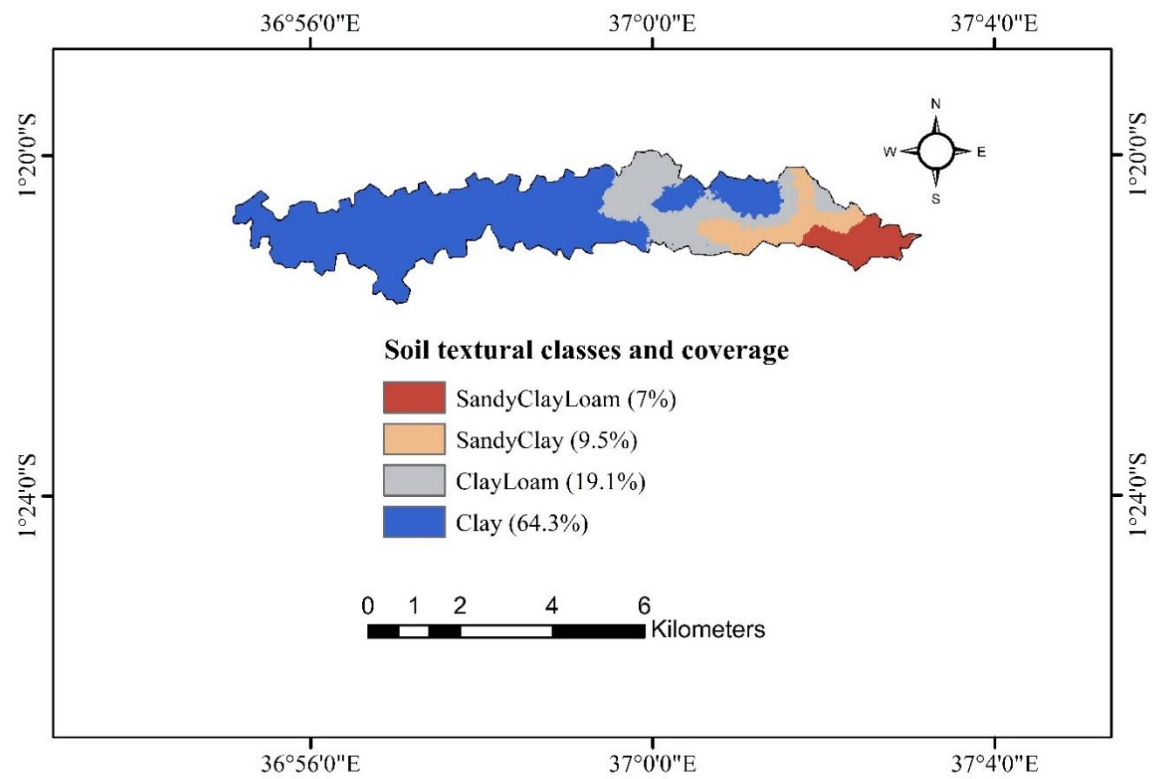
*Map. 4.5: Clay soil distribution map of the Syokimau-Katani area (%)*



*Map. 4.6: Sand soil distribution map of the Syokimau-Katani area (%)*



*Map. 4.7: Silt soil distribution map of the Syokimau-Katani area (%)*

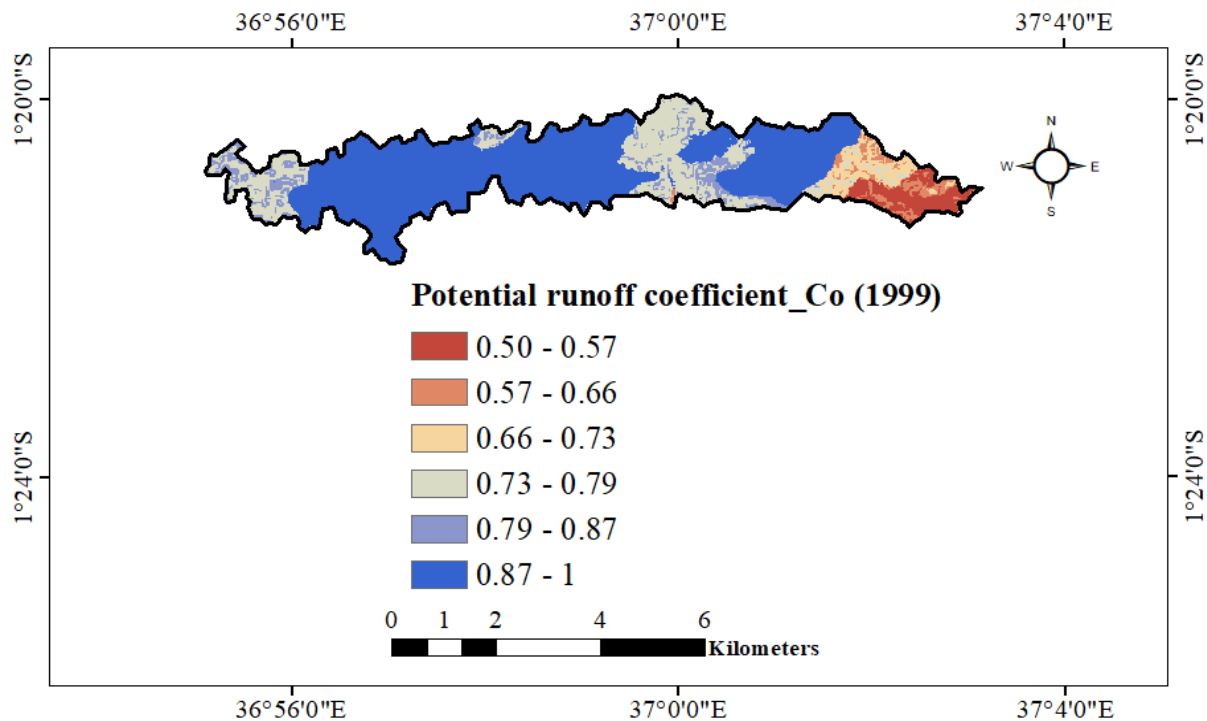


*Map. 4.8: Soil textural and coverage map of the Syokimau-Katani*

The Syokimau-Katani watershed is dominated by clay soils (64.3%) as compared to clay-loam soil (19.1%), sandy-clay soil (9.5%) and sandy-clay-loam soil (7%) textural classes also found in this area. Since clay soils are known to have low porosity values and infiltration rates, this large spatial distribution of clays within the watershed is bound to greatly contribute to flooding in the area.

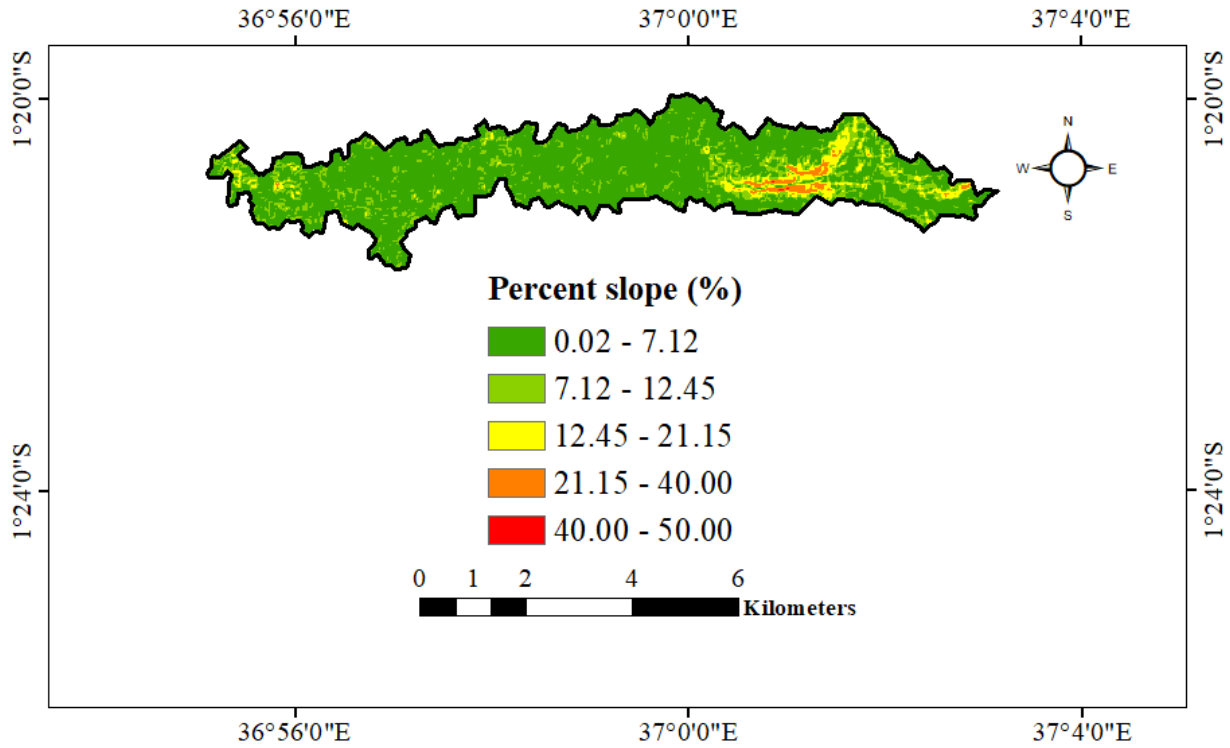
#### 4.1.3 Potential runoff coefficients and ‘hotspots’ of the Syokimau-Katani area

The potential runoff coefficients generated from the soil, land-use and DEM analysis on WetSpa represent the hydrological response of the watershed. These varied land-use map inputs for the years 1999, 2004, 2010 and 2016 yielded the spatial maps for the potential runoff coefficients of the Syokimau-Katani area for these respective years. All the upper limits for the ranges in each map’s legend were matched up for easier comparison.

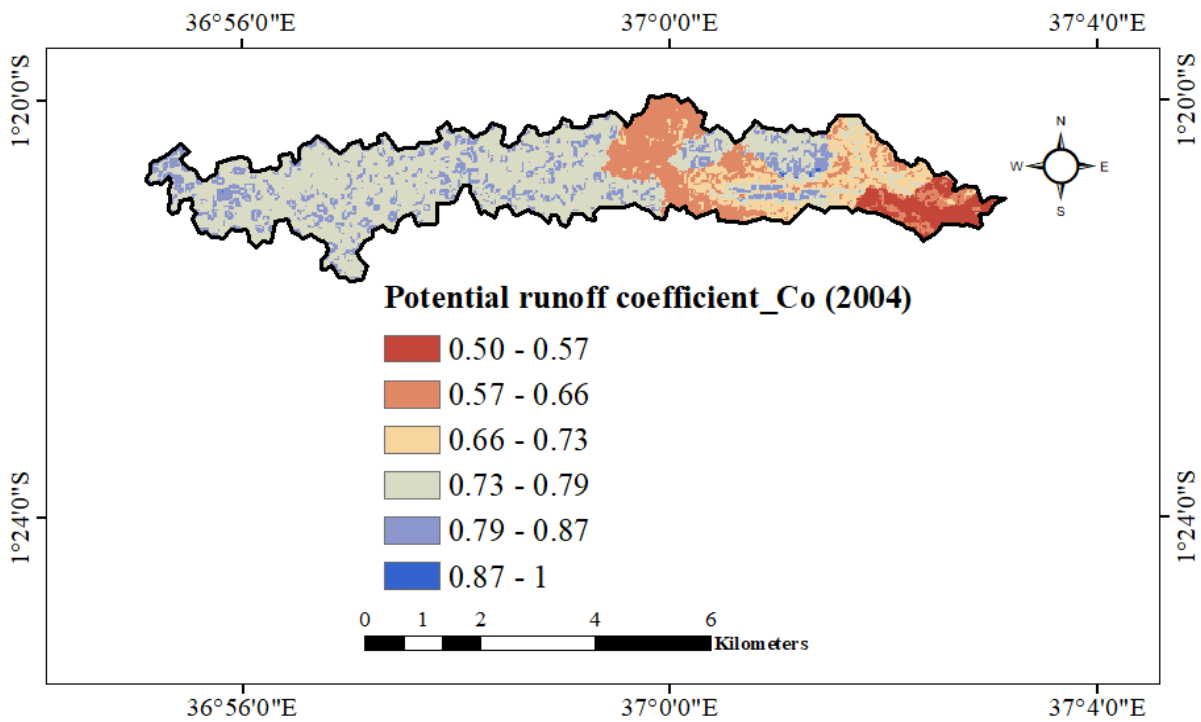


*Map. 4.9: Potential runoff coefficient distribution of the Syokimau-Katani area (1999)*

Over 50% of the watershed in 1999 seems to have had a high potential runoff coefficient within the 0.87 to 1 range as depicted on **Map. 4.9**. This occurrence corresponds to the large percentage of bare/sparsely vegetated land cover noted in the land-use/ land cover map for the same year. The high values towards the eastern side of the watershed also correspond to the steep elevation region that is visible on the slope map of this study area shown on **Map. 4.10**.

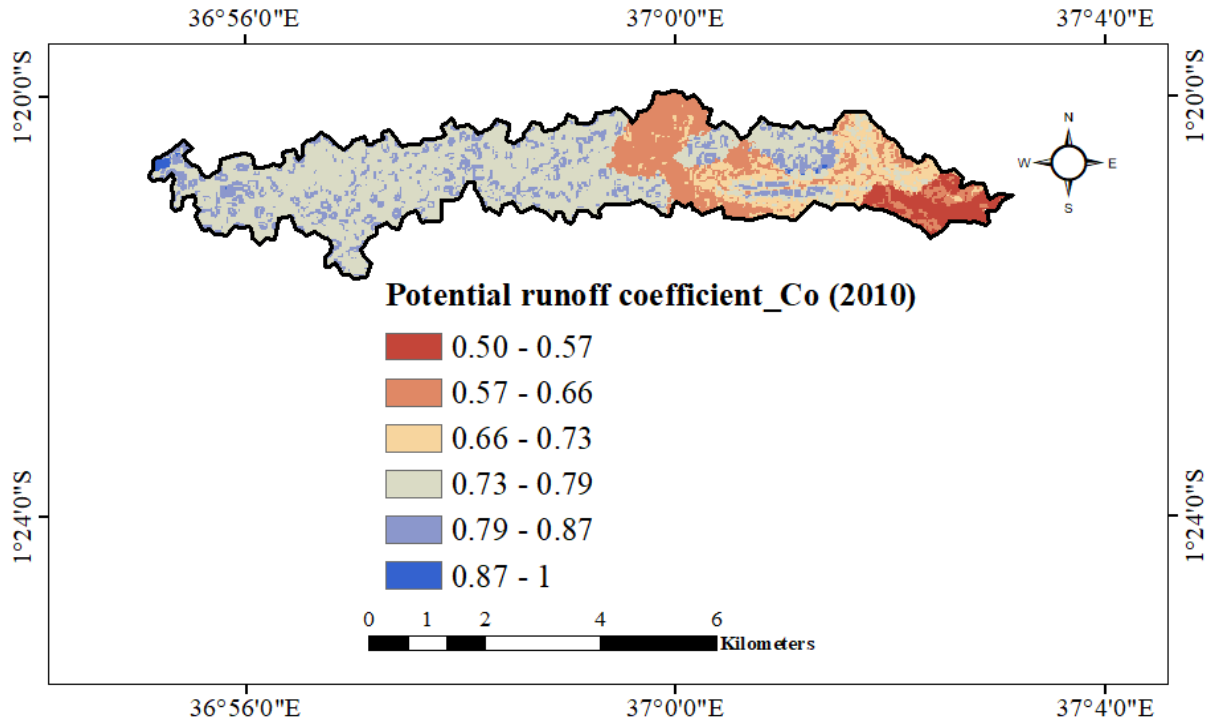


Map. 4.10: Percentage slope distribution in the Syokimau-Katani area



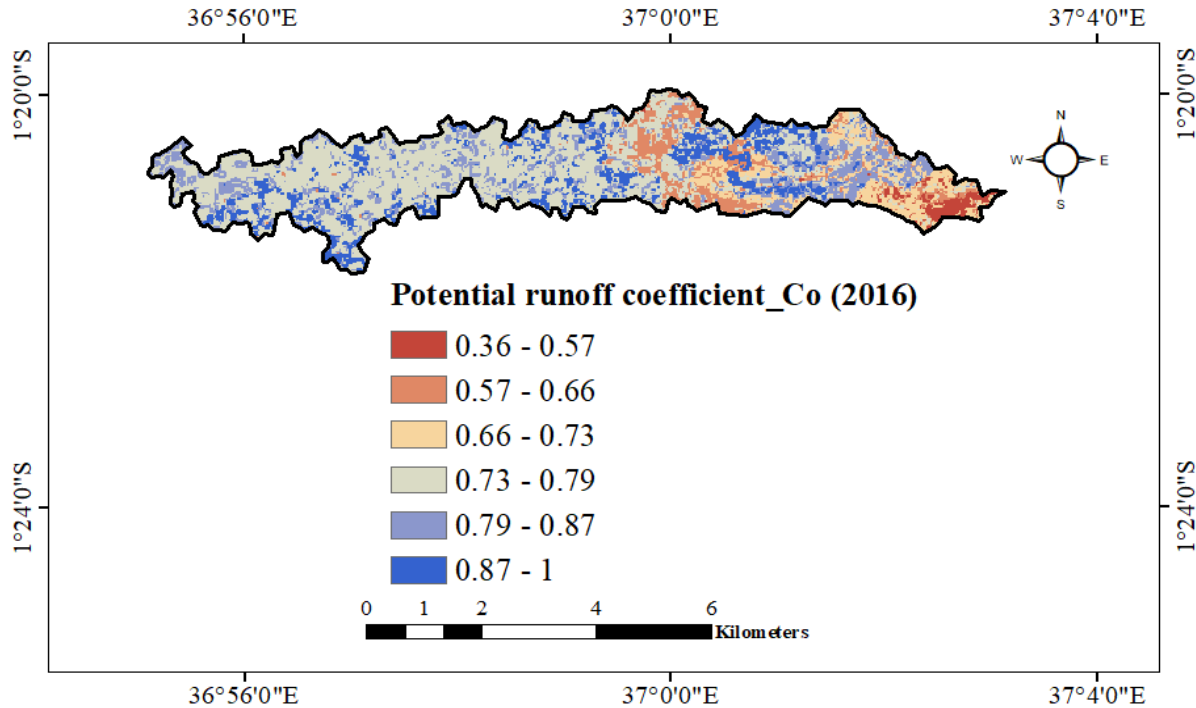
Map. 4.11: Potential runoff coefficient distribution of the Syokimau-Katani area (2004)





*Map. 4.12: Potential runoff coefficient distribution of the Syokimau-Katani area (2010)*

Just like the land-use/land cover maps discussed in *Section Error! Reference source not found.*, a drastic change is also noticed as we move from 1999 to 2004 (with the 0.87 to 1 range decreasing to the 0.73 – 0.87, as is visible on **Map. 4.11**), possibly by the recovery of the watershed from the 1999 – 2000 nation-wide drought. Just as is the case in the land-use/land cover analysis, not much variation is noted between the potential runoff coefficient distribution of 2004 and 2010, except the high-value patch to the western tip of the watershed for the 2010 **Map. 4.12**. This patch appears to be directly linked to the red patch of urban and built-up area in **Map. 4.3**.



*Map. 4.13: Potential runoff coefficient distribution of the Syokimau-Katani area (2016)*

The 2016 map of potential runoff coefficient shows a wider variety of values. The spatial distribution of high values also spreads, showing a higher and more distributed chance of flooding within the Syokimau – Katani area. Therefore, with the understanding that a higher potential runoff coefficient value yields higher amounts of runoff, it is safe to state that the dark blue zones on **Map. 4.13** also represent ‘hot spot flooding zones’, or in other terms, zones with the highest probability of flooding, as of the year 2016. A review of current land-use data would be needed for the current determination of these ‘hot spot flooding zones’.

#### **4.1.4 Topography, land-use and soil overlays with runoff coefficient results**

The topography, land-use and soil map overlays with the runoff coefficient results are as given by:

$$\mathbf{T \times RC \rightarrow I_T}$$

$$\mathbf{LU \times RC \rightarrow I_{LU}}$$

$$\mathbf{S \times RC \rightarrow I_S}$$

Where model **T** overlaid by model **RC** yields an interpretation for **T**, model **LU** overlaid by model **RC** yields an interpretation for **LU** and model **S** overlaid by model **RC** yields an interpretation for

S, as discussed in *section 3.2.1*. The overlays interpreted herein are comprised of the 2016 runoff coefficient map results generated in *section 4.1.3*.

#### 4.1.4.1 Topography overlaid by the 2016 runoff coefficient results

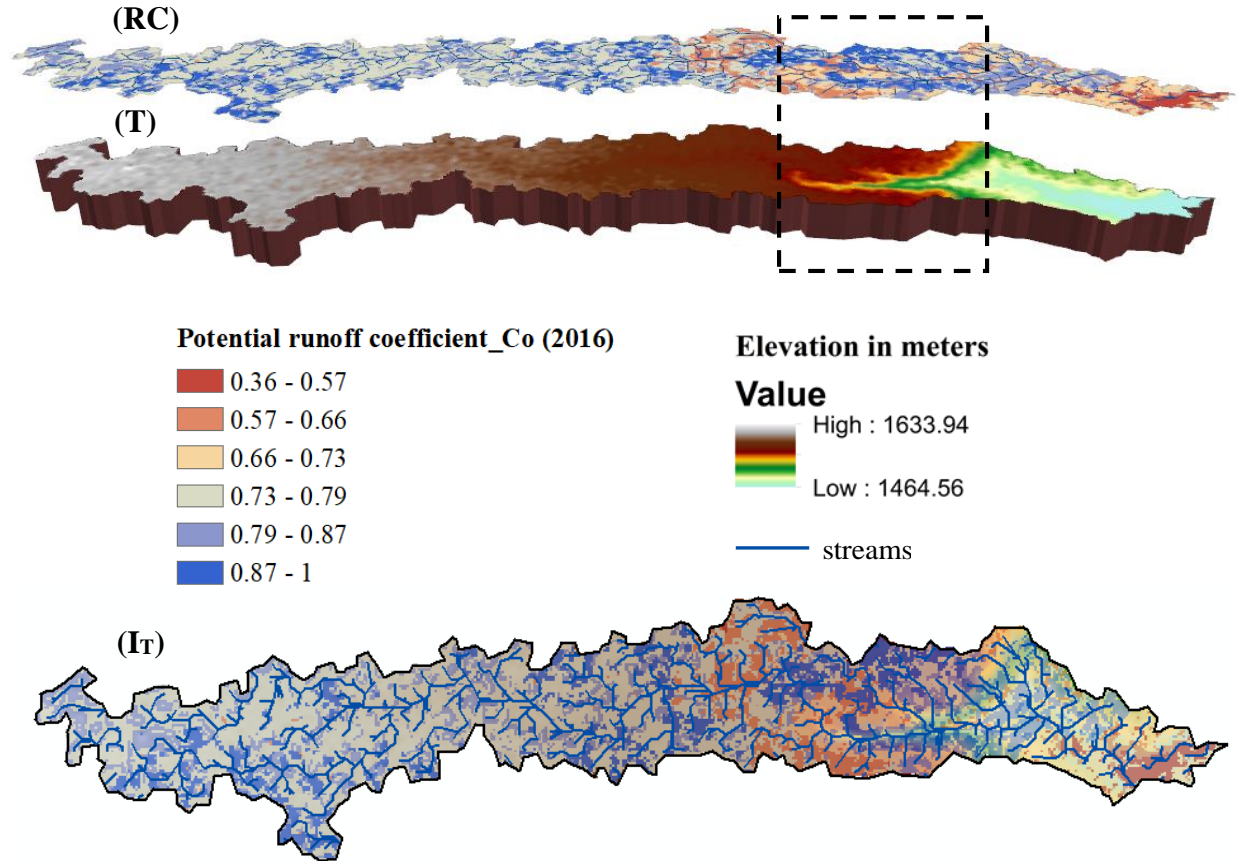


*Fig. 4.2: (RC) A 3-D spatial representation of the 2016 runoff coefficient values in the Syokimau-Katani area with streams generated from DEM, correlated with (T) A 3-D image of the study area's DEM; (IT) A 2-D overlay of runoff coefficient on DEM*

Regions with high runoff coefficient values on the (RC) map displayed on **Fig. 4.2** ranging from about 0.87 to 1 and indicated in a dark blue colour appear to be strewn across varied sections of the study area. It is also evident that the section highlighted by a dotted rectangle towards the east corresponds to the high elevation area on the topography (T) map. We can therefore confidently state that the high runoff coefficient values in this highlighted eastern section are a direct result of the steep slope in this area. This, however, does not explain the equally high runoff coefficient values that appear towards the west where the topography is gently sloping.

## 4.1.4.2 Landuse overlaid by the 2016 runoff coefficient results

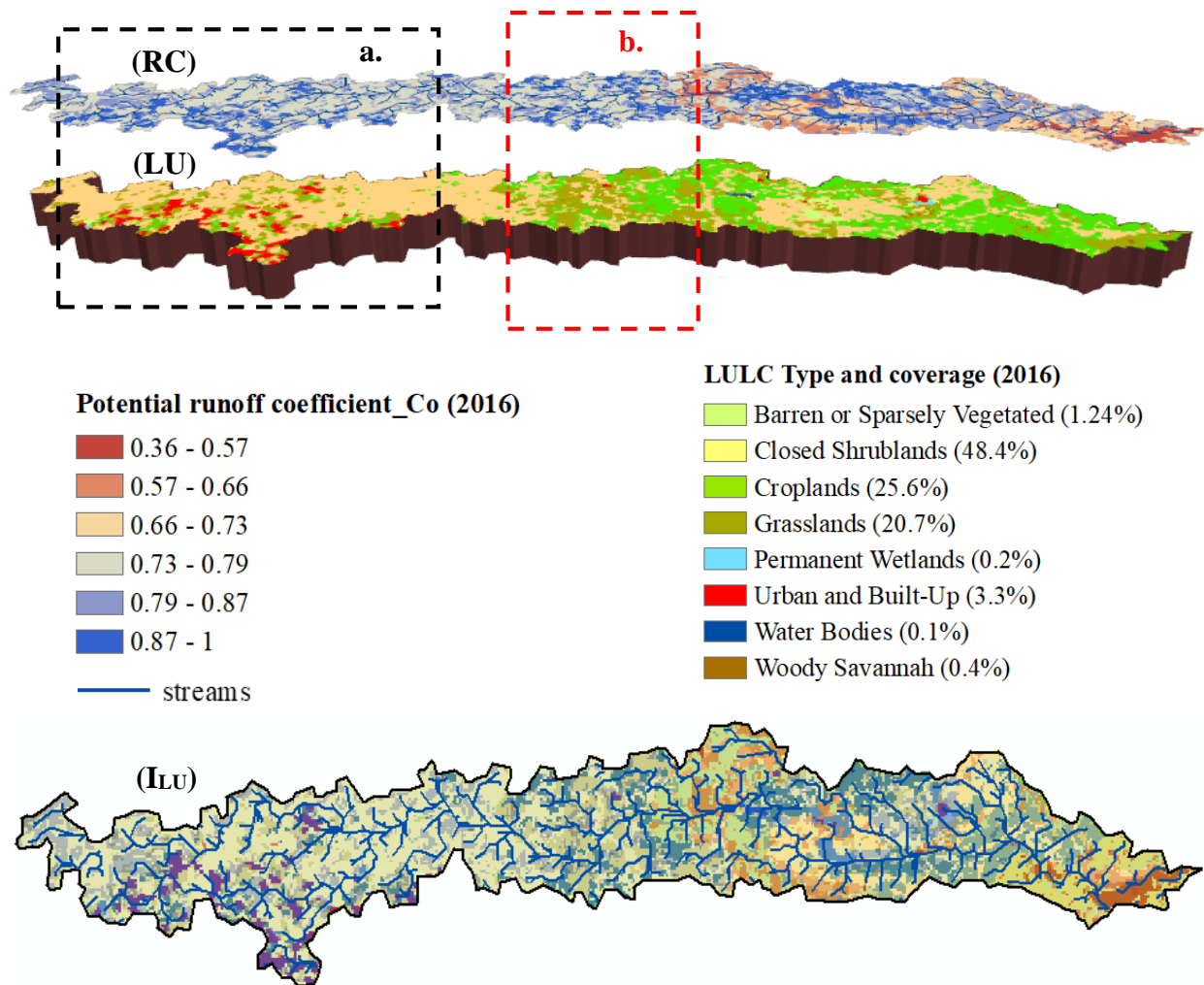


*Fig. 4.3: (RC) A 3-D spatial representation of runoff coefficient values in Syokimau-Katani area with streams generated from DEM correlated with (LU) A 3-D image of the study area's land use map (ILU) A 2-D overlay of runoff coefficient on land-use*

Towards the western side of the study area, two regions (labelled as dotted rectangles **a.** and **b.**) can be highlighted in connection to regions of high runoff coefficient values as shown in **Fig. 4.3**. The farthest western section (**a.**) is evidently due to the rising urbanization in the area and the consequent increase in impermeable surfaces. The central section (**b.**) can be directly linked to the 25.6% cropland cover in the watershed; an area that would be marked as a flooding hotspot for urban/peri-urban developers. This central region of land is fairly gentle in slope and appears safe for settlement but the currently prevailing natural cover or lack thereof already poses as a potential risk to flooding in the area.

#### 4.1.4.3 Soil overlaid by the 2016 runoff coefficient results

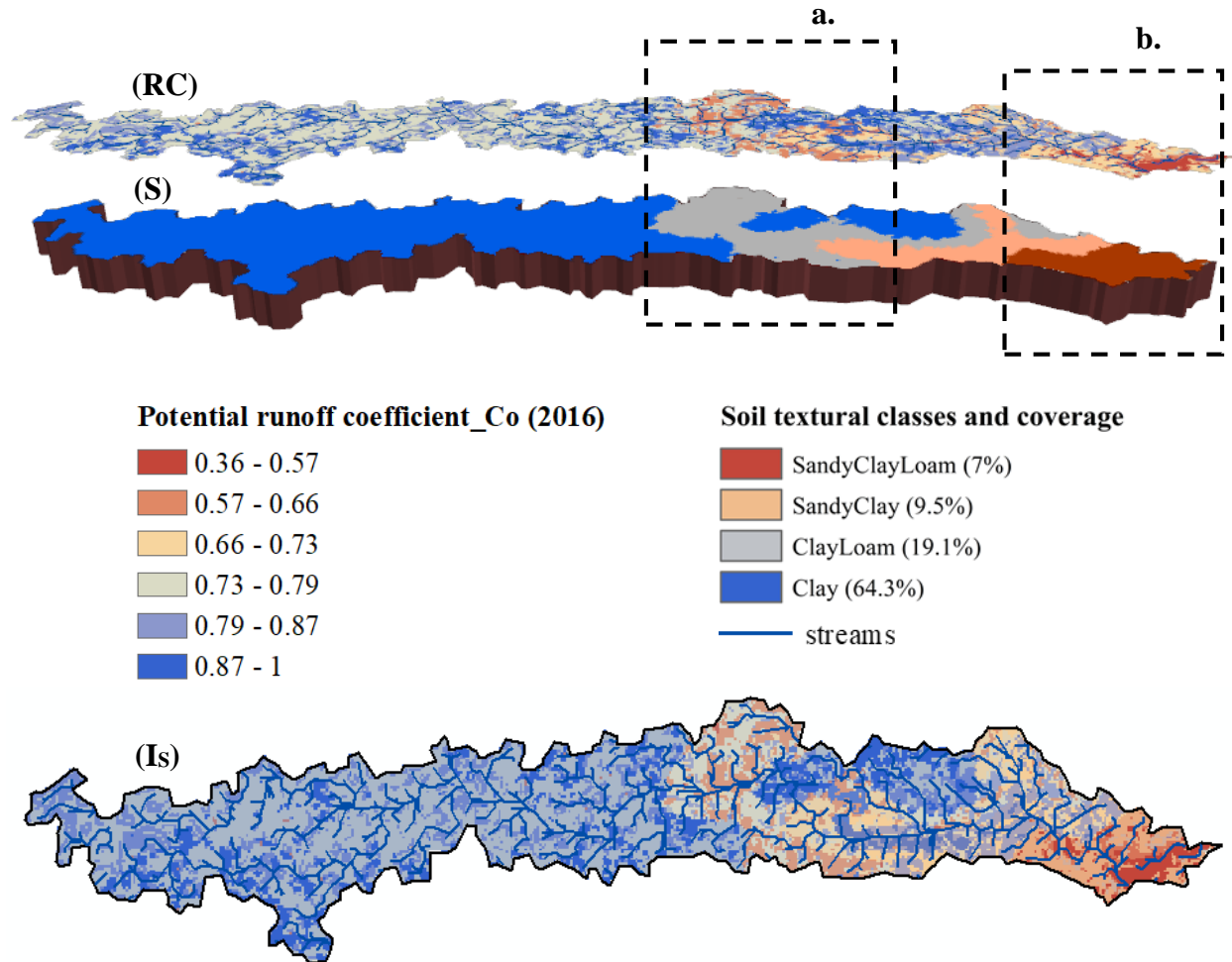


*Fig. 4.4: (RC) A 3-D spatial representation of runoff coefficient values in Syokimau-Katani area with streams generated from DEM correlated with (S) A 3-D image of the study area's soil map (Is) A 2-D overlay of runoff coefficient on soils*

Highlighted regions (a.) and (b.) in **Fig. 4.4** have lower runoff coefficient values ranging from 0.37 to about 0.68 that correspond to the areas of the watershed covered in Sandy-Clay-Loam soils and Clay-Loam soils. These particular regions would be more appealing for their lower flood risk potential as opposed to the regions covered in Clay soils (that tend to have higher runoff coefficient values according to **Table 3.4**).

#### 4.1.5 Runoff depth time series from 1999 to 2016

Using monthly rainfall intensity data for the March-April-May period, the runoff depth profile was generated in two scenarios; the **unique scenario**, in which the runoff depths for each year (among

the years 1999, 2004, 2010 and 2016) were computed using their respective monthly rainfall intensity values, and the **change in LULC only** scenario where the runoff depths for each year were computed using the monthly rainfall intensity values for 2016. The unique scenario aimed to recreate the near-real events of the years chosen, while the change-in-LULC-only scenario was to highlight any effect of land-use/land cover transformation within the watershed.

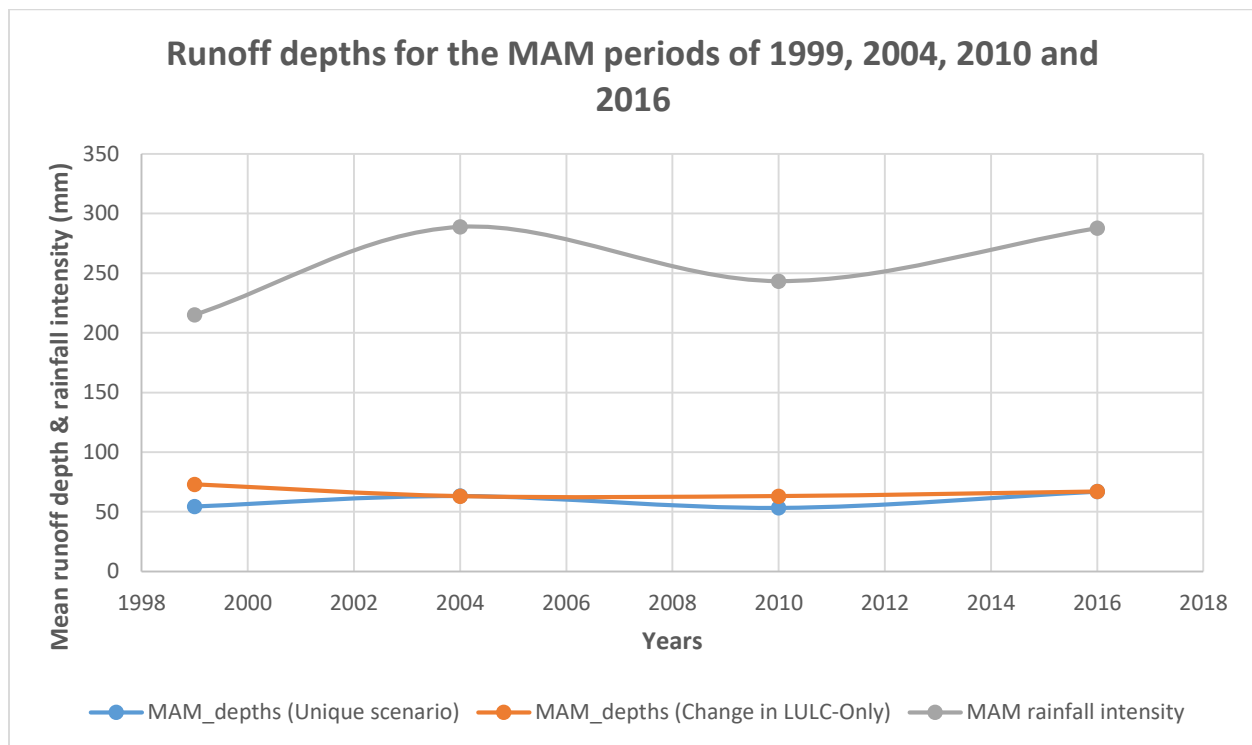


*Fig. 4.5: Runoff depths for the March-April-May periods of the years 1999, 2004, 2010 and 2016*

In **Fig. 4.5**, the two scenarios are plotted against the average rainfall intensity of the MAM periods of the years 1999, 2004, 2010 and 2016. One can note that the unique scenario follows the trend of the average rainfall intensity curve (proving the effect of rainfall intensity on runoff depth), yielding average runoff depth estimates of 54.5mm in 1999, 63.3mm in 2004, 53.35mm in 2010 and 66.9mm in 2016. The change-in-LULC-only scenario yielded average runoff depth estimates of 72.9mm in 1999, 63mm in 2004, 63.1mm in 2010 and 70mm in 2016. Apart from the high runoff depth in 1999 attributed to the bare/sparsely vegetated area that developed during the 1999 – 2000 nation-wide drought, the range of runoff depths from 2004 seems to be increasing steadily with the direct change in land-use/land cover and indirect effects of human activity. **Fig. 4.6** highlights the effects of land-use/land cover on runoff depths, with rainfall intensity data input held constant in calculation.

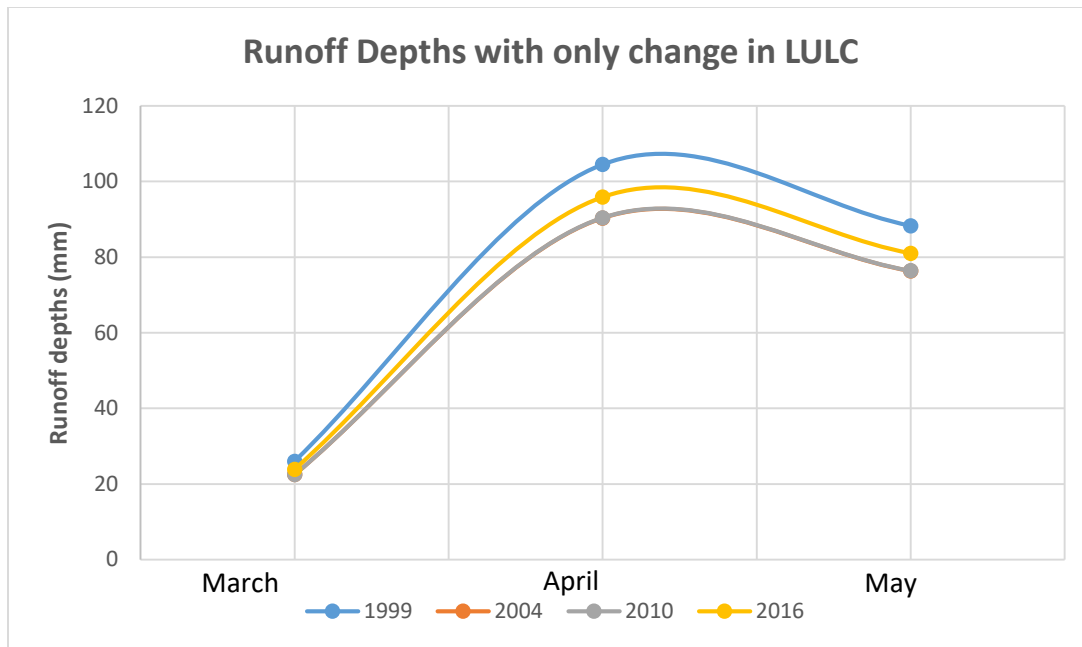


*Fig. 4.6: Runoff depths with only change in land-use/land cover for the March-April-May period in the years 1999, 2004, 2010 and 2016*

In conclusion, the results yielded from the analysis of mapped land-use/ land cover data, mapped soil textural classes, generated potential runoff coefficients, topography, land-use and soil overlays with runoff coefficient results and the graphed runoff depth time series have highlighted the following:

- a) LULC has changed over the years with 1999 – 2000 and 2010 – 2016 registering the highest variations.
- b) The area's slope, soil types and land-use distribution have contributed to the runoff coefficient variations.
- c) Even though weather and climate play a significant role in generating runoff depths in the area, land-use and land cover have also significantly contributed to runoff depth yields as shown from the **LULC only** and **unique scenarios**. Good examples include the 1999-2000 drought case and the 2016 increase in urbanization.

It is important to note that these results have the following limitations:

- 1) An assumption on the reducing factor  $P_j$  – With an estimated minimum relative saturation value of about 0.1 used to compute initial moisture content during simulation and the use

of total monthly rainfall intensity values in the attempt to imitate a real storm, it is assumed that a reducing factor of 0.9 will reduce possible exaggerations.

- 2) The use of low-resolution grid files for input maps – Even with the ability to re-grid and interpolate low resolution maps to high-resolution grid cell sizes, the process in itself does not enrich the data but rather repackages the already available information into a workable grid file purely for simulation purposes.
- 3) Though no faults or fractures have been noted in the study area, the WetSpa tool has no direct way of accommodating for this parameter

## **4.2 Discussion**

The history of the hydrological response of the Syokimau-Katani watershed can be traced from the analysis of the area's soils, land-use/land cover variations over time, topographical landscape (from a high-resolution DEM for high spatial detail) and meteorological information, as evidenced in the research results achieved herein. All these datasets jointly describe the study area's characteristics in a way that is sufficient for the generation of potential runoff coefficient estimates and that can be extracted using physically distributed tools such as WetSpa.

The land-use/land cover variations from 1999 to 2016 define a history of the contributions of both human activities and climate change to the study area's hydrological response. The two scenarios chosen for analysis, i.e. the unique scenario and the change-in-LULC-only scenario represent an attempt at isolating the effects of rainfall intensity and land-use/land cover to the area's runoff depth estimates. From this analysis, it is evident that the rainfall intensity of this region has the most contribution to the runoff depth estimates of the watershed as it was noted in the extreme drought period recorded in 1999-2000. Nevertheless, this scenario-isolating approach has revealed a significant contribution of land-use/land cover variations to the generation of runoff depth estimates and to some extent, highlighted the possible effects, both direct (as seen from the actual presence of urban and built-up zones in the 2016 LULC map) and indirect (from associated human settlement changes such as farming, as stated in literature), of human encroachment – or in other words, urbanization.

Soils are heavily defined by an area's geology, slope and climate. The Syokimau-Katani region shows high amounts and vast coverage of sandy-clay soils believed to be derived from the erosion of the Tertiary volcanic rocks in the area and the depositional nature of the Athi-Kapiti plains that



are greatly defined by the slope. As part of the Upper Athi River basin, this dominance in sandy-clay soils, as expected, contribute significantly to the flooding nature of this watershed from their characteristic low porosity and low infiltration rates as known from literature.

The spatial distribution of the generated potential runoff coefficient estimates has a direct relation to the ‘hotspot’ flood zones targeted in this research. These values or coloured zones serve to provide a relative comparison of the hydrological response of the area constrained by the Syokimau-Katani watershed. The same maps that represent the spatial distribution of the generated potential runoff coefficient values can be used to show ‘hotspot’ flood zones within the area. From these maps, informed decisions can be made in peri-urban planning and for the development of effective storm systems to manage floods in the Syokimau-Katani area, as well as inform human-settlement policy.

## **Chapter 5: Conclusions and Recommendations**

### **5.1 Conclusion**

Through this research, we were able to successfully generate runoff coefficients from the analysis of available topographical, land-use and soil map data. Using the Wetspa tool, we generated models that use predefined constants to define the Syokimau-Katani watershed's hydrological response. We were also able to derive watershed parameters by validating these datasets using additional google earth imagery, borehole data, available geological information and ERT profiles. The processing of the DEM data enabled the derivation of the watershed's extent using a 30m high resolution DEM on ArcGIS and the generation of a slope map.

Even though the acquired ERT profiles' extent covered a relatively small portion of the study area, we were able to confidently extrapolate the interpretation of the top 60m geological surface. This was affirmed by available drillhole data, regional geology and a generated geological cross-section. From this, we were able to correlate resistivity values to the clay soils in the area and hence validate the soil dataset for use on Wetspa.

An analysis of the study area's rainfall-runoff depth estimates and land-use/land cover distribution revealed urbanization (and human activity) to be a significant cause for flooding in the Syokimau-Katani region. Even though the 1999 LULC map recorded large runoff coefficient value attributed to the drought period recorded in 1999-2000, the urban and built-up zones in the 2016 LULC map yield considerably high runoff coefficients towards the western section of the study area. These area high-runoff-coefficient zones or what has been coined herein as 'hotspot zones' can be used for both informed settlement policies and urban planning.

Unfortunately, a correlation between the effects of outcropping rocks on the hydrological response of the Syokimau-Katani area has not been included. This analysis will need the isolation of this area's outcrops to help improve the accuracy of the watershed's texture. In tandem with the rapid response prototyping approach encouraged in this research, this geological analysis may be achieved using processed satellite imagery.

### **5.2 Recommendations**

The results of this work can be used to inform urban development policies and settlement procedures in urban/peri-urban centres and metropolitan spaces. Potential runoff coefficient maps are viable in aiding the placement and design of storm management systems in more effective


ways that can help control the urban-flooding problem in the country. It is thus recommended that these results be used for the improvement and development of the drainage system in the Syokimau – Katani area, and the same approach be adopted in peri-urban spaces within the country.

It is also recommended that these same simulations be redone using WetSpa-Python for the increased spatial and temporal resolution flexibility of the different components since it accounts for the varied distribution of urban catchments.

## APPENDICES

### Appendix 1: Sample page of borehole completion report from WRMA (2018)

The Chief Executive Officer,  
Water Resources Management Authority,  
P.O. Box 45250 - 00100  
NAIROBI



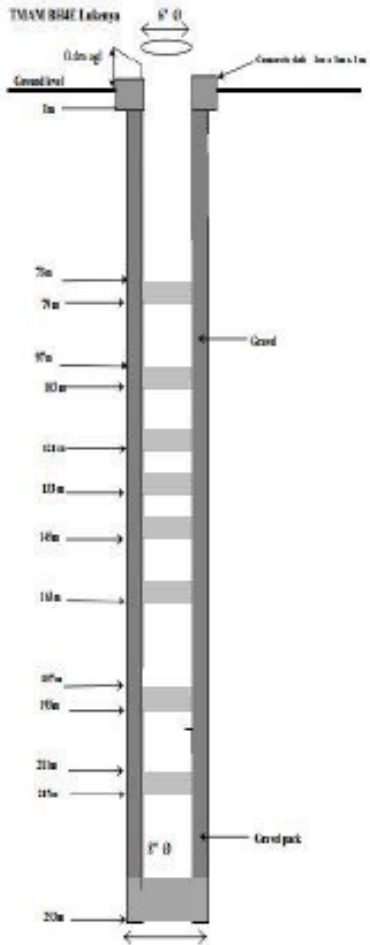
Form: WRMA 009A  
Catchment: \_\_\_\_\_  
WRMA ID : \_\_\_\_\_  
File: \_\_\_\_\_

1. Driller's Log.

0-13m	Highly weathered
15-45m	Fresh trachyte
45-48m	Weathered trachyte
48-54m	Fresh trachyte
55-57m	Weathered trachyte
57-61m	Fresh trachyte
62-64m	Weathered trachyte
64-74m	Highly weathered
74-79m	Fresh trachyte
79-84m	Highly weathered trachyte
84-86m	Brown clayish soil
87-91m	Brown gravel material with quarts
91-98m	Loss of cuttings
98-102m	Highly weathered trachyte
102-103m	Fresh trachyte
104-105m	Yellow/green highly weathered trachyte
105-109m	Highly weathered trachyte
109-113m	Boulder stone
113-116m	Fresh trachyte
116-141m	Highly weathered trachyte
141-156m	Fresh gravel with quarts
157-161m	Highly weathered trachyte
161-163m	Fresh trachyte
163-168m	Highly weathered
168-175m	Fresh trachyte
176-181m	fresh
181-183m	Highly weathered
183-190m	Highly weathered
191-200m	Fresh trachyte
200-205m	Light brown gravels
205-215m	Highly weathered trachyte

12. Sketch of Borehole Construction:



13. Location Sketch: (To be sketched by the driller on the site, showing roads, tracks and prominent land marks, with road distances to the nearest town or trading centre and to water source).

---

**REFERENCES**

- Almasi, P., Soltani, S., 2017. Assessment of the climate change impacts on flood frequency (case study: Bazoft Basin, Iran). *Stochastic Environmental Research and Risk Assessment* 31, 1171–1182. <https://doi.org/10.1007/s00477-016-1263-1>
- Bahremand, A., 2006. Simulating the effects of reforestation on floods using spatially distributed hydrologic modeling and GIS 186.
- Bahremand, A., De Smedt, F., 2010. Predictive Analysis and Simulation Uncertainty of a Distributed Hydrological Model. *Water Resources Management* 24, 2869–2880. <https://doi.org/10.1007/s11269-010-9584-1>
- Bahremand, A., De Smedt, F., Corluy, J., Liu, Y.B., Poorova, J., Velcicka, L., Kunikova, E., 2006. Application of WetSpa model for assessing land use impacts on floods in the Margecany-Hornad watershed, Slovakia. *Water Science and Technology* 53, 37–45. <https://doi.org/10.2166/wst.2006.295>
- Braud, I., Fletcher, T.D., Andrieu, H., 2013. Hydrology of peri-urban catchments: processes and modelling. *Journal of Hydrology* 485, 1–4. <https://doi.org/10.1016/J.hydro.2013.02.045>
- Devi, G.K., Ganasri, B.P., Dwarakish, G.S., 2015. A Review on Hydrological Models. *Aquatic Procedia* 4, 1001–1007. <https://doi.org/10.1016/j.aqpro.2015.02.126>
- Dhami, B.S., Pandey, A., 2013. Comparative review of recently developed hydrologic models 33, 9.
- Ellenkamp, G.R., 2004. Soil variability and landscape in the Machakos District, Kenya 44.
- Fairburn, W.A., 1963. Report Geology of the North Machakos-Thika Area.pdf (No. 59). Geological Survey of Kenya.
- GoK, 2009. Draft National Policy for Disaster Management in Kenya. Government of Kenya.
- Greer, A.D., Wilbanks, Z.B., Clifton, L.D., Wilson, B., Graettinger, A.J., 2018. GIS-Enabled Culvert Design: A Case Study in Tuscaloosa, Alabama. *Advances in Civil Engineering* 2018, 1–10. <https://doi.org/10.1155/2018/4648134>
- Jeremiah, N.A., 2015. Real estate development outside the city county of Nairobi and the escalation of urban sprawl: Could developers be avoiding zoning-related costs in the city? *Journal of Geography and Regional Planning* 8, 261–272. <https://doi.org/10.5897/JGRP2015.0487>
- Karamage, F., Zhang, C., Fang, X., Liu, T., Ndayisaba, F., Nahayo, L., Kayiranga, A., Nsengiyumva, J., 2017. Modeling Rainfall-Runoff Response to Land Use and Land Cover Change in Rwanda (1990–2016). *Water* 9, 147. <https://doi.org/10.3390/w9020147>
- Koti, F., Weiner, D., 2006. (Re) Defining Peri-Urban Residential Space Using Participatory GIS in Kenya. *The Electronic Journal of Information Systems in Developing Countries* 25, 1–12. <https://doi.org/10.1002/j.1681-4835.2006.tb00169.x>
- Kuria, J.N., 2018. Hydrogeological survey report carried out at Syokimau area [Unpublished] (No. HDRG/18/03/13/1).
- Liu, Y.B., De Smedt, F., 2004. WetSpa Extension, A GIS-based Hydrologic Model for Flood Prediction and Watershed Management. Vrije Universiteit Brussel, Brussels, Belgium.
- Matheson, F.J., 1966. GEOLOGY OF THE KAJIADO AREA 57.
- Miller, J.D., Kim, H., Kjeldsen, T.R., Packman, J., Grebby, S., Dearden, R., 2014. Assessing the impact of urbanization on storm runoff in a peri-urban catchment using historical change in impervious cover. *Journal of Hydrology* 515, 59–70. <https://doi.org/10.1016/j.jhydro.2014.04.011>

- Mundia, C.N., 2017. Nairobi Metropolitan Area, in: Murayama, Y., Kamusoko, C., Yamashita, A., Estoque, R.C. (Eds.), *Urban Development in Asia and Africa*. Springer Singapore, Singapore, pp. 293–317. [https://doi.org/10.1007/978-981-10-3241-7\\_15](https://doi.org/10.1007/978-981-10-3241-7_15)
- Naporadean, I., Chira, R., 2006. The hydrological modelling of the Usturoi Valley - Using two modelling programs - WetSpa and HecRas. *Carpth. J. of Earth and Environmental Sciences* 1, 53–62.
- Ngugi, R.K., Mureithi, S.M., Kamande, P.N., 2011. Climate forecast information: the status, needs and expectations among smallholder agro-pastoralists in Machakos District, Kenya. *International Journal of Current Research* 3, 6–12.
- OHPA, O.E.P.A., 2008. *Application of Geophysical Methods for Site Characterization*, in: *Technical Guidance Manual for Groundwater Investigations*. Columbus, Ohio.
- Onyancha, C., Mathu, E., Mwea, S., Ngecu, W., 2011. A study on the engineering behaviour of Nairobi subsoil 6, 12.
- Onyancha, C.K., Mathu, E.M., Mwea, S.K., Ngecu, W.M., 2014. Geophysical Resistivity Survey in Subsurface Characterization for Heavy Construction in Nairobi City, Kenya 5, 9.
- Panyako, O.O., 2018. Urban flooding in Kenya from a psychosocial perspective. *International Research Journal of Management, IT and Social Sciences*. <https://doi.org/10.21744/irjmis.v5n5.276>
- Panyako, O.O., Wakhungu, J.W., Kioli, F.N., 2015. Enhancing household response to flooding in Mavoko peri-urban settlements of Nairobi Metropolis, Kenya 3, 20.
- Reynolds, J.M., 2011. *An Introduction to Applied and Environmental Geophysics* 712.
- Sahoo, S.N., Sreeja, P., 2014. A methodology for determining runoff based on imperviousness in an ungauged peri-urban catchment. *Urban Water Journal* 11, 42–54. <https://doi.org/10.1080/1573062X.2013.765491>
- Shuster, W.D., Bonta, J., Thurston, H., Warnemuende, E., Smith, D.R., 2005. Impacts of impervious surface on watershed hydrology: A review. *Urban Water Journal* 2, 263–275. <https://doi.org/10.1080/15730620500386529>
- Simiyu, N.L., Dulo, S.O., 2015. Spatiotemporal Analysis of Borehole Locations in Nairobi County 1930 - 2013. *IJAIEEM* 4, 9.
- Smedt, F.D., Liu, Y.B., Qiao, Y., 2002. Prediction of floods with the WetSpa model 10.
- Sterrett, R., J., 2007. *Groundwater & Wells: A comprehensive guide for the design, installation, and maintenance of a water well*, 3rd ed. Johnson Screens, United States of America.
- UN-Habitat, 2010. *The State of African Cities 2010: Governance, Inequality and Urban Land Markets*. UN-Habitat, Nairobi.
- UN-Habitat, 2006. *Kenya: Mavoko Urban Sector Profile*.
- Valois, R., Camerlynck, C., Dhemaied, A., Guerin, R., Hovhannissian, G., Plagnes, V., Rejiba, F., Robain, H., 2011. Assessment of doline geometry using geophysics on the Quercy plateau karst (South France): MORPHOLOGY OF DOLINES USING GEOPHYSICS. *Earth Surface Processes and Landforms* 36, 1183–1192. <https://doi.org/10.1002/esp.2144>
- Wirion, C., Bauwens, W., Verbeiren, B., 2017. Location- and Time-Specific Hydrological Simulations with Multi-Resolution Remote Sensing Data in Urban Areas. *Remote Sensing* 9, 645. <https://doi.org/10.3390/rs9070645>
- Xu, C., 2002. *Textbook of Hydrologic Models*. Uppsala University, Department of Earth Science, Hydrology, Uppsala, Sweden.
- Zellner, M., Massey, D., Minor, E., Gonzalez-Meler, M., 2016. Exploring the effects of green infrastructure placement on neighborhood-level flooding via spatially explicit simulations.

Computers, Environment and Urban Systems 59, 116–128.  
<https://doi.org/10.1016/j.compenvurbsys.2016.04.008>

## Turnitin Originality Report

Processed on: 01-Nov-2020 12:19 EAT  
 ID: 1432556266  
 Word Count: 14152  
 Submitted: 1

Similarity Index  <b>2%</b>	<b>Similarity by Source</b>	
	Internet Sources:	1%
	Publications:	1%
	Student Papers:	1%

Karen\_MScThesis\_20201023 By Masila  
 Karen

< 1% match (publications)  
[Qingyun Duan, John C. Schaake. "Total water storage in the Arkansas-Red River basin", Journal of Geophysical Research: Atmospheres, 2003](#)

< 1% match (student papers from 09-Jan-2012)  
[Submitted to University of Leeds on 2012-01-09](#)

< 1% match (student papers from 13-Jun-2017)  
[Submitted to Symbiosis International University on 2017-06-13](#)

< 1% match (publications)  
[Longshan Zhao, Faqi Wu. "Simulation of Runoff Hydrograph on Soil Surfaces with Different Microtopography Using a Travel Time Method at the Plot Scale", PLOS ONE, 2015](#)

< 1% match (student papers from 29-Dec-2017)  
[Submitted to Victoria University College on 2017-12-29](#)

< 1% match (Internet from 29-Aug-2017)  
[http://www.plr.ugent.be/pedon\\_18.pdf](http://www.plr.ugent.be/pedon_18.pdf)

< 1% match (student papers from 05-Apr-2017)  
[Submitted to University of Mauritius on 2017-04-05](#)

< 1% match (Internet from 23-May-2020)  
<http://repositorio.unicamp.br/jspui/bitstream/REPOSIP/243858/1/000363391600008.pdf>

< 1% match (Internet from 28-Apr-2003)  
[http://biometrics.cse.msu.edu/RossCorrelation\\_ECCV02.pdf](http://biometrics.cse.msu.edu/RossCorrelation_ECCV02.pdf)